

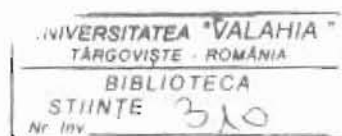
"Valahia" University of Târgoviște
Ministry of Education and Research



THE ANNALS OF "VALAHIA" UNIVERSITY OF TÂRGOVIȘTE

SECTION: FUNDAMENTAL SCIENCE

**Nr. 12
2002**



CONTENTS

<i>Applications of Nuclear Analyzing Methods (PIXE, ICP) in Biology and Environmental at "Valahia" University of Targoviste</i>	
I. V. Popescu, T. Badica, G. Dima, Claudia Stih, M. Jordan, C. Oros	5
<i>X and Gamma Ray N⁺PP⁺ Silicon Detectors With High Radiation Resistance</i>	
Gh. V. Cimpoca	19
<i>Recent Approaches In The Laser Surface Treatment Of Materials</i>	
C. Oros, A. Măriuțan, S. Dinu, Nicoleta Oros	30
<i>PIXE (Particle Induced X Rays Emission) and ICP (Inductive Coupled Plasma) Measurements of Basella Alba L Leaves</i>	
Claudia Stih, Gabriela Busuoc, I. V. Popescu, G. Dima	35
<i>Blood Serum Enzymes Analysis by PIXE Method</i>	
G. Dima, L. Manea, Claudia Stih, I. V. Popescu, Victoria Dima	40
<i>Nonlinear Optical Phenomena</i>	
S. Dinu	43
<i>The Nanophysics Processing of Atomic Units</i>	
Oana Catalina Bute	46
<i>The Influence of Ethanol in Dissolution Test for Antibiotics Capsules</i>	
Ana-Maria Hossu, Mihaela Scripcariu, V. Magearu	53
<i>Study of the Antioxidative Properties of Some Triazinic Skeleton Compounds</i>	
Laura Monica Gorghiu, Crinela Dumitrescu, R. L. Olteanu, S. Jipa	57
<i>The Interaction Between New Synthetized Acid Dyes and a Nonionic Surfactant Alkyl Polyglucosidic</i>	
Irina Moater, Crinela Dumitrescu, Mihaela Olteanu, C. Bendic	64
<i>Engrais retardés sur polymères biodegradable</i>	
Cristiana Radulescu G. C. Constantinescu	70
<i>Synergistic Effects of Some Dyes With Steric Hindered Phenols in i-PP Thermal Stabilization</i>	
Crinela Dumitrescu, Laura Monica Gorghiu, R. L. Olteanu, S. Jipa	74

<i>Reversible Transitions Induced by Light</i> Ionica Ionitã, Crinela Dumitrescu	80
<i>Inorganic Pollutants in the Air, Formed in Photochemical Processes</i> Elena Grigorescu	85
<i>Variational Formulation of the Impulsive Traction for a Plastic Material</i> C. Gbita	91
<i>A Method of Compactness for Hammerstein Equations and Applications</i> C. Mortici	97
<i>Some Properties of Maximal Ring of Quotients</i> Andreea Mihaela Panait	102
<i>Curvilinear $I(C)$ for Problems of Variations Calculus on Supermanifolds</i> V. G. Cristea	105
<i>Un théorème de surjectivité pour opérateurs monotones dans espaces de Hilbert</i> D. Teodorescu	108

APPLICATIONS OF NUCLEAR ANALYZING METHODS (PIXE, ICP) IN BIOLOGY AND ENVIRONMENTAL AT "VALAHIA" UNIVERSITY OF TARGOVISTE

ION V. POPESCU*, TEODOR BADICA**, GABRIEL DIMA*, CLAUDIA STIHI*, MARIN IORDAN*, CALIN OROS*,

Applied Physics Department, Science Faculty, University "Valahia" of Targoviste

** National Institute for Nuclear Physics and Engineering, Bucharest, Romania*

INTRODUCTION

The "Valahia" University of Targoviste was founded in 1994 in Targoviste, Romania. As a part of this young University is the Research Department on Applied Physics and one of the research direction of this department is the application of Particle Induced X-ray Emission (PIXE) for the determination of elements with atomic number greather than 13 in biological, biomedical and environmental samples. The Research Department on Applied Physics of Sciences Faculty from "Valahia" University of Targoviste have many scientific collaborations with Polytechnic University of Bucharest, University of Bucharest, University of Galatzy and Institute for Nuclear Physics and Engineering "Horia Hulubei" Bucharest.

In this paper we present some applications of Particle Induced X-ray Emission (PIXE) and Induced Coupled Plasma (ICP) in biology, veterinary medicine, end environmental studies.

EXPERIMENTAL METHODS

Among the methods designed for the determination of the very low chemical concentrations, the Particle Induced X-ray Emission (PIXE) method is the best one specially for measuring the light elements. This method is based on the fact that the bombardment of the sample with a charged particle beam causes the ionisation of the atomic inner shells followed by a subsequent of the characteristic X-rays. When the X rays spectrum is detected by high-resolution detector, the well-known Z-dependence of the X rays energies, as well as the intensities of the individual X rays line, allow a straight

forward determination of the target element. The detection limit of this method is very good because: i) intense fluxes of exciting radiation are available, ii) the X rays production yields for particles with energies in the MeV range are large and iii) the background associated with the exciting radiation is rather low. The sample preparation technique does not require a special chemical preparation which may cause some losses in concentration or some contamination. A quantitative determination of an element content in a sample by PIXE method can be done both by absolute or relative measurements.

The target samples for **PIXE** were doped with standard solution (1:1) of Yttrium (standard for spectrum normalization and systematical error elimination) consisting of 130 mg/l of Yttrium (prepared from Y_2O_3) in deionised water. Measurements of target elements were made using a 3.2 MeV proton beam extracted from the TANDEM accelerator from IFIN-HH Magurele, Bucharest, and passes through a collimator (3×4 mm) before reaching the target. X-ray spectra were measured with a spectrometric chain having a CANBERRA Ge hyperpure detector (100

mm²×7mm) with a 160 eV resolution at 6.4 KeV of K_{α} line of iron.

At the same time for trace element determinations, we use the **ICP** method. The reason for that choice is the impossibility of measuring the content of Mg with **PIXE** because of the absorption of the X-rays in the windows of the chamber and the detector. On the other hand, we cannot use only the **ICP** because for that type of measurements the quantity of biological sample needed is proportional to the number of the analyzing elements. We prefer to use both methods because **PIXE** requires only a "drop" of sample in order to determine all trace elements with atomic number between 13 and 80.

ICP-OES is a destructive technique that provides only elemental composition. The ICP method has been applied to a wide range of sample types: metals and wide variety of industrial materials, environmental samples (water streams, airborne particles and coal fly ash), and biological and medical samples.

We used ICP method to determine the concentration of Mg – element who can not been determined using PIXE method and concentration of Fe to compared

experimental results obtained using the both methods.

The ICP-OES (Inductively Coupled Plasma-Optical Emission Spectroscopy)

spectrometer used by us are a Baird ICP2070 -Sequential Plasma Specrometer which consists of a sample introduction system, a plasma torch, a plasma power supply and an optical measurement system (figure 1).

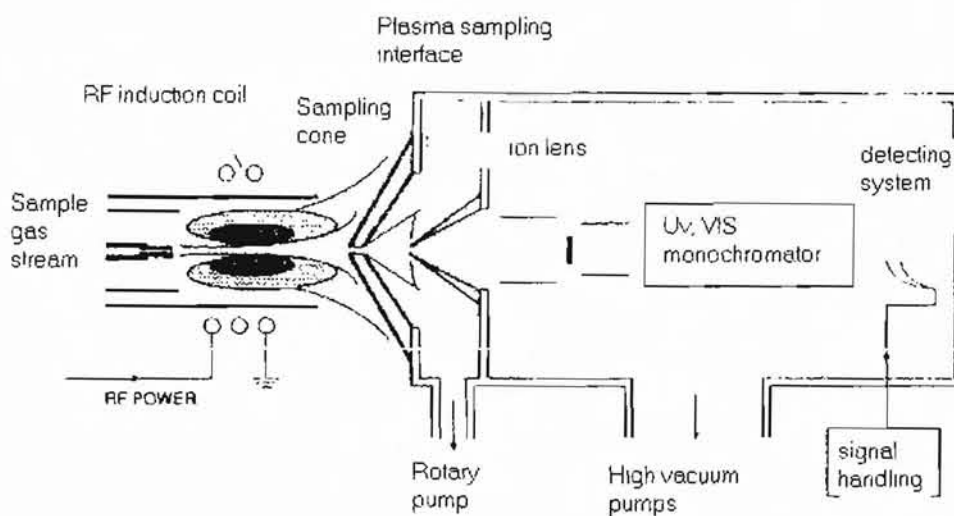


Figure 1: Instrumentation for Inductively Coupled Plasma-Optical Emission Spectrometry

The sample must be introduced into a plasma in a form that can be effectively vaporized and atomized (small droplets of solution, small particles of vapor). The plasma torch confines the plasma to a diameter of about 18 mm. Atoms and ions produced in the plasma are excited and emit light. The intensity of light emitted at wavelengths characteristic of the particular elements of interest is measured and related to the concentration of each element from

samples. Baird ICP2070 -Sequential Plasma Specrometer use as a plasma gas Argon and the plasma is sustained in a quartz torch and the plasma is generated using a radiofrequency generator at 40.68 MHz. Temperatures of 5000-9000K have been measured in the plasma. The detection systems used are a sequential monochromator with a wavelengths range (160-800) nm. The optical emission spectra are made using a personal computer.

EXPERIMENTAL RESULTS

A. IN BIOLOGY

AI. THE BASELLA PLANT.

This quantitative method applicable to Basella plants, is described in this work, along with the results obtained from the elemental analysis of leaves from different Basella plants cultivated in Variety Testing Centre and in Green Houses of Targoviste. Basella plant belong to Basellaceae family is a tropical plant used as a vegetable.

One of the problems of actual foods department is the variety about the vegetables with a great nourishment value.

Is the case of Basella plant like the native spinach (*Spinacea oleracea*). The mineral elements concentration give

information about the nourishment value of Basella plant leaves. Among the reported work we used PIXE analysis method to determine the elemental composition of Basella leaves, cultivated in Variety Testing Centre (VTC) and green houses of Targoviste for a given level of soil fertility.

Particle Induced X-Ray Emission was applied on Basella Alba L leaves, which are listed in table 1. In the experiment we used young Basella Alba Leaves sorted in four groups: Basella Alba - green house (P_1 , P_1'); Basella Alba - VTC (P_2 , P_2'); Basella Alba - VTC cultivated in soil treated with an artificial fertiliser using N (P_3 , P_3'); Basella Alba - VTC cultivated in soil treated with natural fertiliser (P_4 , P_4').

Table 1. Basella Alba L leaves samples

Samples	Green mass [g]	Dried mass [g]
P_1	5	0.2966
P_1'	5	0.3080
P_2	5	0.4412
P_2'	5	0.4133
P_3	5	0.4317
P_3'	5	0.4174
P_4	5	0.4458
P_4'	5	0.4511

The target sample have been prepared in the following manner: the washed leaves were simply air-dried at a temperature of 50⁰ in a clean box preventing further contamination. The dried leaves were grained and after powdering a layer of the samples material were deposited on hostaphan foils.

Using PIXE method we identified and we determined the amount of the following elements: P, Ca, Mg, K, Fe, Mn, Zn. In table 2 are presented the results of PIXE analysis on *Basella Alba* leaves samples with an instrumental error less than 12%.

Table 2. The concentration of elements in *Basella Alba L* leaves samples, mg/100g

Samples	P	Ca	Mg	K	Fe	Mn	Zn
P ₁	67.40	294.31	147.02	230.04	4.80	1.50	1.32
P ₁	67.54	293.27	146.81	231.82	4.72	1.37	1.25
P ₂	82.40	381.37	158.20	228.32	5.20	1.72	1.24
P ₂	82.78	389.33	161.25	225.20	4.98	1.80	1.33
P ₃	88.20	316.38	152.72	202.20	4.92	1.62	0.98
P ₃	89.12	318.02	150.25	200.82	4.80	1.58	0.87
P ₄	94.02	351.22	156.12	227.51	5.12	1.25	1.12
P ₄	94.50	364.71	156.82	225.72	5.02	1.25	1.02

The concentration of elements: Ca, Mg, K is often an essential requirement in agroalimentary domain because theirs presence in a big concentration is beneficial and give a remarkable nourishment value of *Basella* plants.

The use of PIXE technique give possibility to determine the elemental composition of plants with a great sensivity - the limit detection is 1 µg/g, that is genuine

trace-element analysis capability. A series of elements was put in evidence in *Basella Alba* leaves samples, elements which give a great nourishment value of *Basella* plant.

Samples in the ICP experiment, was young *Basella Alba L* leaves plant grown in different conditions at Variety Testing Centre (VTC) of Targoviste, Romania. Six groups of *Basella Alba L* were measured as shown in table . The leaves of the plants

were collected of approximately in some position in two successively months. The washing leaves were simply air-dried at a temperature of 105⁰ C in a clean box preventing further contamination. The dried leaves were grained and after powdering, 2.00g powder leaves have been digested in 40 ml acid nitric.

After a set aside in fume cupboard overnight the obtained liquid was gently boiled (without major loss of volume). For a good digestion 3 ml acid perchloric have been added and 2-3 ml water after cooling. The cooled solution was diluted with water at 250 ml solution and nebulized into plasma.

Table.3 The samples groups of *Basella Alba L* measured by ICP method

Sample	Growth fertiliser conditions
B1(VTC)-July	-
B2(VTC) --July	Natural fertiliser (excrements)
B3(VTC) --July	NPK fertiliser
B4(VTC)-August	-
B5(VTC) --August	Natural fertiliser (excrements)
B6(VTC) -August	NPK fertiliser

Experimental results obtained by ICP method are presented in table 4. The results obtained by ICP for iron concentration are in good concordance with the results for iron

concentration obtained by PIXE method (presented in table 4), so the both method PIXE and ICP are complementary methods for elemental analysis (figure 2).

Table 4: Mg and Fe concentration obtained by ICP method and PIXE method

Elements	B1(VTC) - July	B2(VTC) - July	B3(VTC) - July	B4(VTC) - August	B5(VTC) - August	B6(VTC) - August
Mg	22.65	18.33	16.14	21.00	20.72	18.75
Fe(ICP)	2.53	1.33	0.75	2.87	1.87	0.45
Fe(PIXE)	2.28	1.25	0.64	2.33	1.53	0.15

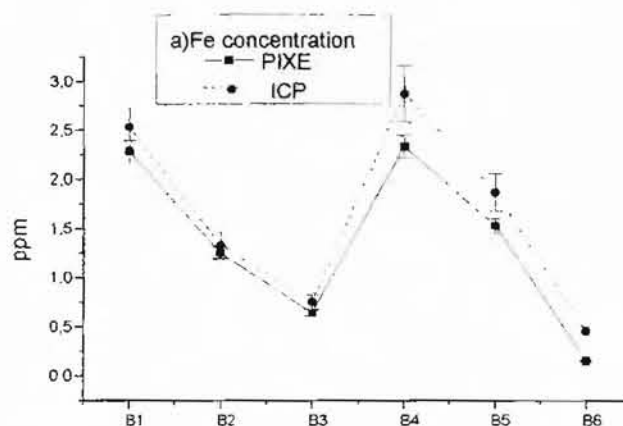


Figure 2: Fe concentration in Basella Alba L. leaves obtained by PIXE and ICP methods

A2. IN VETERINARY MEDICIN

We apply the PIXE method for the microelemental analysis of blood serum samples collected from healthy and ill cows (downer cow syndrome (**DCS**)). Until today the origin of **DCS** is uncertain. At the beginning of our work, we assume some connections among the diminution of some nutritive elements from food, the activity of some enzymes and the origin of **DCS**. The samples were collected from cows at some animal farms on the neighbourhood of Targoviste city. To obtain a microelemental monitoring of these samples, we used a nuclear analysis method **PIXE** (Particle Induced X-Rays Emission) and a

spectrometric one **ICP** (Induced Coupled Plasma). For Ca and P content of the analysed samples, we used **PIXE** based on the internal standard method. The **ICP** analysis method was used for Mg content determination. The determinations of phosphatase alkaline enzyme of analysed blood serum samples were made by a spectrometric analysis using Bessey-Lowry method. In studying diseases, a significant variation in Ca, P, Mg and enzyme contents was observed. Those changes correlate with age, season of alimentation and type of disease.

A typical X-ray spectrum from a blood serum sample collected from a **DCS** cow is shown in figure 3.

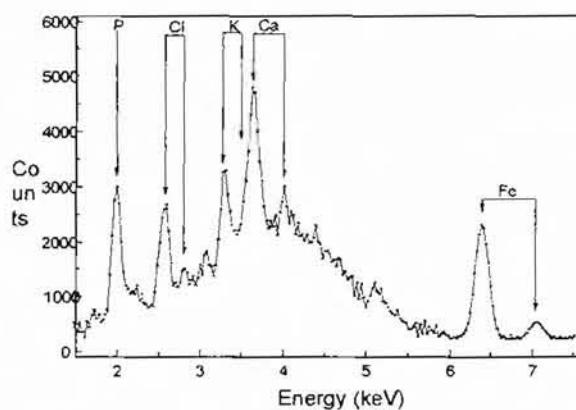


Figure 3. **PIXE** spectrum of blood serum sample of **DCS** cow

At the same time for trace element determinations, we use the **ICP** method. The reason for that choice is the impossibility of measuring the content of Mg with **PIXE** because of the absorption of the X-rays in the windows of the chamber and the detector. On the other hand, we cannot use only the **ICP** because for that type of measurements the quantity of blood serum needed is proportional to the number of the analyzing elements. We prefer to use both methods because **PIXE** requires only a "drop" of sample in order to determine all trace elements with atomic number between 13 and 80.

Phosphatase alkaline enzyme (Pa) is implicated in bone growth process and its activity determines the balance between the

content on Ca and P in blood (for a normal organism, the ratio Ca/P is among 1 and 2, for rachitic organisms is greater than 3, and for osteopourotic ones is less than 1). Magnesium is an activator of the enzyme. To study the metabolic changes produced by phosphatase alkaline enzyme, we have collected blood serum from some cows with interest in medical reasons and to make determinations of P, Ca and Mg contents using the **PIXE** and **ICP** methods.

The reference values for contents of Ca, P, Mg and phosphatase alkaline enzyme are represented in table 5. Concrete dates obtained from healthy and **DCS** cows at the beginning and at the end of the winter of 1998-1999 years are presented in tables 6, 7 and 8.

Table 5. Reference values for contents of Ca, P, Mg and Pa in blood serum of cows

	Ca (mg/dl)	P (mg/dl)	Mg (mg/dl)	Phosphatase alkaline (I.U./l)
Reference value	8.0-11.0	5.0-7.2	2.1-2.8	10.0-36.0

Table 6. Contents on Ca, P, Mg and Pa of blood serum samples collected during december 1998 from healthy cattle (cows with number 3,5,7,8,9,10 are on the first two weeks of lactation and 1,2,4,6 are on the last two weeks of pregnancy)

Cattle number	Ca mg/dl	P mg/dl	Mg mg/dl	P a. I.U./l
1.	9.9	5.4	2.4	9.50
2.	11.8	6.6	2.5	8.82
3.	8.3	6.5	2.4	12.98
4.	12.2	6.0	2.8	12.74
5.	9.7	7.1	2.3	18.86
6.	9.9	6.3	2.4	16.66
7.	9.1	6.4	2.5	12.98
8.	9.2	8.1	2.7	12.25
9.	10.8	7.7	2.9	11.76
10.	9.3	8.1	3.1	10.04
average	10.0±9.4%	6.8± 10.9%	2.6±8.4%	12.66 ± 14.4%

Table 7. Contents on Ca, P, Mg and Pa of blood serum samples collected during march 1999 from healthy cattle (cows with number 2,4,5,7,8,9 are on the first two weeks of lactation and 1,3,6,10 are on the last two weeks of pregnancy)

Cattle number	Ca mg/dl	P mg/dl	Mg mg/dl	P a. I.U./l
1.	9.7	6.5	2.3	25.42
2.	8.2	5.9	3.1	15.19
3.	9.8	7.5	2.3	17.15
4.	9.1	6.6	2.5	19.55
5.	9.2	7.0	2.3	11.27
6.	10.8	5.5	2.6	13.23
7.	10.1	7.0	3.2	12.00
8.	9.3	6.5	2.9	18.57
9.	9.5	7.0	2.7	14.55
10.	11.6	8.1	3.5	19.75
average	9.7±7.0%	6.7 ±8.2%	2.7±10.0%	16.66±17.0%

Table 8. Contents on Ca, P, Mg and Pa of blood serum samples collected during december 1998 - march 1999 from DCS cattle (cows with number 2,5,6,7,9,10 are on the first two weeks of lactation after parturition and 1,3,4,8,11,12 are on the last two weeks of pregnancy)

Cattle number	Ca mg/dl	P mg/dl	Mg mg/dl	P a. I.U./l
1.	7.0	3.9	2.0	63.01
2.	7.5	3.5	2.2	88.12
3.	7.0	3.7	2.0	65.91
4.	7.1	4.4	2.3	64.05
5.	6.9	4.6	3.5	45.50
6.	5.7	3.8	2.4	57.50
7.	9.7	5.5	2.3	40.43
8.	6.8	3.9	2.3	67.51
9.	6.0	4.5	2.3	56.01
10.	6.5	4.6	2.5	45.03
11.	8.2	5.3	2.6	57.44
12.	7.5	5.2	2.0	41.07
Average	7.2±9.9%	4.4±12.0%	2.4±10.8%	57.63±17.5%

As we can see from the results presented before, the mineral and enzymatic parameters in the serum have values in the normal limits for the healthy cows even during the winter, when the mineral content of drying food (hay) is very poor. On the other hand, we can observe important decreases under the normal limits of the amount of Ca, P and Mg in the blood serum of DCS cows. It is easy to see the tendency of the DCS animals to have hypocalcemia and hypophosphatemia. Those perturbations can be the causes of the installations of the ill cows in the lypostatic and decubital attitudes. The enzymatic level is an extremely sensitive parameter in DCS and

can serve as a diagnostic parameter. As the effect of decreases of Ca, P and Mg amount in the blood serum of DCS cows, we observe an increase of the amount of some enzymes like CPK, TGO and Pa. That secondary effect is a very grave phenomenon from the clinical point of view because simultaneous increase of the level of all specified enzymes is in most cases irremediable.

The results obtained in this research work are a preliminary step in order to see the primary causes of the DCS. Those causes can be extremely various and their correct determination is the basic plan of the therapeutically act.

B. ENVIRONMENTAL INVESTIGATIONS

B1. FOUNTAIN WATER

We have analyzed samples collected from underground waters (potable or non-potable) for establish if they are good for consumption. The target samples was prepared by evaporation of 2 l of water; The

obtained dust was mixed with a known amount of Yttrium (internal standard) and depicted on 3 μ m mylar support.

Using a 3MeV proton beam we obtain characteristic X rays spectrums.

We have identify 8 elements: S, Cl, K, Ca, Fe, Zn, Br and Sr and their concentrations are shown in the table bellow:

Table 9. The elemental concentrations of analyzed underground waters

Element	Sample (mg/l)					Ceiling admittance	
	Ruda-Moreni fountain	Salcami-Moreni fountain	Viforata 1 fountain	Viforata 2 fountain	Paltinu-Moreni fountain	Germany	U.S.A.
S	42.5					80	83.5
Cl	51.3		45.3	9.3		250	250
K	8.6	7.0			0.08	12	
Ca	138	140	280	265	3.05	400	
Fe		0.21		1.1	1.4	0.02	0.3
Zn		1.38		0.12			5
Br	0.51		0.08				
Sr	3.29		1.8	0.05			8

Comparing with the ceiling admittance in Germany (S. Eberle, IAEA-Viena 1995) and U.S.A. (Public Law 93-523) we can observe that in two samples (Viforata 2 fountain and Paltinu-Moreni fountain) the concentration of Fe exceeds the maximul admittance levels.

B2. AEROSOLS SAMPLES.

We have analyzed aerosols deposits on filters from ten Romanian towns: Pitesti, Giurgiu, Resita, Ramnicu-Valcea, Baia-

Mare, Craiova, Timisoara, Calarasi, Braila and Arad with different kinds and levels of industrial development by PIXE method.

Sample targets to be annalyzed were collected by the Institute of Hydrology and Waters of Bucharest and prepared in the following manner: aerosol particles were collected on cellulose fiber filter. The flow rate was 15 to 20 liters per minute. Air volume was measured with calibrated gasimeters with a precision of about 5%. We

use PIXE in internal standard variant. We use Yttrium like an internal standard because it is a very rare element in the environment items. The intense peaks of Yttrium in the X-ray spectrum could obscure the peaks of some elements possible existing in the samples: L and K lines of Yttrium overlap SK_{α} and (Rb and Sr) K lines respectively. Therefore we have analyzed targets without Yttrium too and we have not observed any new elements.

A sample of Yttrium on filter was measured too. Weak impurities of Ca, Fe and Zn were found. Concentrations of elements present in the aerosol samples were corrected for these impurities of the filter.

We have identified 15 elements: S, K, Ca, Cr, Mn, Fe, Co, Ni, Cu, Zn, As, Hg and Pb. The measured elemental concentrations are given with respect to the concentration of the Ca for all analyzed samples in the following table 10:

Table 10. The elemental concentrations with respect to the concentration of the Ca for all analyzed samples

City/ Element	Pitesti	Giurgiu	Resita	Rm. Valcea	Baia Mare	Craiova	Timi soara	Calarasi	Braila	Arad
S	0.112						0.02		0.012	0.047
K	0.57	0.272	0.122		0.052	2.51	0.2	0.26	0.174	0.36
Ca	1	1	1	1	1	1	1	1	1	1
Ti	0.14	0.05	0.019	0.063		0.505	0.15	0.66	0.017	0.04
V	0.018			0.012						
Cr	0.002	0.007	0.003	0.007		0.035		0.012	0.006	0.001
Mn	0.027	0.014	0.021	0.017	0.006	0.05	0.007	0.078	0.024	0.017
Fe	1.09	0.49	0.532	0.647	0.075	5.38	0.52	4.32	0.28	0.58
Co						0.015				
Ni	0.009			0.006						
Cu	0.004		0.001	0.021	0.089		0.001	0.008	0.002	0.003
Zn	0.012		0.019	0.023	0.033	0.036	0.002	0.015	0.004	0.011
As				0.004	0.004	0.005				0.001
Hg							0.001		0.003	0.001
Pb				0.006	0.03	0.043		0.005	0.002	0.0003

For the ratio concentrations shown before we could make a comparison between the analyzed filters from all the towns considered here, from the point of view of the pollutant elements: the town Craiova is put in evidence by its high ratios of concentrations Ti/Ca, Cr/Ca, Fe/Ca, Co/Ca, Zn/Ca, As/Ca, Pb/Ca. Calarasi has the highest ratio of Mn/Ca and the filter from Braila is put in evidence by the Hg/Ca. Certainly the level of pollution of a region can not be determined by a single filter and is need of a good statistic to draw conclusions.

B3. ANTARCTIC SAMPLES

Antarctica is supported to suffer minimally from anthropogenic pollution. The recent interest in Antarctica atmosphere, due to the "Antarctic ozone Hole" had resulted in recognition of the need for long term background environmental characterization studies.

In this work we have analyzed samples of ice from different depths of a glacier from Antarctic zone. The samples have been collected during a Bulgarian Antarctic Expedition. We have applied Proton Induced X-Ray (PIXE) and Neutron Activation Analysis (NAA) methods in order

to determine polluting elements. The samples of 200 ml of molten ice have been passed through Nucleopore filters.

For PIXE analysis the samples together blank Nucleopore filters have been irradiated by a 3 MeV proton beam supplied by the FN-tandem accelerator from INPE-Bucharest. The beam current varied between 5-10 nA, to mention a count rate below 300 counts/s. X-rays have been detected by means of a Si(Li) detector with a 160 eV resolution at 6.4 KeV, and an associated electronic equipment. The X-ray spectra have been fitted off-line and after the subtraction of the contribution given by the blank filter, the concentration data have been obtained for 15 elements: Si, P, S, Cl, K, Ca, Cr, Mn, Fe, Ni, Cu, Zn, As, Sr and Pb. The results of the analysis of Antarctic ice samples by PIXE method are shown in the table . The precision of the PIXE analysis was less then 5% for Ca, Cr, Mn, Fe, Ni, Cu and Zn, less then 8% for K, As, Sr and Pb and less then 13% for Si, P, S and Cl.

Some filters with the samples of ice and the blank filter have been irradiated with thermal neutrons at the rabbit system of the Nuclear Reactor from INPE, Bucharest, at a flux of 2×10^{12} neutrons/cm².sec, a period of

time of 1 min, for the determination of short-lived isotopes. The counting system for the measurement of induced radioactivity in the samples consisted of a Ge(Li) detector with appropriate amplification equipment, and a personal computer. The energetic resolution was 2.3 KeV at 1.33 MeV. NAA method, used for short irradiation permitted the determination of some elements which could not be observed by PIXE method: Na, Al, V and In.

REFERENCES

1. S.A.E. Johansson, J.L. Campbell, PIXE: *A Novel Technique for Elemental Analysis*, Wiley, 1988
2. O. M. Radostils, D.C. Blood, C.C. Gay: *Veterinary medicine*, Bailliere Tindall, Eighth edition, London, 1994
3. S. Ghergariu: *The basis of medical pathology of animals*, All Pub, 1995
4. D. Mihai: *Nutrition and metabolic diseases of animals*, Ceres Pub, 1996
5. H. Barza: *The synoptic presentation of downer cow syndrome*, Rev. Roum. Of Veterinary Med., vol.4 (1), 68-69.
6. R. Walter: *Chaire de nutrition et alimentation*, E.N.V., Lyon Cedex, 1975
7. D. Mihai: *The differential clinical diagnosis on internal diseases of animals*, Ceres Pub, 1990
8. W.E. Glasseggen, J.W. Metzger, S. Heuer, *Phytochemistry*, Vol. **33**, No.6, pp 1525-1527, 1993;

The concentration of Al ranges between 9.96-43.0 mg/g, of V: 0.13-0.266 mg/g and for In: 0-0.075 mg/g. More elements will be determined by longer periods of irradiation in further measurements, which will be then make possible the interpretation the results and the analysis of the evolution of the pollution as a function of the depths of the ice layer in the glacier, in the Antarctic zone.

X AND GAMMA RAY n^+pp^+ SILICON DETECTORS WITH HIGH RADIATION RESISTENCE

GHEORGHE - VALERICA CIMPOCA,

Physics Department, Science Faculty, "VALAHIA" University of Targoviste

ABSTRACT: *The paper describes some results concerning technology and behaviour of X-and gamma-ray n^+pp^+ silicon detectors used in physics research, industrial and medical radiography and non-destructive testing. These detectors work at the room-temperature and can be used individually to detect X-and soft gamma-rays, or coupled with scintillators for higher incoming energies. Electrical characteristics of these photodiodes, their modification after exposure to radiation and results of spectroscopic X-and gamma-ray measurements are discussed. Devices manufactured under this technology proved to be stable after an exposure in high intensity gamma field with the dose range of 10 Krad-5 Mrad. Nuclear radiation resistance was studied by irradiation with ^{60}Co gamma source (1.17 and 1.33 MeV) at dose rates of 59 Krad/hour and 570 Krad/hour. Results indicate that proposed structures enable the development of reliable silicon detectors to be used in a high gamma-radiation environments encountered in a lot of applications.*

Keywords: Silicon detectors, X-ray, Gamma-ray, Radiation resistance

INTRODUCTION

Silicon detectors are widely used in X-and gamma-ray spectroscopy for direct detection or coupled with scintillators in high energy nuclear physics (modern collider experiments are representative), medicine and industrial applications. In X and gamma dosimetry, a low detection limit (under 6 KeV) with silicon detectors becomes available. Work at the room temperature is now possible due to the silicon processing evolution, which assures low reverse current and high life time of carriers.

For several years, modern semiconductor detectors have been the primary choice for the measurement of nuclear radiation in various scientific fields¹. Nowadays the recently developed high resolution silicon detectors found their way in medical applications². As a consequence many efforts have been devoted to the development of high sensitivity and radiation hardened X-and gamma-ray detectors for the energy range of 5 - 100 KeV. Most authors have studied the silicon detectors made on N-type

material because it is easy to process it by planar technology.

We have investigated the use of p-type silicon as the starting material for X- and gamma-ray detectors because of several potential benefits it would bring. High purity, p-type silicon grown by the float-zone process exhibits better radical dopant uniformity than n-type float-zone silicon. Also it is readily available and quite inexpensive. In addition, p-type float-zone silicon is free of radiation damage caused by the neutron transmutation doping process. Recently, position-sensitive silicon drift detectors were designed and manufactured on p-type substrates³ and efforts are in progress to get avalanche photodiodes (APD), which are on high resistivity p-type materials, too⁴.

However, p-type silicon in combination with a passivating layer of SiO_2 , lead to a more complex detector layout since the positive charge in the oxide causes an inversion in the surface layer. These features set stringent requirements for the technology in the construction of p-silicon detectors. In high-purity silicon, the electron density can be large enough to invert the surface region of p-type silicon under the silicon dioxide. Consequently, it would be expected that silicon n+p diodes would have higher leakage current than p+n. All these have

been demonstrated experimentally.⁵ Also p-type silicon is more resistant to the radiation damage since acceptor-like centres are mainly created through the exposure, the result being only the necessity of a higher bias voltage to fully deplete the volume and not the conversion of the bulk material. Thus the importance of the p-material radiation resistance investigation was constantly signalled in the last decade⁶.

The paper presents two new geometries and an improved technology on p-type high resistivity material to obtain low noise radiation detectors. Test structures were characterised before and after gamma exposures with cumulative doses between 10^4 to 10^7 rad (^{60}Co). Results indicate that proposed structures and their technology enable the development of reliable n^+pp^+ silicon detectors to be used to measure X- and gamma-ray radiations.

For some specimens (0.8 mm^2 - 12 mm^2), extremely low reverse currents were obtained and that, combined with low noise preamplifiers made possible the detection of low energy X- and gamma-rays at the room temperature. Detectors with thin dead layer demonstrate excellent energy resolution for X-rays close to a value of 2 KeV (for 13.9 KeV line of ^{241}Am).

DETECTOR LAYOUT AND TECHNOLOGY

The present work investigates the possibility to manufacture n^+pp^+ silicon detectors by conventional planar technology. Detectors are made of p-type silicon with (111) orientation, resistivity between 6 000 Ωcm and 20 000 Ωcm , thickness between 260 μm and 360 μm .

Both layouts proposed are shown in Fig. 1, 2. These structures were designed first time as PIN detectors for visible and near infrared light, especially to detect YAG:Nd laser (1064 nm). Electrical parameters needed as nuclear radiation detectors are quite the same: low reverse current at total depletion, low capacitance and noise and high responsivity.

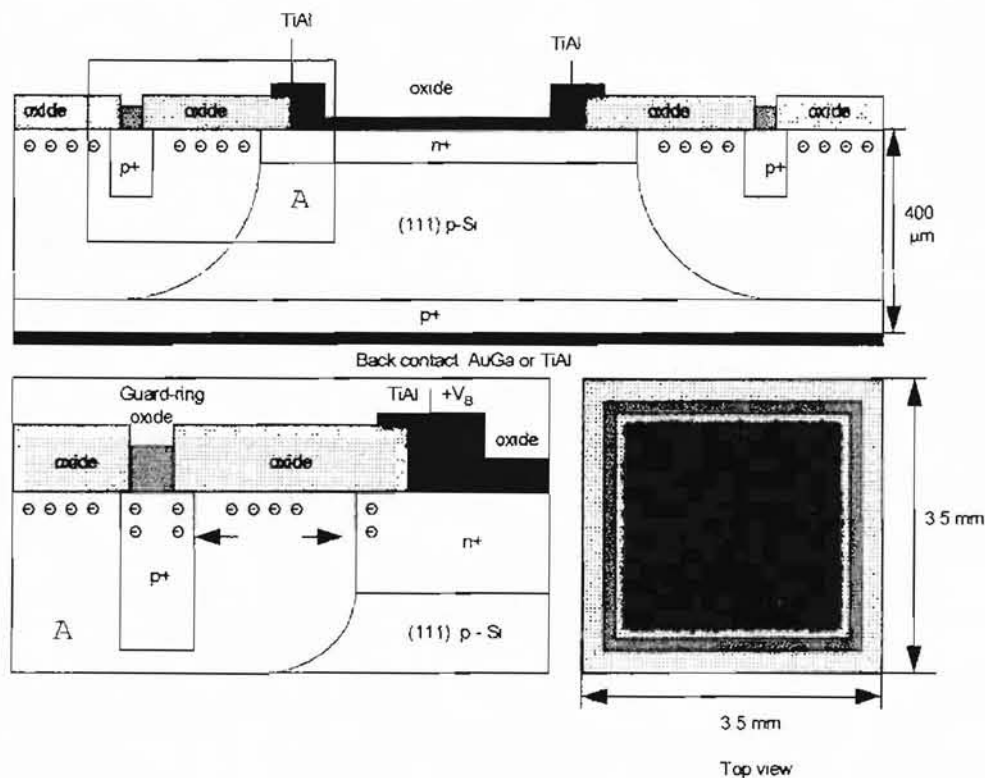


Fig. 1 n^+pp^+ silicon detectors with p^+ guardring

Parameters obtained (especially reverse current) allowed us to select a fraction of the manufactured batch to be tested as radiation detectors for X-and gamma-rays.

The 3 inch diameter wafers were first oxidised at 950 $^{\circ}\text{C}$ in dry oxygen with

Devices consisted of a square (Fig. 1) or round (Fig. 2) geometry n^+pp^+ diodes with guardring: the first with p^+ guard and the second with a n^- guard sticked to the n^+ contact

2-3 % TCE (trichlorethylene) in order to obtain a high quality initial oxide on the

silicon surface. The oxidation step was followed by an in-situ high temperature N_2 annealing (950 °C) to reduce the interface charges. The thickness of the oxide layer was 700 Å.

A 0,7 μm layer of SiO_2 was next deposited on the wafers in an LPCVD hot wall reactor using TEOS as the source. The thermal treatment was performed at 850 °C in N_2 . P-type high resistivity silicon wafers with these oxides present very good stability at interface Si/SiO_2 . The additional p^+ stop ring (Fig.1) and n^- stop

ring (Fig.2.) are used for the termination of the inverse layer at the surface of the silicon, and also it decreases the surface component of the reverse current. The p^+ ring is formed by boron diffusion at 975 °C (from BN wafers) together with p^+ back contact. The n^- ring is formed by glass deposition doped with phosphorus. After the first photolithography, boron was diffused simultaneously in the guard ring and in the p^+ back contact.

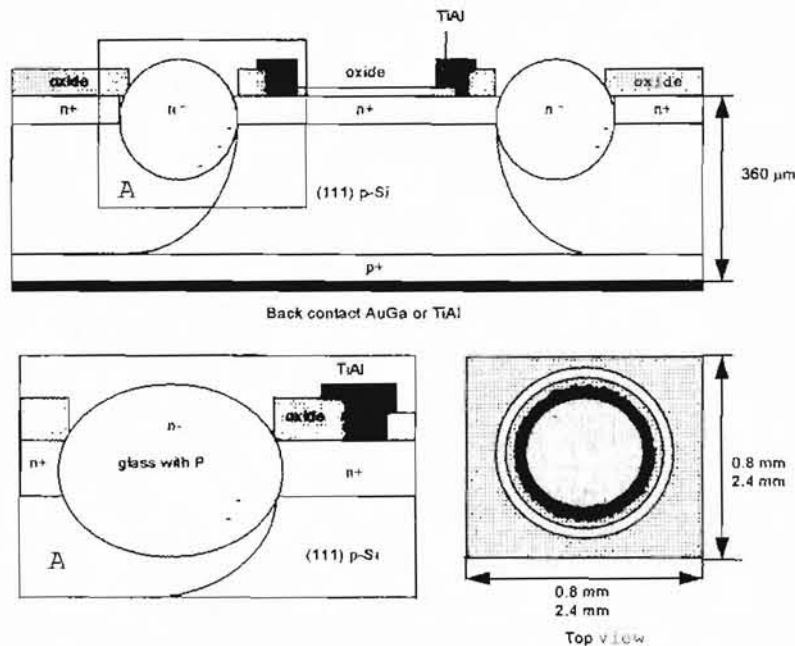


Fig.2. N^+PP^+ silicon detectors with n^- guardring

A second phosphorous implantation was made on the front side of silicon wafers with an energy of 20 KeV and a

dose of 10^{16} cm^{-2} . Implanted impurities were activated at 700 °C in N_2 . A 0,3 μm layer of SiO_2 was next deposited on the

wafers in an LPCVD using TEOS as the source. The final thermal treatment was performed at 850 °C in N₂, followed by a very slow cooling to 600 °C for gettering the unwanted impurities from the silicon active zones. Contact windows were opened on the surface by standard photolithography. An TiAl layer (1000 Å Ti and 10 000 Å Al) was deposited on the wafer surface and a TiAl (or AuGa) layer was deposited on the back side of the wafer.

After electrical characterisation selected detector test structures were mounted on TO-18 and TO-5 cases as to illuminate the chip through the n⁺ electrode polarised at a negative potential with respect to the p⁺ one. A transparent epoxidic resin layer was molded on the case. Photodiodes obtained by the described process have a sensitivity higher than 0.65 A/W at 900 nm and 0.45 A/W at 1060 nm for 90% of the batch. Main characteristics of manufactured structures are shown in the Table 1.

Table 1

Type	P resistivity	Guardring	Area	Id*	C _D *
n ⁺ pp ⁺ square	6 000 Ωcm	p ⁺	12 mm ²	< 2 nA	< 10 pF
n ⁺ pp ⁺ round	15 000 Ωcm	n ⁻	3.14 mm ²	< 2 nA	< 5 pF
n ⁺ pp ⁺ round	20 000 Ωcm	n ⁻	0.8 mm ²	< 1 nA	< 1.5 pF

* Id and C_D at total depletion

EXPERIMENTAL MEASUREMENTS.

RESULTS

In order to test silicon diodes behaviour after the irradiation with gamma rays, the entire diode batch was exposed to a ⁶⁰Co source at a quasiconstant

temperature of 15 °C, using facilities existent at the Institute of Nuclear Physics and Engineering in Bucharest. The exposure range was of 10 krad ÷ 5 Mrad with dose rates of 59 krad/h or 570 krad/h and diode parameters measurements were

performed after cumulative doses of 10, 20, 50, 100, 500 krad, 1 M and 5 Mrad. The following parameters were monitored: leakage current, junction capacitance and X and gamma rays spectral response. The diode leakage current vs. reverse voltage was measured using a Keithley model 419 picoammeter and the corresponding curves are shown in the Fig.3, 4 with the

cumulative dose as parameter. It is shown, after 1Mrad the leakage current begin to gradually increase for n^+pp^+ structures with p^+ guardring. For n^- guardring the current degradation starts earlier than 500 krad. The main reason of this alteration with the exposure dose is considered to be interface states and oxide traps generation in intense gamma field.

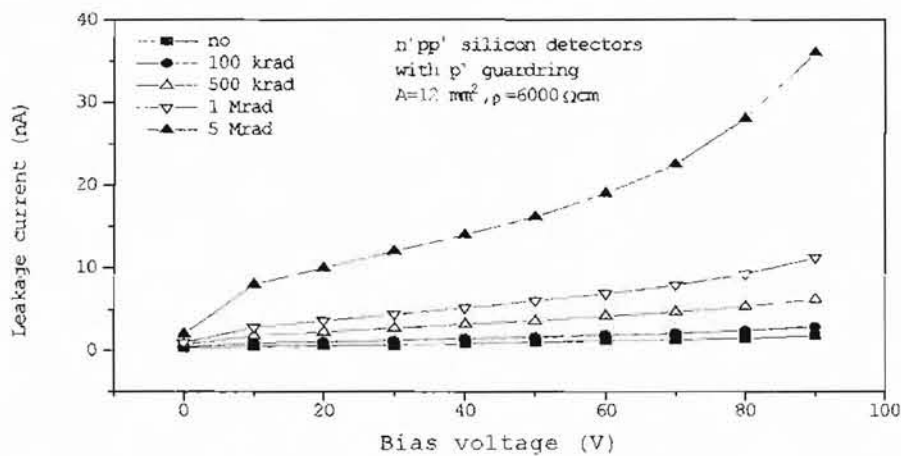


Fig.3. The reverse current vs. reverse voltage for the n^+pp^+ structure (p^+ guardring) with the gamma dose as parameter

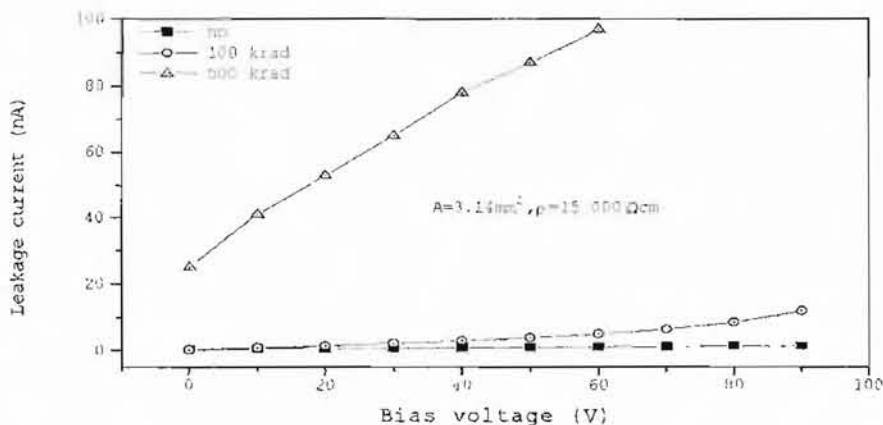


Fig.4. The reverse current vs. reverse voltage for the n^+pp^+ structure (n^- guardring) with the gamma dose as parameter

The junction capacitance vs. reverse voltage was measured using a C-V plotter at the frequency of 1 MHz and the curves family is shown in the Fig 5.

Concerning the junction capacitance, no spectacular modifications were observed. For spectral response test in the X-ray range, the Rb K_{α} line (13,39 keV) was recorded and for a more complex spectrum with X and soft gamma rays a spectroscopic ^{241}Am source was

used. Spectra were recorded using a charge sensitive preamplifier with a 7 mV/100 keV intercept (silicon), an Ortec 572 spectroscopy amplifier, a variable voltage power supply for diode biasing and a PC-based multichannel analyser. The noise contribution of the entire measurement chain in the line width was of 2,2 keV full-width at half medium (equivalent silicon), with an unirradiated diode mounted in front of it.

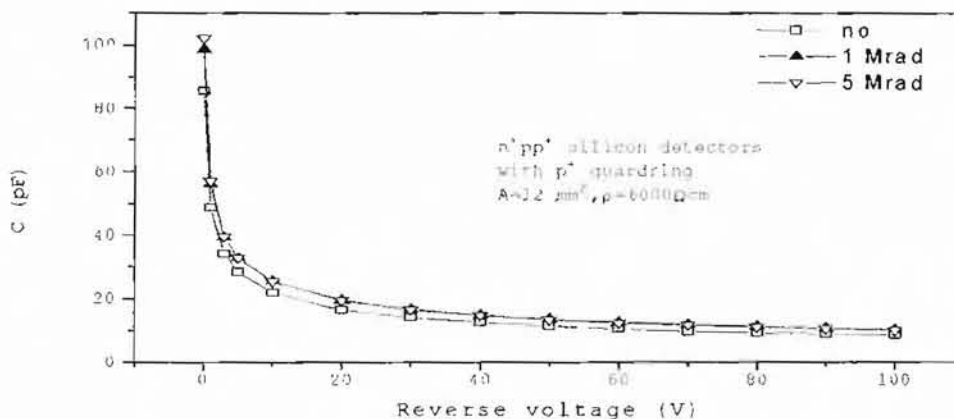


Fig.5 Junction capacitance vs.reverse voltage for the n^+pp^+ structure with the gamma dose as parameter

Fig.6 shows ^{241}Am spectra obtained with a representative diode in the batch measured with the diode unirradiated and after cumulative exposures of 0.1, 0.5, 1 and 5 Mrad. Clearly two effects are visible: the 59.5 keV gamma photopeak decreases in intensity with the dose, widens and moves toward low energies and the second is the broadening of the

spectrum in the X-ray region and its low energy tail, present even at the unirradiated diode, is accentuated as the dose increases.

For both diode families the spectrum shape evolution with the dose was the same, excepting the fact for n^+pp^+ silicon detectors with n^- guardring the degradation appeared at lower doses, so

that after 100 krad the noise and the line shape begin to produce irrelevant spectra.

In order to separate noise contribution and gamma-ray-induced secondary effects (characteristic lines excitation in the metallic case or silver glue used to fix the chip on the base could be one of them), from charge collection degradation as a result of the high dose exposure, two other kind of measurements

were done: one was to record the noise spectrum and to subtract it from the energy spectrum and the other, to get the energy spectrum of only a gamma-ray ^{241}Am source (^{241}Am encapsulated in a steel case). Both of them showed no significant contribution in our energy range of interest (10÷60 keV) excepting, for the gamma source, the increase of the low energy tail given by poorly collected events.

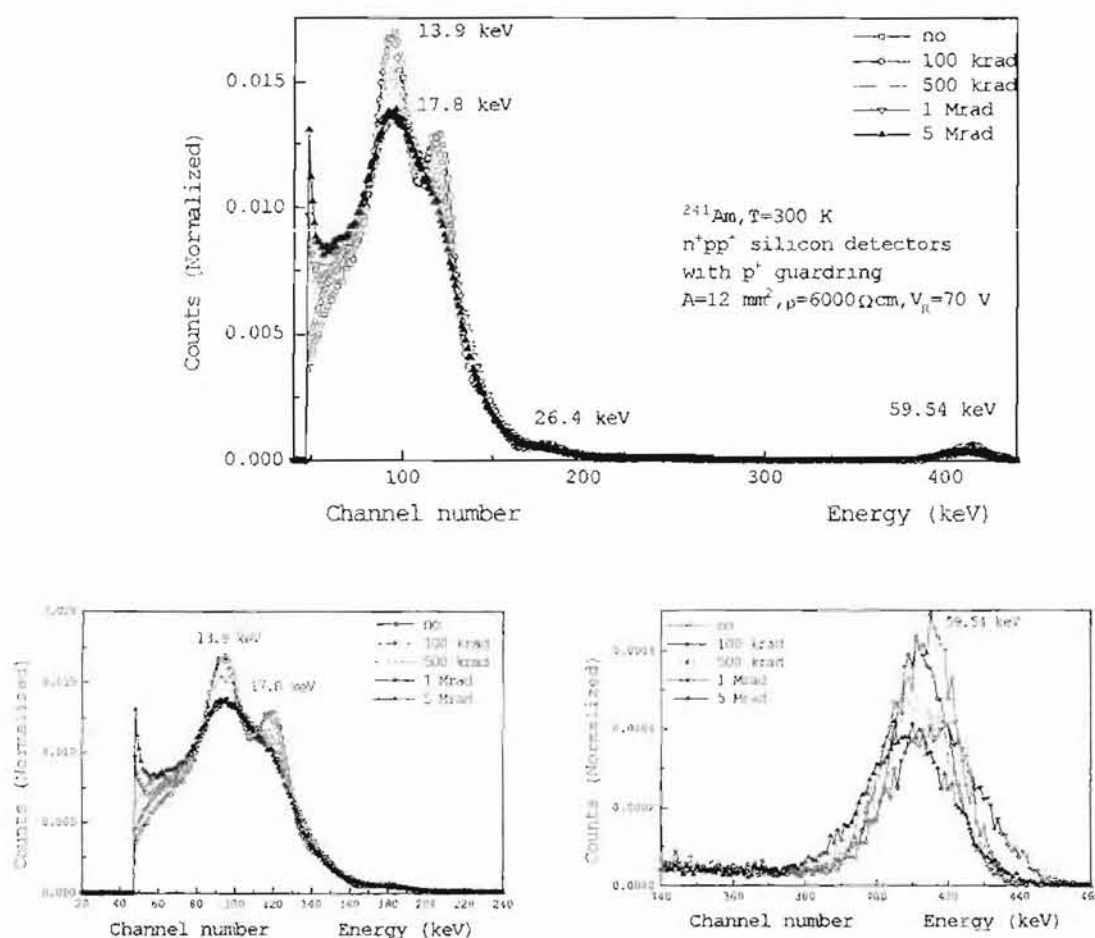


Fig.6 ^{241}Am spectra for 6 000 Ωcm n^+pp^+ detectors (p^+ guardring) after various doses.
b) X-ray region, c) gamma ray region

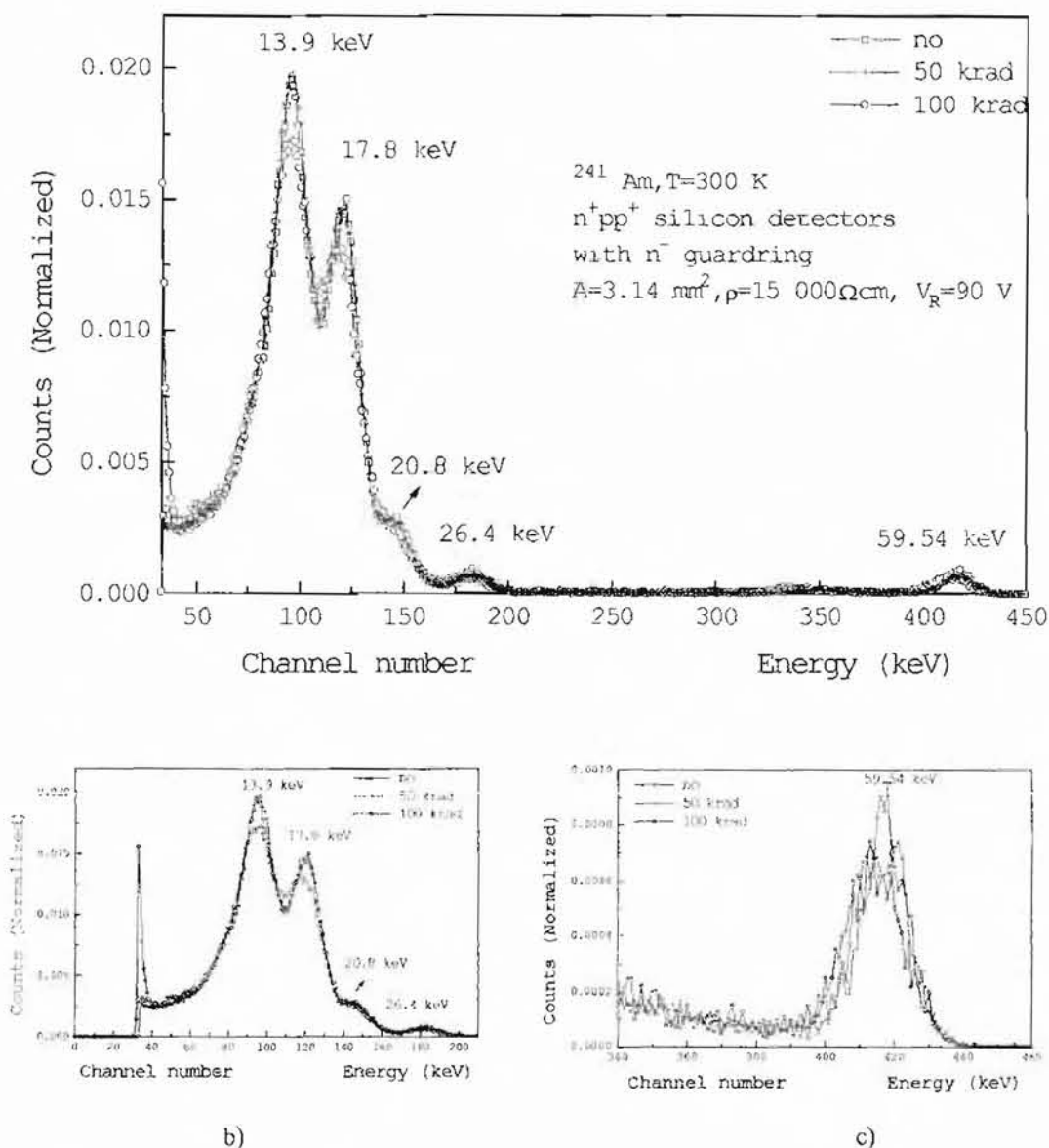


Fig.7 ^{241}Am spectra for $15\,000\,\Omega\text{cm}$ n^+pp^+ detectors (n^- guardring) after various doses.

b) X-ray region, c) gamma ray region

Fig.8 shows the evolution with the dose of a X-ray spectrum shape. For this measurement, diodes were polarised at a somewhat higher voltage (100 V) overdepleting the volume and the $K\alpha$ line

of Rb (13.39 keV) was recorded. Same kind of degradation is observed: loss of the efficiency, noise increase and poor charge collection.

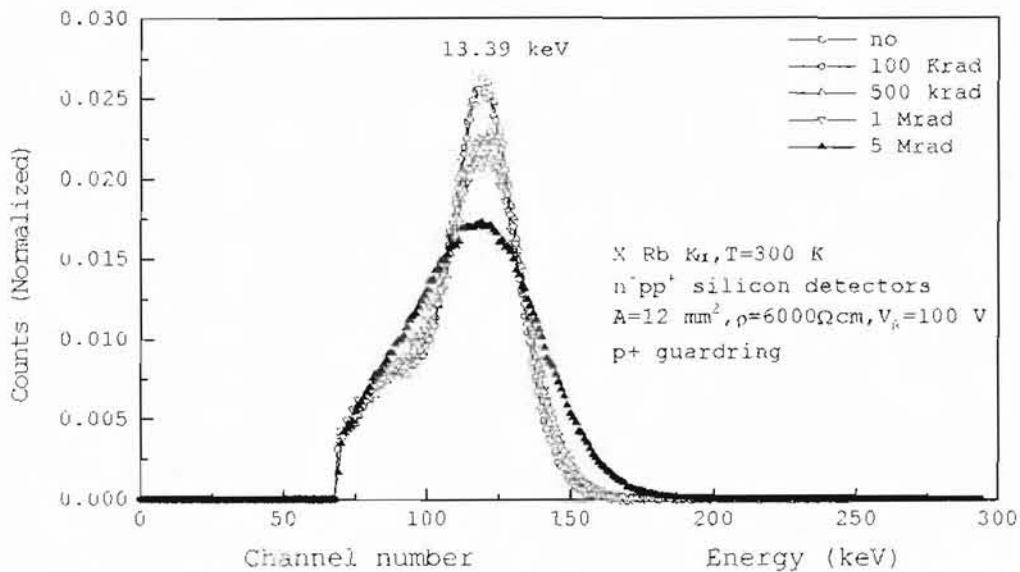


Fig.8 Rb- $K\alpha$ line (13.39 keV) recorded with n^+pp^+ (p^+ guardring) structure over depleted with gamma dose as parameter.

CONCLUSIONS

These structures and their technology does allow the manufacture of p-type silicon detectors with high radiation resistance. Tests performed indicate a good charge collection in Si-p material and an improved stability of collection efficiency with the exposure dose.

Even this technology offers devices with higher leakage current than n-material standard technology and thus more noisy and, for surface interactions, holes with a lower mobility are transported through the volume these drawbacks are compensated by the fact in radiation exposure acceptor-like centers are created⁶ which affect

mainly electrons but they, in this geometry, have shorter collection distance.

Low resistivity structures proved to have a better radiation behaviour. This could come from the p^+ -type guard ring which is also deeper than the junction and interrupts the inversion layer accentuated by the gamma exposure. Specific to the p^+ -type guard ring for Si-p in our geometry is the fact it avoid the MOS parasitic structure which would appear if a n^+ guard ring will be used, only one ring is needed to insure the breakdown protection and it does not ask for a separate supply voltage.

REFERENCES

1. H.Struder, H.Soltau, Radiation protection dosimetry, Vol.61, No.1-3, pp.39-46,1995.
2. A.Thomson, Handbook for Synchrotron Radiation, Plenum Press, N.Y., pp. 583, 1994
3. I.T.Walton, D. Krofcheck, R. O'Donnell, G. Odynice, M.D. Pantlar, N.W. Wang, Nuclear Instruments and Methods in Physics Research A377 (1996) 357-361).
4. R.Farrel, F. Olschner et al, Nuclear Instrument and Methods in Physics Research, A288 (1990), pp.137-139
5. Jack T. Walton, "Silicon Detectors: New Challenges" , Nuclear Instruments and Methods in Physics Research 226 pp 1-11, 1984
6. D.Sueva, V.Spassov et al., I.E.E.E. Transaction on Nuclear Science, Vol 40, No.3, 1993, pp. 257-261
7. F.Lemeilleur, M. Glaser et al., IEEE Transactions on Nuclear Science, vol. 41, No. 3, June 1994
8. A.Bischoff, N.Findeis, D.Hauff, P.Holl, J.Kemmer, P.Klein, P.Lechner, G.Lutz, R.H.Richter and L. Struder, Nuclear Instruments and Methods in Physics Research A326 (1993) pp.27-37
9. R.Hartmann, D.Houff, P.Lechner, R.Richter, L.Struder, J.Kemmer, S.Krisch, F.Scholze, G.Ulml, Nuclear Instruments and Methods in Physics Research, A377 (1996), pp.191-196.

RECENT APPROACHES IN THE LASER SURFACE TREATMENT OF MATERIALS

CĂLIN OROS*, ALEXANDRU MĂRIUȚAN*, SERGIU DINU*, NICOLETA OROS**

**Physics Department, "Valahia" University of Targoviste, 28 Unirii Blvd., 0200 Targoviste, Romania*

Tel.: +40.45.620611, Fax: +40.45.217683, E-mail: oros@valahia.ro

***"I.H. Rădulescu" High School, 26 Unirii Blvd., 0200 Târgoviște, Romania*

ABSTRACT: *The experimental dependence of surface hardness on Nd:YAG laser parameters (laser intensity, laser pulse duration, number of laser shots and laser spot diameter) for aluminum, titanium, nickel, copper and two kind of steel (21CrMoV57 and 40Cr130) targets is given. It is shown that the target surface hardness increases with laser intensity, with number of laser shots and laser pulse duration. Also, the target surface hardness decreases when the laser spot diameter increases. From these experiments result that the laser hardness is rather a function on laser surface energy density than laser energy.*

Subject terms: surface hardness, laser surface energy density

INTRODUCTION

In thermal processing with laser radiation energy deposition and heating in a material are a consequence of the balance between the deposited energy, governed by optical materials properties and characteristics of the laser radiation, and the heat diffusion, determined by thermophysical materials properties and the interaction time. For temperatures below melting temperature the light-induced changes of properties occur within the solidus-range. In surface treatment with a laser, the metallic surface is heated locally extremely rapidly

and after the laser is switched off it cools very rapidly. The temperature rises very rapidly to almost melting temperature. Only a thin layer is heated, the other parts of the target remain cold. Due to the high temperature gradients, thermal conduction to the bulk material will cause sufficiently rapid cooling of the heated parts and the resultant structures are often metastable structures with particular properties. Heating and cooling rates are of the same order $\sim 10^6$ K/s. The advantages and disadvantages of surface treatment with laser beams are thus apparent: precise local

treatment, non-equilibrium structures with specific proprieties, difficult procedure for covering large areas with each track influencing the structure of the previous one if the laser beam is moving on the target surface [1]. The laser is not a universal tool and should not be considered simply as a possible substitute for existing methods. It is very effective for treatment of thin surface layers. If thick layers are to be treated then other heat sources are more appropriate. Laser transformation hardening offers decided advantages in local or partial hardening of components or treatments of components which are too large for treatment other by flame hardening.

The hardness of the material is strongly related to its binding behaviour [2]. The metallic binding gives not the highest hardness values but allows a certain amount of plastic deformation. The highest hardness values are obtained for covalent bindings, like diamond. Heteropolar bindings are found for a number of ceramic materials which apart from their hardness show a good oxidation resistance. In reality, the binding behaviour is more complicated and mixed types of binding are possible.

The equation governing absorption of laser energy on the metallic target is given by:

$$I = I_0(1 - R)e^{-\sum_i \alpha_i z} \quad (1)$$

where I is the laser intensity of the absorbed laser beam and I_0 is the intensity of the incident laser beam. The fraction of the incident light intensity reflected by the target is given by R . The factor α_i represents the coefficient for the light absorption by the i^{th} process which summed over the different absorption processes occurring at the irradiated surface, and z is the penetration depth of the radiation in the material. In the case of laser hardfacing the laser intensity must be below the critical value for melting of material. For same lower laser intensity we account a single term in equation (1) which represent the classical absorption of the electromagnetic radiation by a metallic material.

The critical laser intensity required for melting the surface of the target can be theoretically estimate by the following relationship:

$$I_m = \frac{k_r T_m}{2(1 - R)\sqrt{\chi_r \tau_p}} \quad (2)$$

where T_m and k_T are the melting temperature and the thermal conductivity of the material, respectively.

It is known that in the case of laser interaction with the metallic targets the depth of the damage or the interaction corresponds closely to the depth of thermal penetration l_{th} given by the following relationship:

$$l_{th} = \frac{1}{2} \sqrt{\pi \chi_T \tau_p} \quad (3)$$

where χ_T is the thermal diffusivity of the metal and τ_p is the laser pulse duration.

LASER AND TARGETS LASER

Experiments have been performed with the neodymium-YAG laser of our laboratory operating at 1.064- μm wavelength. The laser delivers Gaussian pulses of 2 ms, 2.5 ms and 3 ms full width at half-maximum (FWHM) with a repetition rate till 20 Hz. The laser output energy can be ranging between 0 and 15 J. The laser spot diameter can also be modified from 0.3 mm to 8 mm. In instance the maximum laser intensity is about $1.06 \times 10^7 \text{ W/cm}^2$.

For the hardness experiments we have used lower laser intensities. All experiments were performed in air at normal conditions.

TARGETS

For experiments we have used metallic targets of aluminum, titanium, nickel, copper and two kinds of steel: 21CrMoV57 and 40C130, with 1.5-mm thick and 10-mm diameter. Their surfaces were polished using a P 1000 grade polishing paper. In order to improve the laser absorption the surface of the targets was painted with a very thin black paint. The measurements of the target surface hardness were performed with a microhardness device.

EXPERIMENTAL RESULTS

First we have calculated the critical laser intensity for melting the target surface using equation 2. The results for our target materials are given in table 1. Then we have measured the experimental values for critical laser intensity obtained when we use our laser. In order to compare these values the results are given in same table.

Table 1. Calculated and measured values of critical laser intensity.

Targets	Al	21CrMoV57	40C130	Ti	Cu	Ni
I_{cr} (W/cm^2)	4.2×10^3	1.7×10^4	1.5×10^4	9.5×10^3	1.1×10^4	6.5×10^3
	7.6×10^3	6.9×10^3	6.5×10^3	7.5×10^3	7.9×10^3	7.5×10^3

The calculated depth of thermal penetration, equation 3, is given in table 2

for three values of laser pulse duration.

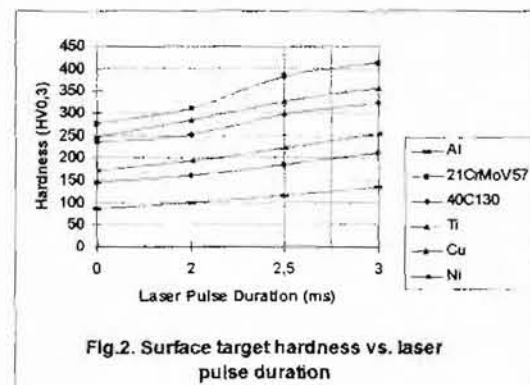
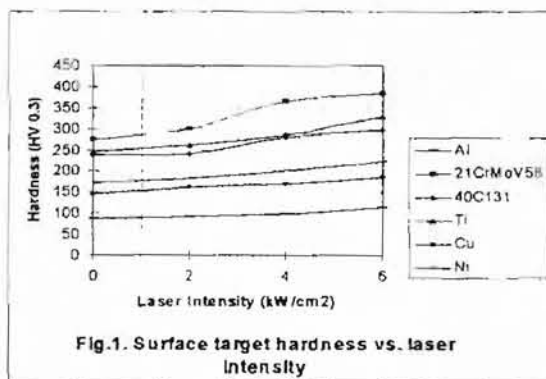
Table 2. Calculated values of thermal penetration depth for three laser pulse durations

Targets		Al	21CrMoV57	40C130	Ti	Cu	Ni
l_{th} (μm)	$\tau_p=1$ ms	261.6	97.1	104.8	68.6	296.5	118.9
	$\tau_p=2$ ms	369.9	137.3	148.2	97.0	380.4	168.2
	$\tau_p=3$ ms	453.1	168.2	181.5	118.8	513.5	205.9

We have performed a first experiment in order to obtain the dependence of surface target material hardness on laser intensity. The results are given in figure 1. The laser irradiation parameters were: pulse duration 2.5 ms, the laser spot diameter 5 mm, and the number of laser shots 600.

In other experiment we have

analyzed the dependence of surface target material hardness on laser pulse duration. The results are given in figure 2. The laser energy for each target material was close below the critical value for melting given by table 1. The laser spot diameter was 5 mm and the number of laser shots was 600 as in previous experiment.

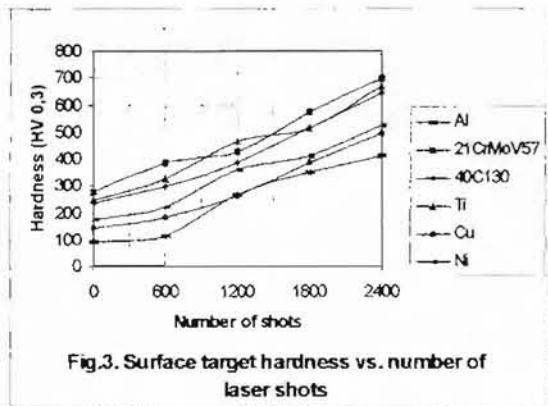


The dependence of surface target material hardness vs. number of laser shots is given in figure 3. The laser energy for

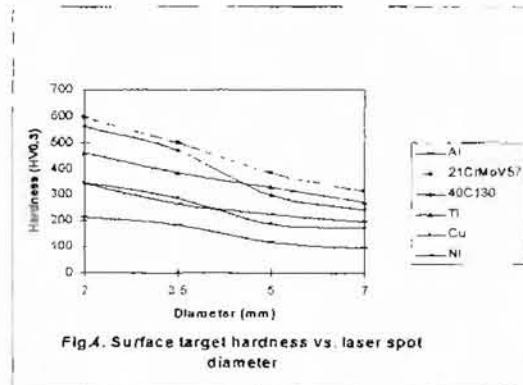
each target material and the laser spot diameter were same as in previous experiment. In our last experiment we have

analyzed the dependence of surface target material hardness vs. laser spot diameter.

The laser pulse duration was 2.5 ms,



the laser energy for each target material was same as in previous experiment and the number of laser shots was 600. The results are given in figure 4.



CONCLUSIONS

We have measured the metallic target surface hardness before and after laser irradiation below melting temperature in order to study the hardness dependence on Nd:YAG laser parameters: laser intensity, laser pulse duration, number of laser shots

and laser spot diameter. From our experiments result that the laser surface hardness increases with laser intensity, laser pulse duration, number of laser shots and decreases when laser spot diameter increases.

REFERENCES

1. A. Gasser, E. W. Kreutz, K. Wissenbach, "Physical Aspects of Surface Processing with Laser Radiation", *SPIE*, 1020, 70-83 (1989)
2. H.W. Bergmann, R. Kupfer, D. Muller, "Laser hardfacing", *SPIE*, 1276, 375-390 (1990)

PIXE (PARTICLE INDUCED X RAYS EMISSION) AND ICP (INDUCTIVE COUPLED PLASMA) MEASUREMENTS OF *BASELLA* *ALBA L* LEAVES

CLAUDIA STIHI*, GABRIELA BUSUIOC**, ION V. POPESCU*, GABRIEL DIMA*

**Applied Physics Department, Science Faculty, University "Valahia" of Targoviste*

***Agromontology Department, Environmental Engineering and Biotechnology Faculty,
University "Valahia" of Targoviste*

INTRODUCTION

In this paper we present the quantitative methods PIXE (Particle induced X-ray emission) and ICP (Inductively Coupled Plasma) applicable to *Basella* plants, together with the results obtained from the elemental analysis of leaves from different *Basella* plants cultivated in Variety Testing Centre and in Green Houses of Targoviste. Using PIXE method we identified and we determined the amount of the following elements: P, Ca, K, Fe, Mn, Zn with an instrumental error less than 6%. Using ICP method we determined the amount of elements: Mg and Fe with an instrumental error less than 10%.

EXPERIMENTAL METHODS

Particle Induced X-ray Emission (PIXE) method is based on the fact that the bombardment of the sample with a charged

particle beam causes the ionization of the atomic inner shells followed by a subsequent of the characteristic X-rays. When the X rays spectrum is detected by high resolution detector, the well-known Z-dependence of the X rays energies, as well as the intensities of the individual X rays line, allow a straight forward determination of the target element. The detection limit of this method is very good because: i) intense fluxes of exciting radiation are available, ii) the X rays production yields for particles with energies in the MeV range are large and iii) the background associated with the exciting radiation is rather low. The sample preparation technique does not require a special chemical preparation which may cause some losses in concentration or some contamination. Measurements of target elements were made using a 3.2 MeV proton beam

extracted from the TANDEM accelerator from IFIN-HH Magurele, Bucharest, and passes through a collimator (3×4 mm) before reaching the target. X-ray spectra were measured with a spectrometric chain having a CANBERRA Ge hyperpure detector (100 mm²×7mm) with a 160 eV resolution at 6.4 KeV of K_α line of iron.

Samples in the PIXE experiment, was young *Basella Alba L* leaves plant grown in different conditions at Variety

Testing Centre (VTC) of Targoviste, Romania. Six groups of *Basella Alba L* were measured as shown in table 1. The leaves of the plants were collected of approximately in some position in two successively months. The washing leaves were simply air-dried at a temperature of 105⁰ C in a clean box preventing further contamination. The dried leaves were grained and after powdering a layer of the samples material were deposited on hostaphan foils.

Table.1 The samples groups of *Basella Alba L* measured by PIXE and ICP method

Sample	Growth fertiliser conditions
B1(VTC)-July	Soil without fertiliser
B2(VTC) –July	Natural fertiliser (excrements)
B3(VTC) –July	NPK fertiliser
B4(VTC)-August	Soil without fertiliser
B5(VTC) –August	Natural fertiliser (excrements)
B6(VTC) -August	NPK fertiliser

At the same time for trace element determinations, we use the ICP (Inductively Coupled Plasma) method. The reason for that choice is the impossibility of measuring the content of Mg with PIXE because of the absorption of the X-rays in the windows of the chamber and the detector. On the other hand, we cannot use only the ICP because for that type of

measurements the quantity of biological sample needed is proportional to the number of the analyzing elements. We prefer to use both methods because PIXE requires only a "drop" of sample in order to determine all trace elements with atomic number between 13 and 80.

ICP-OES is a destructive technique that provides only elemental composition.

The ICP method has been applied to a wide range of sample types: metals and wide variety of industrial materials, environmental samples (water streams, airborne particles and coal fly ash), and biological and medical samples.

We used ICP method to determine the concentration of Mg – element who can not be determined using PIXE method and concentration of Fe to compared

experimental results obtained using the both methods.

The ICP-OES (Inductively Coupled Plasma-Optical Emission Spectroscopy) spectrometer used by us is a Baird ICP2070 -Sequential Plasma Spectrometer which consists of a sample introduction system, a plasma torch, a plasma power supply and an optical measurement system (figure1).

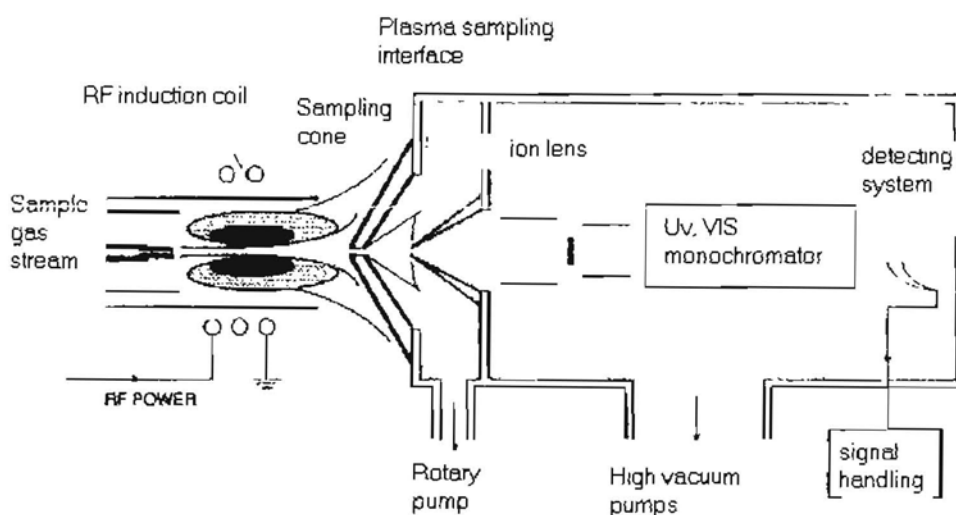


Figure 1: Instrumentation for Inductively Coupled Plasma-Optical Emission Spectrometry

The sample must be introduced into plasma in a form that can be effectively vaporized and atomized (small droplets of solution, small particles of vapours). The plasma torch confines the plasma to a diameter of about 18 mm. Atoms and ions produced in the plasma are excited and emit light. The intensity of light emitted at wavelengths characteristic of the particular

elements of interest is measured and related to the concentration of each element from samples. Baird ICP2070 - Sequential Plasma Spectrometer use as a plasma gas Argon and the plasma is sustained in a quartz torch and the plasma is generated using a radiofrequency generator at 40.68 MHz. Temperatures of 5000-9000K have been measured in the

plasma. The detection systems used are a sequential monochromator with a wavelengths range (160-800) nm. The optical emission spectra are made using a personal computer.

Samples in the ICP experiment, was young *Basella Alba L* leaves plant grown in different conditions at Variety Testing Centre (VTC) of Targoviste, Romania. Six groups of *Basella Alba L* were measured as shown in table 1. The leaves of the plants were collected of approximately in some position in two successively months. The washing leaves were simply air-dried at a temperature of 105⁰ C in a clean box preventing further contamination. The dried leaves were grained and after powdering, 2.00g powder

leaves have been digested in 40 ml acid nitric. After a set aside in fume cupboard overnight the obtained liquid was gently boiled (without major loss of volume). For a good digestion 3 ml acid perchloric have been added and 2-3 ml water after cooling. The cooled solution was diluted with water at 250 ml solution and nebulised into plasma.

EXPERIMENTAL RESULTS AND DISCUSSION

Using PIXE method we identified and we determined the amount of the following elements: P, S, Cl, K, Ca, Mn, Fe, Cu, Zn, Sr. In table 2 are presented the results of PIXE analysis on *Basella Alba* leaves samples with an instrumental error less than 6%.

Table 2. The microelemental concentrations (in ppm) measured by PIXE normalized to the concentration obtained for a control group

Element	B1(VTC)- July	B2(VTC)- July	B3(VTC) -July	B4(VTC)- August	B5(VTC)- August	B6(VTC)- August
P	0.38	0.35	0.72	0.30	0.33	0.75
S	0.40	0.71	0.13	0.65	0.66	0.18
Cl	1.75	2.26	0.36	0.43	3.81	0.20
K	56.22	56.69	126.96	48.21	49.22	106.77
Ca	43.22	37.90	38.93	46.61	49.83	103.77
Mn	0.05	0.18	0.012	0.06	0.23	0.02
Fe	2.28	1.25	0.64	2.33	1.53	0.15
Cu	0.03	0.03	-	0.1	0.08	-
Zn	0.08	0.08	0.07	0.06	0.04	0.03
Sr	0.64	0.44	0.92	0.62	0.42	0.87

Experimental results obtained by

ICP and PIXE methods are presented in table 3.

Table 3: Mg and Fe concentration obtained by ICP method and PIXE method

Element	B1(VTC) -July	B2(VTC) -July	B3(VTC) -July	B4(VTC)- August	B5(VTC) -August	B6(VTC) -August
Mg	22.65	18.33	16.14	21.00	20.72	18.75
Fe (ICP)	2.53	1.33	0.75	2.87	1.87	0.45
Fe (PIXE)	2.28	1.25	0.64	2.33	1.53	0.15

The results obtained by ICP for iron concentration are in good concordance with the results for iron concentration

obtained by PIXE method (presented in table 3), so the both method PIXE and ICP are complementary methods for elemental analysis (figure2).

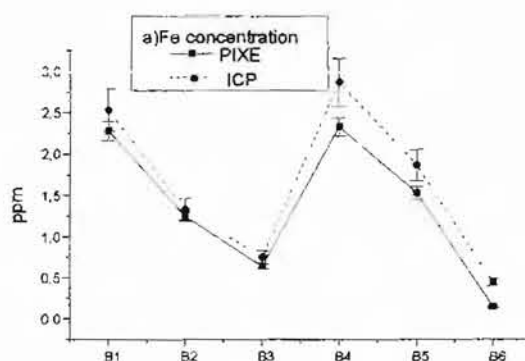


Figure 2: Fe concentration in Basella Alba L leaves obtained by PIXE and ICP methods

REFERENCES

1. S.A.E. Johansson, J.L. Campbell, PIXE: *A Novel Technique for Elemental Analysis*, Wiley, 1988
2. W.E. Glassegen, J.W. Metzger, S. Heuer, *Phytochemistry*, Vol. 33, No.6, pp 1525-1527, 1993;
3. C. Stihl, I.V. Popescu, G. Busuioc, T. Badica, A. Olariu, G. Dima, Particle induced X-ray emission (PIXE) analysis of *Basella Alba L* leaves, *Journal of radioanalytical and Nuclear Chemistry*, Vol 246, No. 2(2000), 445-447;
4. C. Stihl, I.V. Popescu, G. Busuioc, G. Dima, T. Badica, A. Olariu, Microelemental analysis of *Basella alba L* plants by using PIXE, *Balkan Physics Letters*, BPL, 8(2), pp. 84-88 (2000)

BLOOD SERUM ENZYMES ANALYSIS BY PIXE METHOD

GABRIEL DIMA*, LAUR MANEA**, CLAUDIA STIHI*, ION V. POPESCU*, VICTORIA DIMA***

**Valahia State University of Targoviste, Regele Carol I Street, no.2, 0200 Targoviste, Romania*

***Agromontanology Department, Environmental Engineering and Biotechnology Faculty,
University "Valahia" of Targoviste*

****"I.L.Caragiale" College, Moreni*

ABSTRACT. *The phosphatase alkaline enzyme is responsible of the bone formation and growth (Ca/P ratio). Microelemental analysis of blood serum samples is made by PIXE (Particle Induced X-Rays Emission) method in internal standard variant and the measurements are made on normal, rachitic, paretic and osteoporotic animals (cattle's) in order to making correlation's with phosphatase alkaline enzyme activity. We used PIXE method in internal standard variant for systematically errors elimination's. As an internal standard element for spectrum's normalisation we used Yttrium. The samples introduced into the reaction chamber are bombarded with 3.2 MeV proton beam. The characteristics X-rays spectra were detected by a Ge hyperpure detector with the energy resolution of 160 eV at the $K\alpha$ 6.4 keV X-ray iron line are recorded using an acquisition computer. Using the calibration curve and the LEONE software were making determinations on Ca, P, Fe and Mg content of analysed samples. We find a dependency between Ca/P ratio and Mg content of blood serum samples.*

INTRODUCTION

Phosphatase alkaline enzyme is implicated in bone growth process. In order to study their activity we have collected blood serum of some cattle's, interesting from medical reasons and

make determinations of P, Ca and Mg content using the PIXE method. For a normal organism, the ratio Ca/P is among 1 and 2, for rachitic organisms is grater then 3 and for osteoporotic ones is less then 1. The Mg is an activator of the enzyme.

SAMPLES PREPARATIONS

Blood serum samples are collected from jugular zone of cattle's selected by following criteria:

-the season of food alimentation (winter/summer), great milk productions,

advanced pregnancy steady (last weeks); the weight of cattle's.

After the serum separation (24-36 hours), the target samples were doped with standard solution (1:1) of Yttrium for spectrum normalisation and deposited on

mylar foils who are attached on aluminium supports in order to introduce them in irradiation chamber (a multitarget irradiation chamber). We have prepared 10 samples. The cattle's having the experience number 4,5,6,7,8,9 are cattle's in the first days after born of the young's cattle's. The cattle's having the experience number 2,3,10 are cattle's in the last week of pregnancy.

THE EXPERIMENTAL SET-UP

Measurements of mineral substances were made using a 3.2 MeV protons beam extracted from the TANDEM accelerator from IFIN-HH Magurele, Bucharest. X-ray's spectra were measured with a spectrometric chain, with a CANBERRA Ge hyperpure detector with a 160 eV resolution at 6.4 KeV of XK_{α} line of iron. Amplification, generation and analysis of electric signals were achieved by an adequate electronic device: a sensitive preamplifier with field effect cooled at the liquid nitrogen temperature, a linear amplifier and a multichannel analyser with 4096 channels having an acquisition computer for data output - PDP11. For each sample target were recorded the characteristic X-ray spectra. The X-ray spectrum's analyses were made

off-line using a computer fitting programme - **LEONE**. The calibrations of experimental set-up were made using standard targets witch are prepared by evaporating pure elements (Ni, Cu, Ge, Ag, Sn, Au, Pb) on mylar foil.

The determinations of phosphatase alkaline enzyme is analysed blood serum samples were made by spectrometric analysis using Bessey-Lowry method (the enzyme is a cathabolit for chemical reaction: $R-O-PO_3H_2 + H_2O \rightarrow ROH + H_3PO_4$).

RESULTS AND CONCLUSIONS

A typical X-ray spectrum of blood serum samples is shown in figure 1.

The contents of Ca, P, Mg, alkaline enzyme of analysed samples and the normal values are shown in table 1. Analysing our data, we can see a good level of Ca. The samples number 1 is from a young cattle having a dismorexy's syndrome. We can see a great level of enzyme content. The sample number 10 have a great level of Ca and P than the normal one, and the result shows that in a young organism there are compensatory mechanisms for balancing the loses of Ca by a great milk production. The content of Mg in the same sample is grater than the normal value, because Mg is an activator of phosphatase alkaline enzyme.

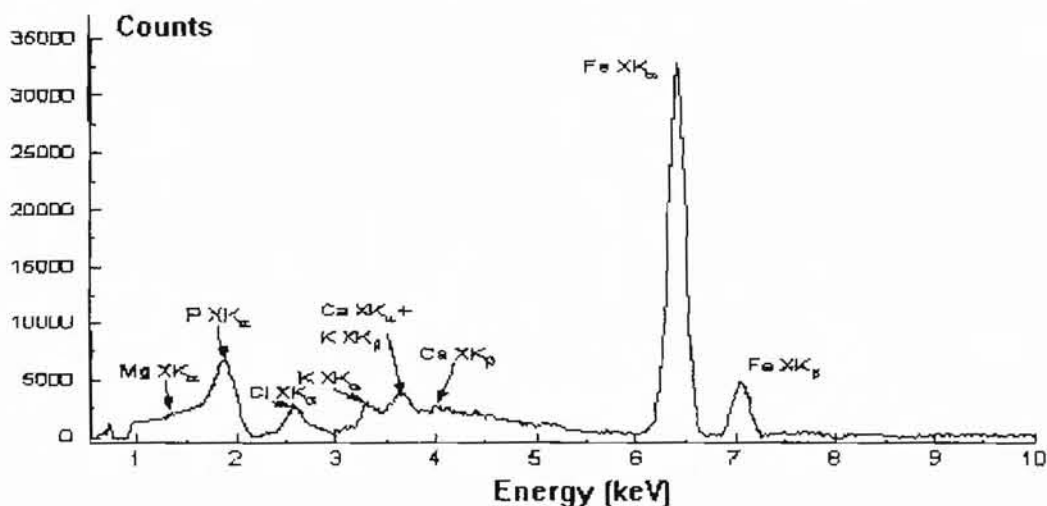


Figure 1

Table 1

Sample	Ca (mg/dl)	P (mg/dl)	Mg (mg/dl)	Phosphatase alkaline (I.U./l)
1	9.7	6.5	2.3	40.42
2	12.2	5.9	3.1	15.19
3	9.8	7.5	2.3	17.15
4	9.1	6.6	2.5	9.55
5	9.2	7.0	2.3	11.27
6	10.8	5.5	2.6	13.23
7	10.1	7.0	2.7	9.55
8	9.3	6.5	2.9	8.57
9	9.5	7.0	2.7	9.55
10	12.3	8.1	3.5	29.75
Reference value	8-11	5-7.2	2.1-2.8	10-36

REFERENCES

1. S.A.E. Johansson, J.L. Campbell, K.G. Malmqvist, Particle Induced X-Ray Emission Spectrometry (PIXE), Vol.133, John Wiley & Sons Inc., 1995
2. M. Aspiazu, R. Policroniades, R. Vivero, M. Jimenez, Nucl. Instr. And Meth. in Phys. Res., B101(1995), 453-458
3. Z. Szokefalvi-Nagy, I. Demeter, C. Bagyinka, K. Kovacs, Nucl. Instr. And Meth. in Phys. Res., B22(1987)156-158
4. Z. Szokefalvi-Nagy, I. Demeter, C. Bagyinka, K. Kovacs, Nucl. Instr. And Meth. in Phys. Res., B75(1993)160-165

NONLINEAR OPTICAL PHENOMENA

SERGIU DINU

Valahia State University of Târgoviște, Regele Carol I Street, no. 2, 0200, Târgoviște, Romania

Until lasers were invented people used to believe that the optical properties of a medium depend only on the frequency of the radiation which goes through it and not on its intensity, because, when it came to classical light sources, the intensity of the electric field of the wave was not higher than 10^5 V/m, while the intensity of the electric field inside the atom is 10^9 V/m (for semi-conductors) and 10^{11} V/m (for the insulators).

The discovery of lasers led to getting intensities of $I \sim 10^{27}$ W/m² and, knowing that

$$\left. \begin{aligned} I &= \frac{E^2}{Z} \\ \text{cu } Z &= 380\Omega \end{aligned} \right\} \Rightarrow E \approx 10^{14} \text{ V/m}, \quad \text{which}$$

maybe compared to the intensities of the inter-tomic fields.

It is obvious that, in this case, the properties of the medium depend on the intensity of the radiation as well. A new science has developed - nonlinear optics - which describes phenomena that can be

observed on a macroscopic scale based on the influence that the medium has on the optic radiation which goes through it and, on the corrections which appear with it.

Thus, the main phenomena emphasized by the nonlinear optics are:

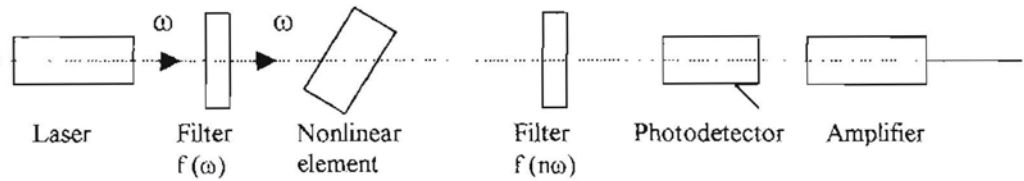
1. OPTICAL REDRESSATION

This means creating an electric field inside the medium where the laser radiation spreads. The intensity of this field is proportional to the intensity of the light wave field.

2. GENERATING OPTICAL HARMONICS

This means creating inside the medium some light waves of 2ω , 3ω , ..., $n\omega$ pulsations, starting from a laser wave of ω pulsations which interacts with the medium.

The experimental scheme of an assembly used to obtain optical harmonics is:



When referring to these harmonics we can add:

-the strength of an harmonic is related to the variance of the medium indices.

-we get an increase of the strength density while getting through the medium.

-the strength of the order n the harmonic alternates with the fundamental strength as in $I_{n\omega} = (I_{\omega})^n$ for slight enough entrance radiation.

3. PARAMETRICAL GENERATION OF LIGHT

We can get this when we spend a fraction of the energz of a ω_1 pulsation light eave to generate 2 new light waves of ω_2 and $\omega_1 - \omega_2$ pulsation (ω_2 is ajustable in the field $[0, \omega]$)

Thus, talking the nonlinear polarisation

$$P_{NL} = \alpha E^2$$

and nepposing the 2 fields have the same direction, meaning

$$E = E^{\omega_1} \cos \omega_1 t + E^{\omega_2} \cos \omega_2 t \quad \text{we get}$$

$$P^{\omega_1 + \omega_2} \cos(\omega_2 + \omega_1)t \text{ and}$$

$$P^{\omega_2 - \omega_1} \cos(\omega_2 - \omega_1)t \quad \text{where}$$

$$P^{\omega_2 + \omega_1} = P^{\omega_2 - \omega_1} = \alpha E^{\omega_2} E^{\omega_1}.$$

This, the interaction of the pulsation waves ω_2 and ω_1 inside a nonlinear medium leads to creating new pulsation waves $\omega_2 + \omega_1$ and $\omega_2 - \omega_1$ which is a parametrical generation of light.

4. LIGHT SELFIFOCUS

This means that light focuses inside a fine filament if its intensity gets over a certain point and it is created by the variation of a light wave field, as in:

$$n = \left[\epsilon_0 (1 + \chi_e) \right]^{1/2} + \frac{3}{2} \frac{\pi \theta}{\left[\epsilon_0 (1 + \chi_e) \right]^{1/2}} E_{\omega}^2$$

5. STIMULATED DIFFUSION OF LIGHT

We should mention: - Raman diffusion

- Brillouinn diffusion

- Rayleigh diffusion

6. DARHENING THE MEDIUM

This means that a medium which is optically transparent under a low intensity radiation (classical source) becomes

opaque under an high intensity radiation (laser)

7.LIGHTING UP THE MEDIUM

When this the case, the medium, which was initially opaque under a low intensity radiation becomes transparent (it lights up) under a high intensity radiation.

8.THE SATIETY EFFECT

This means a slowing-down of the increas in the saturation of the radiation and its stabilization at certain value while the processed of stimulated emission overcome the absorbation ones.

9.THE DISAPPEARANCE OF THE RED LIMIT OF THE PHOTOELECTRIC EFFECT

This shows when the intensity of the laser light wave is high enough to prove that the external photoelectric effect appears for frequencies which are much lower than its standard frequency - ω_0 .

All the above mentioned phenomena (and much more) are found in many applications in optics, electro-optics, creating new materials whit special properties.

THE NANOPHYSICS PROCESING OF ATOMIC UNITS

OANA CATALINA BUTE

Physics Department, Science Faculty, Valahia University of Targoviste

INTRODUCTION

In order to observe the atomic dimension, Scanning Probe Microscope (SPM), Scanning Tunnelling Microscope (STM), represent today the main current, as well as, an essential device for the nanotechnology. Scanning Tunnelling Microscope can process atom by atom, and, at the same time, it can measure the immediately result after processing.

1.1. A method that was advanced from the conception of STM is

“The evaporation in electric field of particular atoms”.

The schematic diagram of the evaporation in electric field is shown in figure No. 1.1. The system consists of an electrode with sharp top made of wolfram which is controlled by a three-dimensional positioning unity. This unity is based on a piezoelectric system with a subnanometric resolution, high accuracy and a source of permanent current about few volts.

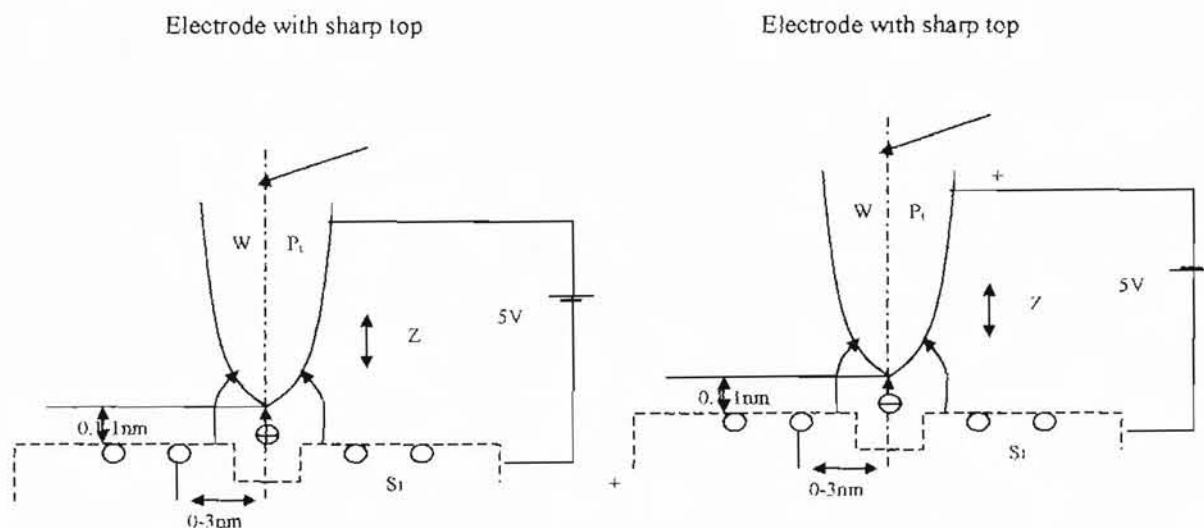


Figure 1.1.

Models for the evaporation in electric field:

- a) a electrode with sharp top controlled by a positioning piezoelectric device with a subnanometric resolution.
- b) P_t shows the drive force due to concentrated electric field at the sharp border. The piece to be processed, made of a conductor material is placed to a distance by 01.nm or similar to it under an electrode. The intensity of electric field is by $5 \times 10^{10} \text{ V m}^{-1}$ in the workspace what creates a drive force or an extraction force over an ionized atom from the surface by $8 \times 10^{-8} \text{ N}$. On the other hand the bound force aver an atom placed in the knot of the crystalline net is estimated to be by $5 \times 10^{-8} \text{ N}$ for Si, so we can wait for an atom placed on the surface can be removed by an electric field like this.

Another strong instrument in the science of surfaces, which bases on the STM is Scanning Probe Microscope (SPM). SPM supplies précis and high resolute topography of the molecular structure at an atomic scale, in the real space, using the probe's heads placed very near by the surface.

Further on are presented the SPM systems. With this new type of microscope is possible the exceeding of resolution limit of optic microscopes and electronic microscopes.

1.2. In the figure 1.2. are shown the components of a typical SPM. In this case, a physics magnitude- like the tunneling current, the magnetic force, the atomic force- is measured by the probe top, the XYZ scanner and the regulator of command.

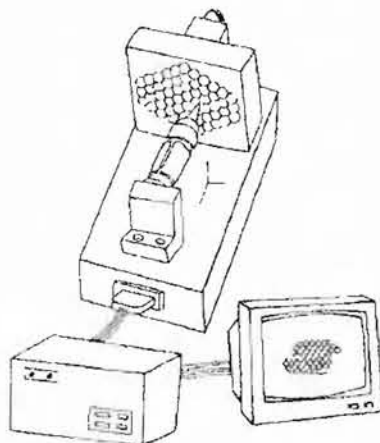


Fig. 1.2. SPM system

THE ATOMIC MANIPULATION

Eigler and Schweizer from IBM described how independent atoms can be positioning and how can be built the models with STM. In this order they were capably to cool specimens at 4 K and to keep clean their surfaces whole days. So, when the xenon atoms are introduced towards a clean nickel surface, in vacuum, they remain on the surface in a physics adsorption state. Eigler and Schweizer have cleaned their surface perfectly by a spraying process of argon atoms, a hardening process for the carbon moving off from the surface and fast hardening and they reduced the

contamination of specimen surface by absorption of residual gases until a level in which was impossible the detection of another contamination for a long time.

The adsorbed xenon atoms on nickel (110) with a superficial potential about some electron volts are very stable and unreactive when they are cooled at 4 K. So when to probe tip is placed above of a xenon atom and is approached to this, the individual xenon atom and the probe tip are easily attracted one to the other because of the interaction van der Waals force (see the figure 1.2.1.)

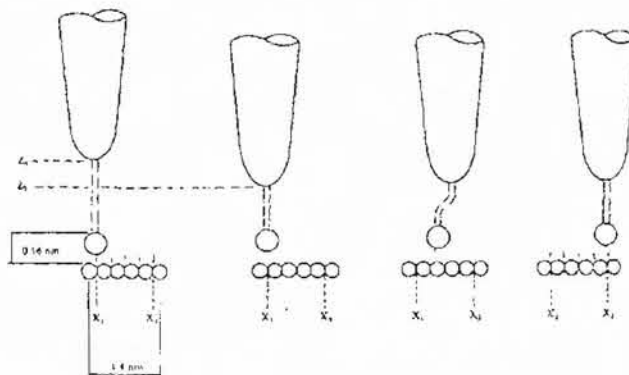


Figure 1.2.1. The translation of xenon atom from X1 to X2 using a probe STM

In the time of STM tunneling, if the tunneling current is increased while the polarization voltage is maintained constantly, the tip moves nearer to the specimen.

So in order to increase the van der Waals interactions between the tip and the specimen, the current is increased beyond the used level for the simple surface visualizing.

The top specimen current with tunneling through the electronic barrier is fixed at ~ 1 nA when we must visual the topographic surfaces, at Z1 high of the top. This operation is shown in the 1.2.1. figure. In the first stage, Eigler and his colleagues increased the current of a value about 10-60 nm. So, in the figure 1.2.1. is shown that the probe top is taken down to the atom and is positioned at Z2 high; the xenon atom is adsorbed at the border of the probe top, easily. Then, the top with the xenon atom is removed from X1 to X2, along the surface,

with a speed by 0.4 nm s^{-1} . The point X2 represents the new position where the atom is put down. In this position the probe top is taken back at X1 by the decrease of tunneling current at the reference voltage used for the visualing. An individual xenon atom is placed in every unitary cell which contains 6×5 Ni atoms which occupy an area about $1.4 \times 1.5 \text{ nm}$. For now haven't been possible the amplasation of xenon atoms nearer than that presented above.

Next figure (1.2.2.) shows an example of writing with xenon atoms.

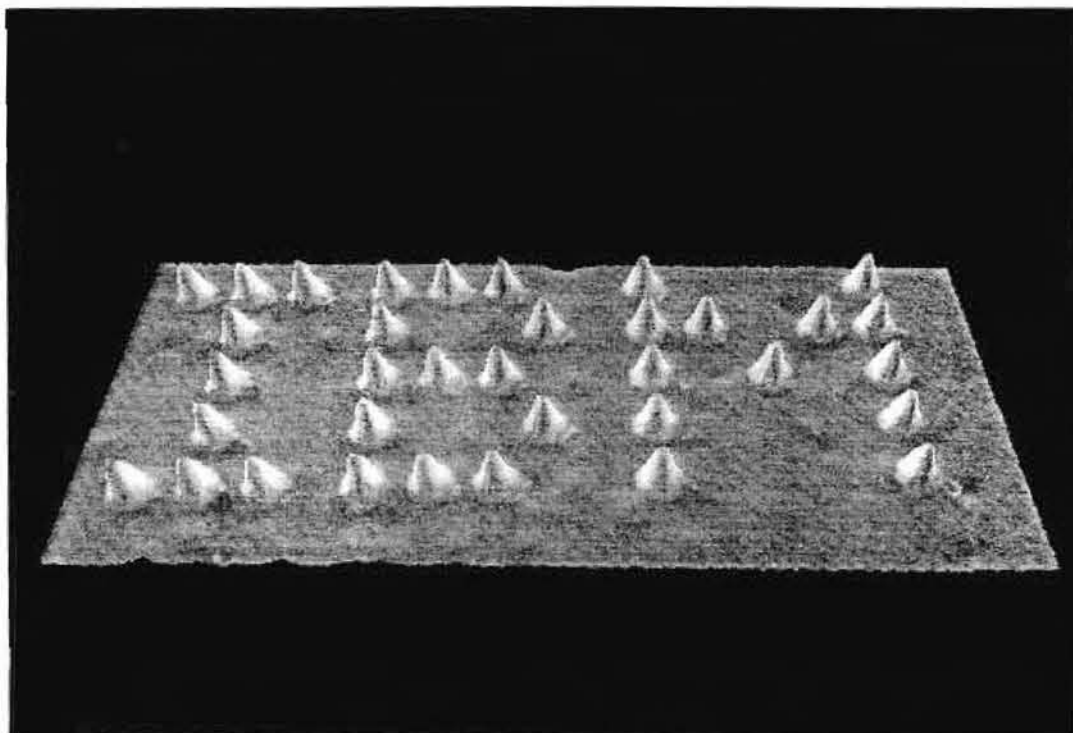


Figure 1.2.2.

THE ATOMIC COMMUTATION.

The figure 1.2.3. shows the probe top and the xenon atom are placed on a terrace of nickel (110) surface, with the distance between the probe top and terrace is about 0.38nm, and the polarization voltage applied

is by -0.02 V. The xenon atom remains in an ell made of the steps a nickel surface. This atom is stable when is in contact with three nickel surfaces, so it has a small probability to be removed to another position from the nickel surface. (1.2.2.)

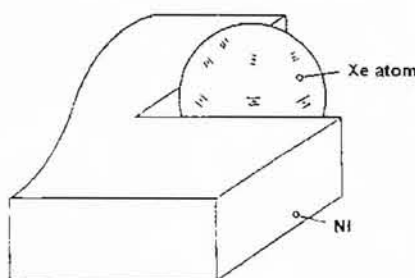


Fig. 1.2.3. The ell position. The xenon atom is surrounded by three nickel surfaces.

STM can function like an atomic switch if the probe top is placed above the xenon atom as you can see in the figure 1.2.4

In the first stage, the polarization is

maintained at -0.02 V. The application of a pulse by $+0.8$ V for 64ms brings about the change of place of the atom from specimen surface to the probe top.

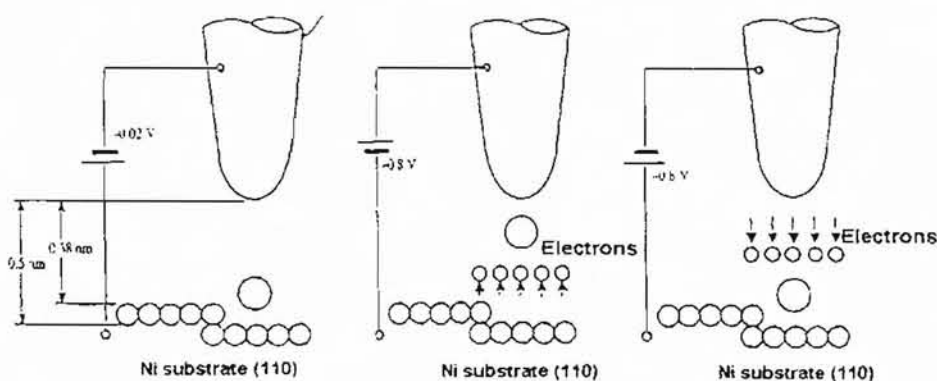


Fig. 1.2.4. The principle of the atomic switch.

After that is applied a pulse by -0.8 V, so, the atom is put back in the first position. The surface is visualized using the tunneling current, which is present in the time of all operation phases for to confirm the final localization of the atom.

In the figure 1.2.5., the level A of the current corresponds to the probe top and nickel surface from the figure 1.2.4. (a), were the current is decreased and stable and the top is polarized at -0.02 V.

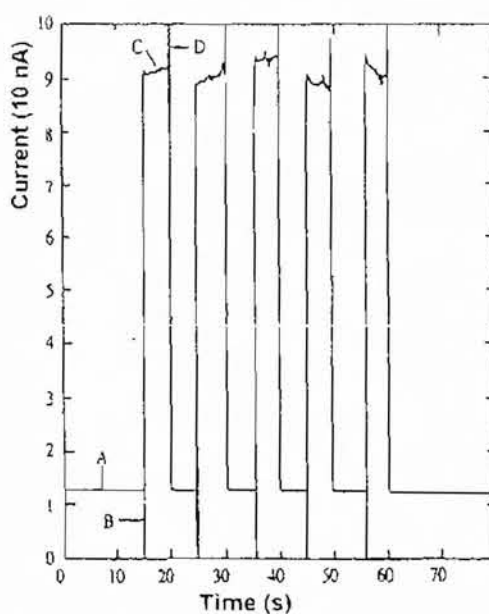


Figure 1.2.5

When is applied the pulse by $+0.8$ V on the top for 64 ms, a transitory current appears (state B). High conduction state (state C) appears when the xenon atom is removed to the top in this state the current isn't stable as in state A because of the xenon atom from state A is localized in the

ell position and it is in contact with three surfaces, while in state C this atom is adsorbed at the border of the top, so it can move a little to the top. The transitory current in state D appears when is applied a pulse by -0.8 V for 64 ms which removes back on the surface the xenon atom.

REFERENCES

1. Scott, V, D, and Love, G, (1983),
Quantitative electronprobe microanalysts.
Ellis Horwood
2. Binning, G. and Rohrer, H. (1982)
Scanning tunneling microscope.
Helvetica Physica Acta, 55, 726
3. Taniguchi, N. 2000, *Nanotechnology*,
Ed. Tehnica, Bucuresti

THE INFLUENCE OF ETHANOL IN DISSOLUTION TEST FOR ANTIBIOTICS CAPSULES

ANA – MARIA HOSSU*, MIHAELA SCRIPCARIU**, VASILE MAGEARU***

*Chemistry Department, Science Faculty, Valahia University of Targoviste

**Institute from control of biological products and drugs of use veterinary, Str. Duduza, nr. 37, sec. 6, Bucharest

***University of Bucharest, Faculty of Chemistry, Bd. Regina Elisabeta, nr. 4-12, sec. 3, Bucharest

ABSTRACT: The present study is devoted to the dissolution test for ampicillin capsules and the influence of ethanol in activity of this antibiotic in the human body. The test is used to determine the dissolution rate of the active ingredients of solid dosage forms (for example capsules). The conclusions had been drawn on one example namely ampicillin capsules.

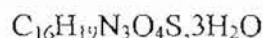
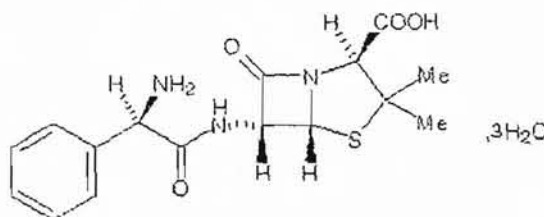
INTRODUCTION

Capsules are solid preparations with hard or soft shells of various shapes and capacities, usually containing a single dose of active ingredient. They are intended for oral administration. The capsule shells material is consist in gelatin or other substance, the consistency of wich may be adjusted by the addition of substances such as glycerol or sorbitol. Excipients such as surface – active agents, opaque fillers, antimicrobial preservatives, sweeteners, coloring matter authorized by the competent authority and flavouring substances may be added.

The contents of capsules may be solid, liquid or of paste – like consistency. They consist of one or more active ingredients with or without excipients such

as solvents, diluents, lubricants and disintegrating agents. The contents do not cause deterioration of the shell. The shell, however, is attacked by the digestive fluids and the contents are released [3].

Ampicillin capsules contain Ampicillin or Ampicillin Trihydrate.



It is a white, crystalline powder, slightly soluble in water, practically insoluble in alcohol, in ether and in fatty oils. It dissolves in dilute solutions of acids and of alkali hydroxides.

The aim of this work is the influence of alcohol (ethanol) in medical treatment with antibiotics.

EXPERIMENTAL PART

The choice of the apparatus to be used depends on the physical and chemical characteristics of the dosage form. All parts of apparatus that may come into contact with the preparation being examined or with the dissolution medium are chemically inert and do not adsorb, react with or interfere with the preparation being examined. All metal parts of the apparatus that may come into contact with the preparation or the dissolution medium must be made from a suitable stainless steel or coated with a suitable material to ensure that such parts do not react or interfere with the preparation being examined or the dissolution medium.

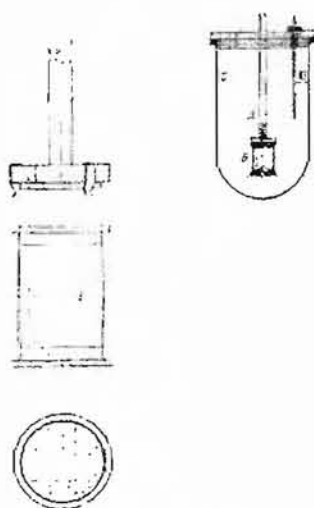


Fig. 1. Basket apparatus

The main components of testing apparatus are listed below:

- (a) A cylindrical vessel, C, made of borosilicate glass or other suitable transparent material, with a nominal capacity of 1000ml. The vessel has a flanged upper rim and is fitted with a lid that has a number of openings, one of which is central.
- (b) A motor with a speed regulator able to keep a constant rotation speed of the basket within $\pm 4\%$ of that specified in the individual monograph. The motor is fitted with a stirring element which consists of a drive shaft, A, and a cylindrical basket B. The basket consists in two components. The top part, with a vent, is attached to the shaft. It is fitted with three spring clips, that allow removal of the lower part for introduction of the preparation being examined.
- (c) A water bath that will maintain the dissolution medium temperature at $36,5^{\circ}\text{C}$ to $37,5^{\circ}\text{C}$.

Introduce the stated volume of the dissolution medium into the vessel of the apparatus. Warm the dissolution medium to between $36,5^{\circ}\text{C}$ and $37,5^{\circ}\text{C}$. [2]

In the case of ampicillin capsules 250mg, we used as the medium 900ml of distilled water and rotate the basket at 100 revolutions per minute, for 45 minutes.

Measure the absorbance of the filtered sample directly at the maximum at 268nm.

Etalon solution contains 29 mg ampicillin trihydrate (25 mg anhydrous ampicillin). It was passed in a glass balloon of 100ml and was brought at sign with distilled water.[1]

$$C\% = \frac{(A_{\text{sample}} - A_{\text{e.c.}}) \cdot 3600 \cdot 25}{A_{\text{etalon}} \cdot 1000},$$

e.c. = empty capsule.

RESULTS AND DISCUSSION

First, we carried-out the dissolution test of ampicillin capsules and the results are showed in table 1.

Table 1

Ampicillin samples	Absorbance ($\lambda = 268\text{nm}$)	Admissibility conditions (min. 75%)
Etalon (29mg AT/100ml)	0,160	-
1.	0,240	95,6
2.	0,246	99
3.	0,231	90,5
4.	0,248	100
5.	0,242	95,6
6.	0,233	91,6
Empty capsule	0,07	-

In each sample was added alcohol in different concentrations and it caused a

decrease of the absorbance of ampicillin (table2).

Table 2

Samples	Alcohol (% vol)	Absorbance ($\lambda = 268\text{nm}$)
1.	0	0,216
2.	5	0,209
3.	10	0,206
4.	15	0,205
5.	20	0,195
6.	30	0,184
7.	40	0,178
8.	50	0,167

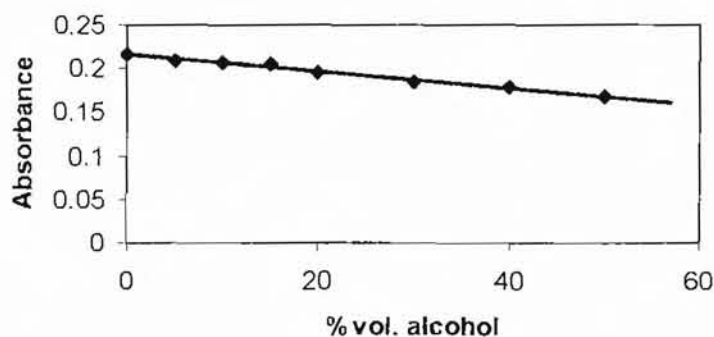


Fig. 2 – The variation of absorbance of ampicillin with the concentration of alcohol.

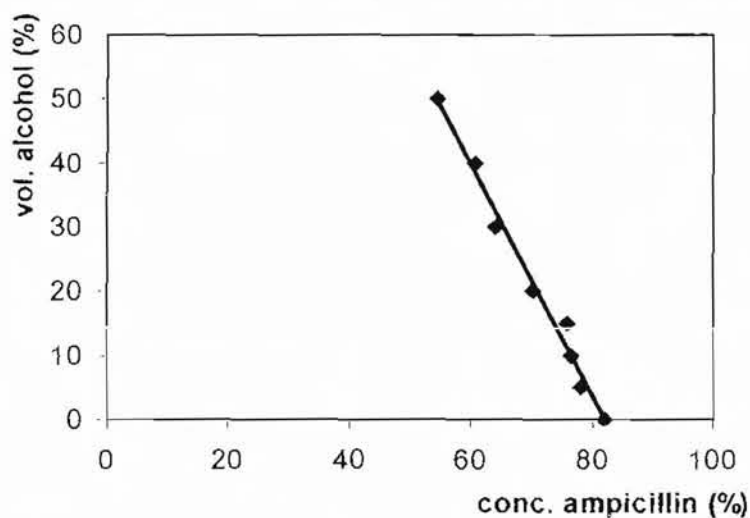


Fig. 3 - The variation of concentration of ampicillin with the concentration of alcohol

CONCLUSIONS

The results of quantitative control obtained with this analytical method are shown that the consuming of alcohol in the

same time with the antibiotics causes a decreasing in activity of these substances in human body.

REFERENCES

1. *** "Farmacopeea Romana", ed. X, Editura Medicala – Bucuresti – 1993;
2. *** "British Pharmacopoeia Volume II" 1999;

3. D. Dobrescu, "Farmacodinamie", ed. II, Editura Didactica si Pedagogica – Bucuresti – 1977 ;

4. C. Podina, Analele Universitatii Bucuresti, anul IV (serie noua), 1995.

STUDY OF THE ANTIOXIDATIVE PROPERTIES OF SOME TRIAZINIC SKELETON COMPOUNDS

LAURA MONICA GORGHIU, CRINELA DUMITRESCU, RADU LUCIAN OLTEANU, SILVIU JIPA

Chemistry Department, Science Faculty, Valahia University of Targoviste

ABSTRACT: *There is a considerable interest in thermal stabilization of commercial polyolefins because their service life depends on a large extent by the stabilization efficiency of additives.*

One of the most sensitive procedures used for the determination of antioxidative ability is chemiluminescence.

An important class of antioxidants that has a continuous developing is the triazines skeleton antioxidant compounds class. In the case of these compounds an important decrease of the oxidation effect in comparison with the same effect of the simple phenolic or aminic antioxidants is observed.

In this paper the influence of some new synthesized triazinic antioxidants on the polyolefines is studied. The stabilization efficiency of these additives is also studied.

INTRODUCTION

Organic matter has a strong tendency to react with oxygen and oxidize. This is true for most commercial organic materials, e. g. plastics, elastomers, fibers, fuels, lubricants and foods.

A. W. Von HOFMANN (1861) first made the connection between oxygen and the deterioration of polymer properties in his studies on the aging of gutta-percha [1]. The concept of antioxidants and the discovery that small amounts of reducing agents could protect materials susceptible to oxidation were attributed to S. L. BIGELOW (1898) for sodium sulfite solution [2]; to P. SISLEY (1903 and 1940) for stabilization of dyed silk to

oxidation; to A. LUMIERE, L. LUMIERE and A. SEYEWETZ (1905) for the protection of photographic developers (these authors first used therm antioxidant); and to CH. MOUREU and CH. DUFRAISSE (1920) for the protection of acrolein.

The development of methods of production and testing of new highly efficient antioxidants for polymeric materials have a great practical importance. From this viewpoint the skeleton derivatives are of interest for the polyethylene stabilization. Chemiluminescence (CL) has found a wide application in the studies of solid state oxidation of polymers [3-7]. A sensitive

photomultiplier is used to measure the weak light accompanying oxidation of organic molecules. It is generally believed that the luminescence originates from excited ketones [8-10].

In the present work the evaluation of protective action of some triazinic skeleton derivatives using CL method has been performed.

EXPERIMENTAL

The new triazinic antioxidants were synthesized by the condensation of cyanuric chloride with different amines and/or thiols by refluxing in xylene [11].

As oxidative substrates the specified polymers of table 1 were used:

Table 1: The polymeric substrats

Polyethylene type	Sort	Producer	Density (g/cm ³)	Flow (*) Index (g/10min)
LDPE	A-23FB/035	Arpechim Pitesti	0.921	1.83
LDPE	K-322	Brazi	0.920	0.5
LLDPE	LLN 1001xF (E29996)	EXXON MOBIL	0.915	2.07
HDPE	A-53-MB/084P	Arpechim Pitesti	0.966	6.15

(* 190°C, 216 kg)

These polymers were purified by precipitation with ethanol from hot o-xylene solutions. The resulted powders were rinsed with acetone and dried at the room temperature.

The triazinic additives were mixed with polymers as chloroformic paste. After the solvent evaporation the samples were powerfully mixed.

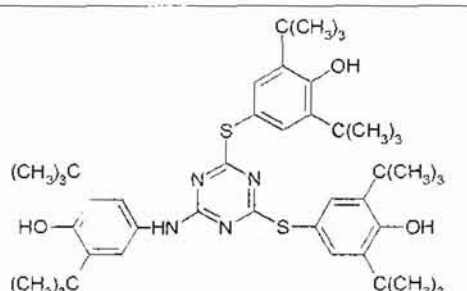
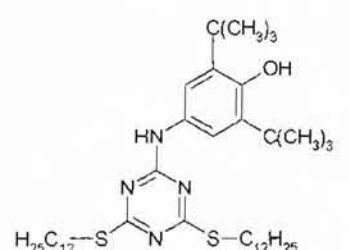
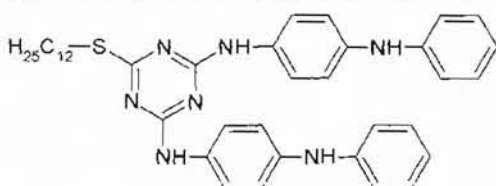
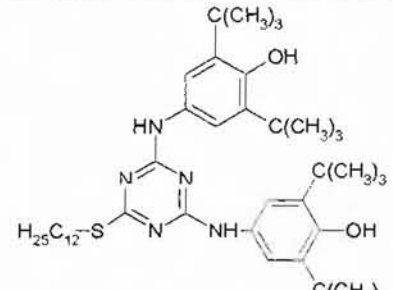
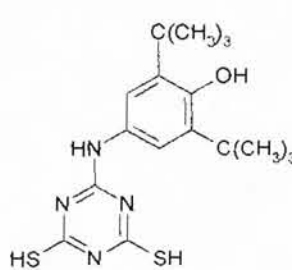
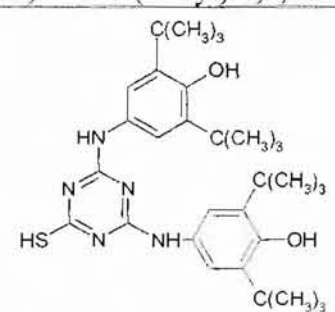
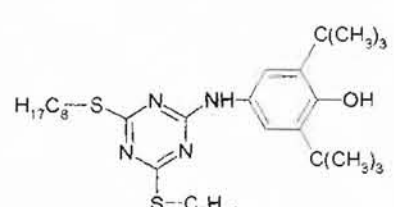
Molecular structure and denomination of these compounds are presented in Table 2

near a standard antioxidant (Irganox-565) which has also a triazinic skeleton.

Isothermal chemiluminescence emission measurements were performed in air at 200°C for all polymers and 190°C for HDPE and LDPE using OL-94 Oxyluminograph [12].

The CL-parameters used for the kinetic description of thermal oxidation process were presented in a previous work [12].

Table 2: Molecular structure and denomination of mercapto-s-triazines used for the stabilization of polyolefins

Code	Structure and denomination	Code	Structure and denomination
A ₁	 <p>2,4-thio-bis-(2,6-di-tert-butyl-phenol)-6-(4-hydroxy-3,5-di-tert-butyl-aniline)-1,3,5-triazine</p>	A ₄	 <p>2,6-thio-bis-(lauryl)-4-(4-hydroxy-3,5-di-tert-butyl-aniline)-1,3,5-triazine</p>
A ₂	 <p>2,6-bis-(N-phenyl-p-phenylen-diamine)-4-thio(lauryl)-1,3,5-triazine</p>	A ₅	 <p>2,4-bis(4-hydroxy-3,5-di-tert-butyl-aniline)-6-thio-(lauryl)-1,3,5-triazine</p>
A ₃	 <p>2,6-bis-(mercapto)-4-(4-hydroxy-3,5-di-tert-butyl-aniline)-1,3,5-triazine</p>	A ₆	 <p>2,4-bis-(4-hydroxy-3,5-di-tert-butyl-aniline)-6-mercapto-1,3,5-triazine</p>
A ₇	 <p>2,4-bis(n-octyl-thio)-6-(4-hydroxy-3,5-di-tert-butyl-aniline)-1,3,5-triazine (IRGANOX-565)</p>		

RESULTS AND DISCUSSION

The stabilized samples leads to a substantial increasing of the oxidation

induction period and oxidation decreasing rate as is shown in 2-5 figures in comparison with figure 1.

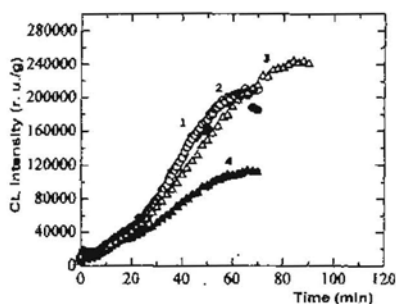


Figure [1]- CL-traces of LDPE(A-23FB/0.35P) (1); HDPE (A-53MB/0.84P) (2); LDPE (K-322) (3) and LLDPE (EXXON MOBIL) (4) - free of additive

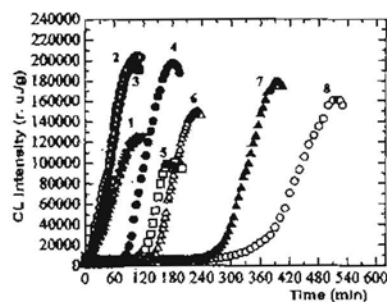


Figure [2]- CL-spectra of LDPE (K 322) unstabilized (1) or protected with A2 (2), A1 (3), A3 (4), Irganox-565 (5), A6 (6), A5 (7) and A4 (8) (0,25 wt %) additives

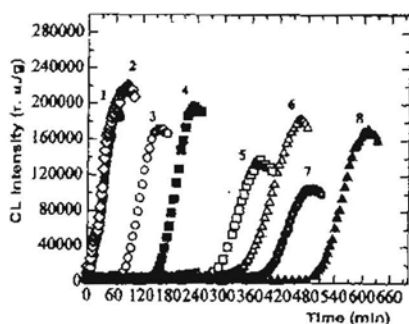


Figure [3] - CL-spectra of LDPE (A-23FB/035P) unstabilized (1) or protected with A2 (2), A1 (3), A3 (4), A6 (5), A5 (6) Irganox-565 (7) and A4 (8) (0,25 wt %) additives

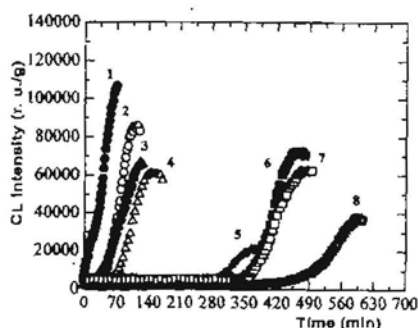


Figure [4] - CL-spectra of LLPE (EXXON MOBIL) unstabilized (1) or protected with A1 (2), A2 (3), A3 (4), Irganox-565 (5), A5 (6), A4 (7) and A6 (8) (0,25 wt %) additives

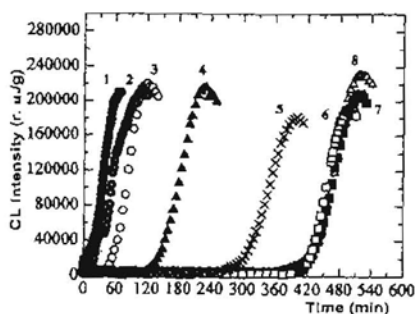


Figure [5] - CL-spectra of HDPE (A-53MB/084P) unstabilized (1) or protected with A2 (2), A1 (3), A3 (4), Irganox-565 (5), A6 (6), A5 (7) and A4 (8) (0,25 wt %) additives

The kinetic parameters resulted from the comparative data from each of these figures are presented in tables like table 3. For all of

substrats the same data of this table were obtained.

Table 3: Kinetic parameters for thermal oxidation of LDPE (A-23FB/035P) stabilized with the studied mercapto-s-triazines in 0,25 wt %. CL data.

Antioxidant	t_i (min)	t_{i2} (min)	V_{ox}^{max} (r.u./g/min)	I_{max} (r. u./g)	t_{max} (min)	A	S
none	12	32	4140	163131	61	-	-
A ₁	82	111	2958	171500	155	0.186	0.714
A ₂	16	33	6026	190873	81	0.011	1.456
A ₃	160	190	3203	197050	235	0.393	0.774
A ₄	510	542	2310	171150	610	1.321	0.558
A ₅	350	400	1907	182488	465	0.897	0.461
A ₆	293	333	1933	137562	380	0.745	0.467
Irganox-565	389	425	1502	106040	495	1.000	0.363

In those tables are also presented the relative activities (A) and relative stabilities (S) defined in (1) and (2) equations.

$$A = [(t_i)_x - (t_i)_0] / [(t_i)_s - (t_i)_0] \quad (1)$$

where: $(t_i)_x$, $(t_i)_0$ and $(t_i)_s$ are the induction periods of the sample protected by the studied antioxidant, of unprotected sample and also of the standard antioxidant protected sample.

$$S = (V_{ox}^{max})_x / (V_{ox}^{max})_0 \quad (2)$$

where: $(V_{ox}^{max})_0$ and $(V_{ox}^{max})_x$ are the maximum oxidation rates for unprotected and stabilized samples.

From the presented data analysis, it results that remarkable induction periods and great activities for A₆, A₅ and A₄ triazines

are obtained. On the other hand the A₃ compound has a similar behavior with the standard antioxidant (Irganox-565) while A₁ and A₂ have a lower activity.

The relative stability is improved in all the analysed triazines. This aspect shows that some of the reaction products of the triazinic antioxidants with peroxi radicals keep also the protector effect in the propagation oxidating step.

We have also observed that the main stabilization parameter – induction period – increases with flowing index increasing, like table 4 presents.

Table 4: Kinetic parameters

Polymer	Density (g/cm ³)	Flow (*) Index (g/10min)	Induction period t _i (min)			
			A5	A6	A2	None
LDPE (K322)	0.920	0.5	280	144	14	10
LDPE (A-23FB/035)	0.921	1.83	350	293	18	10
LLDPE (LLN 1001xF)	0.915	2.07	368	480	29	10
HDPE (A-53-MB/084P)	0.966	6.15	430	430	33	16

The induction period increasing of the polymer with lower maximum flow index sample may be explained by higher antioxidant mobility in ramification. This behaviour is better illustrates in figure 6 for A5 antioxidant.

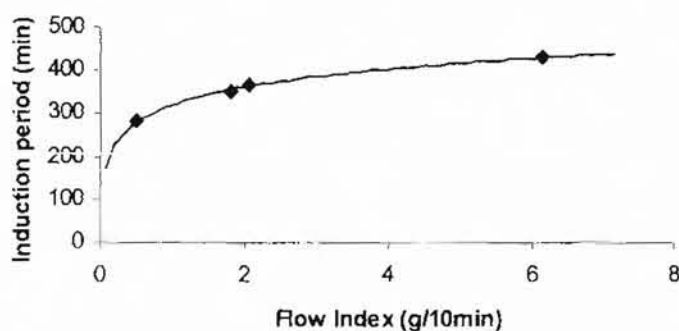


Fig. [6] - Induction period-flow index dependence for A5 antioxidant

CONCLUSIONS

The presented data on LDPE and HDPE confirm the remarkable antioxidant activity of the triazinic compounds. The studied antioxidants present in the HDPE case a medium increasing of the induction period with approximately 35% greater than the LDPE (K322) case and 18.6% than LDPE (A-

23FB/035) case. This increasing effect of the antioxidative protection is explained through the higher cristalinity content of the oxidation substrate.

The antioxidative efficiency evaluation has to be performed for every polymer. An extrapolation result from each polymer to other is not recommended.

REFERENCES

- [1] A. W. VON HOFMANN, *J. Chem Soc.* **13**, p. 87, 1861
- [2] A. SEYEWETZ, P. SISLEY, *Bull. Soc. Chim. De France*, **31**, p. 672, 1922
- [3] A. KRON, B. STENBERG, T. REITBERGER, N.C BILLINGHAM, *Polym. Deg. Stab.*, **53**, p. 119 1996
- [4] L. MATISOVA-RYCHLA, J. RYCHLY, L. C. ROGER, N.C. BILLINGHAM, K.T.GILLEN (editors), *Polymer durability – degradation stabilization and life time prediction*, Advances in Chemistry Series 249, Washington D. C., Am. Chem. Soc., Chapter 12, 1996
- [5] L. MATISOVA-RYCHLA, B. LANSKA, J. RYCHLY, *J. Angew. Makromol. Chem.* **216**, p. 169, 1994
- [6] L. ZLATKEVICH, editor, *Luminescence techniques in solid state polymer research*, New York: Marcel Dekker Inc, 1989
- [7] S. JIPA, R. SETNESCU, T. SETNESCU, T. ZAHARESCU, *Polym. Degrad. Stab.*, **68**, p. 159, 2000
- [8] G. A. GEORGE In: N. G. GRASSIE, editor, *Developments in Polymer Degradation*, vol. 3, Chapter 6, London: Applied Science Publisher, 1981
- [9] L. REICH, S. S. STIVALA, *Die Makromol. Chem*, **103**, p. 74, 1967
- [10] R. F. VASILEV, *Die Makromol. Chem*, **126**, p. 231, 1969
- [11] M. GIURGINCA, J. M. HERDAN, L. CIRA, G. VALEANU, G. IVAN, *Polym. Degrad. Stab.*, **36**, p. 53, 1992

THE INTERACTION BETWEEN NEW SYNTHETIZED ACID DYES AND A NONIONIC SURFACTANT ALKYL POLYGLUCOSIDIC

IRINA MOATER*, CRINELA DUMITRESCU*, MIHAELA OLTEANU**, CEZAR BENDIC**

* Chemistry Department, Science Faculty, Valahia University of Targoviste

**University of Bucharest, Faculty of Chemistry, Bd. Regina Elisabeta, nr. 4-12, sect. 3, Bucharest, ROMANIA

ABSTRACT: The study of the interaction between an acid dye and nonionic surfactant is very important in clarifying the mechanism of wool dyeing and color preservation and also for the washing conditions determination. It was examined the possibility of the formation of the complexes between a series of acid dyes, newly synthesized, from the class of azoic dyes derived from aminonaphtolsulphonic acids [1] and a nonionic surfactant from the class of the alkyl polyglucozides [2]. The tensiometric method has the advantage that we can monitor the surfactant- dye one interaction over a large scale of concentrations. The formation of some surfactant- dye complexes was made evident in the different molecular ratios in the submicellar range compared to the micellar range of concentration of the surfactant. The equilibrium constants, the free energy of the complex formation in the absence of nonionic micelles or mixed micelles, were determined. There are different equilibrium in the system which compete one another over a large scale of surfactant concentration (adsorption, micellisation, small complex formation, large complex – mixed micelles formation).

INTRODUCTION

The study of the interaction between an acid dye and a nonionic surfactant is very important in clarifying the mechanism of wool dyeing and color keeping, and also in establishing the washing conditions. The wool dyeing mechanism is affected by the addition of a nonionic surfactant, due to the formation of the dye-surfactant complex. The goal of this work is to study the possibility of the formation of complexes between a series of new synthesized dyes from the class of azoic dyes and a nonionic surfactant, by measuring the surface tension for a large

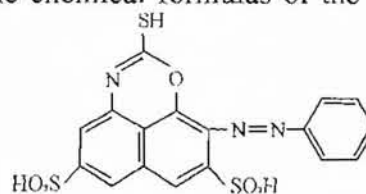
scale of surfactant concentrations. The nonionic surfactant, alkyl polyglucosidic class, was chosen due to its less aggressive properties against the natural fibre.

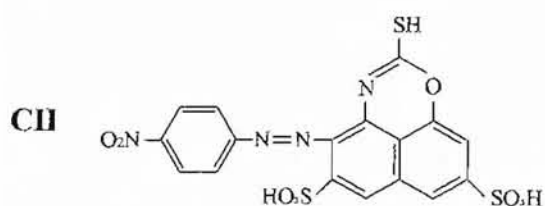
MATERIALS AND METHODS

The acid dyes abbreviated C I and C II were used, derived from 1-amino 8-naphtol 3,6 sulphonic acids, with the reactive system represented by the isothiocyanic group. [1]

The chemical formulas of the dyes are:

C I





The two compounds were purified by the recrystallisation from the water and characterized by IR spectrum.

The nonionic surfactant is an alkyl polyglucoside with an alkylic chain between 8-16 carbon atoms, short named APG, and an average molecular mass of 390 u.a.m., a product of Caspho-Europe [2].

It is a surfactant obtained from vegetal sources with a "soft" action upon the wool fibres.

The surface tension determination for aqueous solutions of the dyes, with concentrations of 10^{-4} – 10^{-3} mole/liter, showed that the surface tension for these solutions is identical with the distilled water surface tension, where from comes that the two dyes are not tensioactives.

There were made surface tension measurements for dye-surfactant mixtures over a large surfactant concentrations 10^{-4} – $12,5 \cdot 10^{-4}$ mole/liter.

The surface tension determination method was the Du Nouy method. The Pt-Ir ring was attached to a torsion balance (Spiralfederwaage Germany) with an

accuracy of 0,1 mN/m and a reproductibility of 0,05mN/m [3].

The tensiometric method has the advantage that one can monitor the surfactant-dye interaction over a large scale of concentration.

The surface tension measurements furnish data upon the adsorption of the surfactant molecules at the solution-air interface, because the surfactant-dye complexes are not adsorbed at the interface.

RESULTS AND DISCUSSION

The tensiometric results are shown in figures 1 and 2.

In the absence of dye the surface tension decreases linearly with increasing surfactant concentration and attains a constant value at the critical micelle concentration, of the surfactant, as typical for the amphiphile molecules, with a hydrocarbonated part with at least 8 metilenic groups. At 21 °C the $[APG]_{CMC} = 2,5 \times 10^{-4}$ mol/l. In surfactant-dye mixtures, in which the surfactant concentration is lower then CMC, the surface tension increase, due to the presence of the dye, indicates the existence of an association process dye-surfactant and that the associated form is not tensioactive.

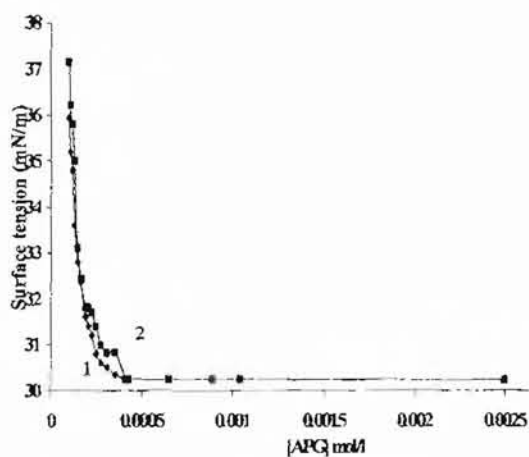


Fig. 1 - Surface tension vs alkyl poliglocozide (APG) concentration in aqueous solution (1) and for the mixture APG – C I dye (2). The dye concentration 1×10^{-4} mol/l, at 21°C .

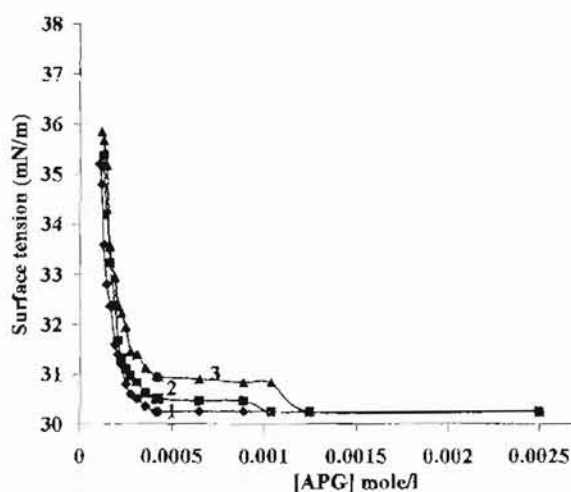


Fig. 2 - Surface tension vs $[\text{APG}]$ mol/l at various constant concentration of C II in mixture. (21°C) : 1- APG in water, 2- mix APG + CII 1.10^{-4} mol/l, 3- mix APG + CII $1.6.10^{-4}$ mol/l.

Table 1: The critical micelle concentration CMC, values of the APG surfactant in mixtures with the dyes CI and CII and the number of surfactant molecules bound to dye, in the submicelle range (n) in the range micelle (l) (21°C).

Composition	CMC (mol/l)	n	l
APG in water	$2,5.10^{-4}$		
mix APG + CI 1.10^{-4} mol/l	$3,75.10^{-4}$	2.3	10-30
mix APG + CI $1,6.10^{-4}$ mol/l	$12,5.10^{-4}$	3.0	
mix APG + CII 1.10^{-4} mol/l	$12,5.10^{-4}$	1.2	
mix APG + CII $1,6.10^{-4}$ mol/l	$22,5.10^{-4}$	2.0	10-40

In the presence of C I and CII, on the surface tension isotherm can one observed a short plateau which enhance with the increase of dye concentration in the bulk, and leads directly to the modification of the CMC for the dye-surfactant mixtures (Table 1).

When the concentration of nonionic surfactant increases, the surface tension initially decreases, reaches a short plateau at the first transition, decreases again, and finally attains a constant value at the second transition, where the surface tension is identical with that at the $[APG]_{CMC}$ of surfactant solution in the absence of dye.

Such a multiplicity of transitions also has been observed by Jones [3] in the interaction of sodium dodecyl sulfate with polyethylene oxide. Multiple transitions revealed through the method used in the present work or (and) through the other methods (conductometry, light diffusion, viscosimetry) were put in evidence also in the case of other surfactant-dye, surfactant-polymer solutions [4].

Figures 1 and 2 show that in the submicelle domain to reach a given surface tension value, a solution which contains dye needs a greater quantity of surfactant than in the absence of the dye. The extra quantity of surfactant in the case of the surfactant-dye mixture, involves the

existence of a strong surfactant-dye interaction.

We may assume that the surface tension both dye and surfactant would be a measure of the free surfactant quantity existant the solution by means of the adsorption equilibrium of the free surfactant molecules on the solution surface, because the complexes are not adsorbed at the interface. This supposition is reasonable since the surface tension at the critical micellar concentration of the surfactant is identical with the surface tension at the critical micellar concentration of the solution which contains both surfactant and dye.

The assumption can be further reasonably sustained in what concerns the proprieties of the complex by the fact that the complex should be more hydrophilic, the formation of the complex being allowed by the hydrophobic bound, which leads to a solubilization in micelles. An other probable variant is that the interaction between the studied acid dyes and the nonionic surfactant occurs by means of the etheric oxygens, like the interaction between the anionic and those nonionic polyetoxilated surfactants [5].

The formation of some surfactant-dye complexes in different molecular proportions in the micelle range compared to the submicelle range of the surfactant

concentrations was put into evidence. It is likely that the dye should prevent the formation of the surfactant micelles so that the first micelles could be small with an aggregation number lower than in the absence of the dye.

When a complex DS_n is formed according to the equation:



the following equation may be,

$$[C] = K ([D] - [C])([S] - n[C])^n, \quad (2)$$

assuming that the value of activity coefficients is unity, where K represent the equilibrium constant, $[C]$ the concentration of the complex, $[D]$ the total concentration of the dye, $[S]$ the total concentration of the surfactant, and n the number of surfactant molecules bound to the dye.

Equation (2) can be rewritten as:

$$[X]/n = K([D] - [X]/n)([S]^*)^n \quad (3)$$

$$\text{since } [C] = [X]/n, [S] - n[C] = [S]^* \quad (4)$$

Therefore, the difference in the surfactant concentration, $[X] = [S] - [S]^*$ represents the quantity of nonionic surfactant that interactions with the dye, since $[S]^*$ is the amount of the free surfactant in the dye – containing solution.

In equation (3) $[D]$ and $[S]^*$ are known and $[X]$ is measured, and consequently K can be calculated if only n is determined. The values of n might be

determined by the following approximation of equation (3):

$$\log ([X]_i/[X]_j) = n \log ([S]_i^*/[S]_j^*) \quad (5)$$

provided that $[D] \gg X/n (= [C])$ for any pair of solutions, both i and j represent, respectively, $[X]$ and $[S]^*$ at the surfactant tension γ_i and γ_j . When $\log ([X]_i/[X]_j)$ is plotted as a function of $\log ([S]_i^*/[S]_j^*)$ a straight line of slope n is obtained. (Table 1) The values of n , the number of surfactant molecules bound to a dye molecule, for the submicelle range, is 2 or 3 for CI and 1 or 2 for C II (Table 1). For K , there were obtained values between $2 \cdot 10^8$ – 10^{13} in function of the n value (21 °C).

An other complex, DS_l , different from DS_n , would be formed above the first transition point, the formation of DS_l causes the increase of $[X]$. It is supposed that there is no more formation of DS_l above the second transition point ($[S]_{CMC}$), due to the absence of the dye.

The l values would be determined by the difference, $[S]_{CMC} - [S]_{CMC}^*$, supposing that $[DS_n] \ll [DS_l]$ at $[S]_{CMC}$. The plot of $[S]_{CMC} - [S]_{CMC}^*$ as a function of $[D]$ give a straight line whose slope gives the l value. (Table 1).

The mechanism for the interaction system consisting of acid dye and nonionic surfactant may be divided into four kinds of process:

- 1- surface adsorption of free surfactant molecules;
- 2- small complex formation;
- 3- large complex (mixed micelle) formation;
- 4- ordinary surfactant micelle formation.

These processes vary with the concentration of surfactant through various equilibria, competing with one another.

CONCLUSIONS

There is an interaction between

REFERENCES

- [1] - DUMITRESCU C.¹, GUTU I.², GUTU E.³, MARIUS F.⁴, TARABASANU C.⁴. *Derivates of 1-amino-8-naftol-3,6 disulfonic acid new reactive izothiocyanic dyes*, 2nd International Conference of the Chemical Societies of the South –Easten European Countries on Chemical Sciences for Sustainable Development, Book of Abstracts, vol.1, pag.307, 2000.
- [2] - WOLFGANG VAN RYBINSCHI* AND KARLHEINZ HILL AUGEW. *Chem. Int. ED.* 1998;37, 1328-1345.
- [3] - JONES M.N., *J. Colloid Interface Sci.* 23, 36, 1967.
- [4] -D.M. Bloor and Wyu- Yones "The Structure, Dynamics and Equilibrium Properties of Colloidal Systems' 1990, Kluwer Academic Publishers, Netherlands, p. 149-160.
- [5] - MEGURO K., MINORU U., KUNIO E., *Nonionic Surfactants. Physical Chemistry*, Martin J. Schich ed., Manel Dekker inc. New York - Basel, 1987.

ENGRAIS RETARDÉS SUR POLYMÈRES BIODEGRADABLE

CRISTIANA RĂDULESCU, G. C. CONSTANTINESCU

Département de Chimie, Faculté des Sciences, Université „Valahia” Târgoviste,

RESUME: En utilisant le xanthane, le houillon xanthanique ou la cellolignine fourfouronique comme supports à la fois organique et biodégradables on a réussi à retarder par voie chimique l'urée et les phosphates d'ammonium. En résulte des engrais complexes organiques et minéraux contenant l'azote et respectivement le phosphore dans la plus grande partie insolubles dans l'eau, qui deviennent accessibles aux plantes après une dégradation microbiologique du support organique on a établi les limites du processus.

Les processus de lévigation dans le sol accompagnés de phénomènes de rétrogradation ainsi que la protection du milieu ont imposés depuis longtemps une autre direction de recherche dans la fabrication des engrais chimiques (1) par la diminution de la solubilité des sels minéraux solubles dans l'eau. Dans des cultures irriguées la lévigation s'amplifie d'une manière impressionnante dans cette situation la diminution de la solubilité s'impose avec une force économique supplémentaire.

Le premier choix était l'application des sels minéraux dont la solubilité augmente avec la diminution de pH. Une autre idée fructueuse, était l'enveloppement dans des produits organiques. Cet idée peut être concrétisée aussi par l'intermède d'un greffage sur polymères. La combinaison chimique réalisée entre le polymère (véhicule tractant ou support) et un composé chimique contenant de l'azote ou du phosphore sous forme assimilable par des plantes, réalisées par des liaisons estheriques ou amidiques (idée empruntée de l'industrie de médicaments retardés) suppose la scission de la liaison chimique substrat-engrais par une action chimique (hydrolise) ou par voie micro-biologique.

Dans le cas d'ions nitrate ou encore ammonium, leurs inclusion dans une structure de gel ou dans une microcapsule représentent des variantes applicables.

La technique de microcapsulation utilisée par Mankins et Hill (2,3) en 1971 a subi d'importants développements notamment dans l'utilisation de microcapsules de gélatine ou de polymères, ayant un diamètre de $\approx 10\mu$ (4,5).

Il y a des systèmes qui réalisent l'élaboration d'une molécule biologiquement active comme sont celles de médicaments, pesticides, stimulateurs de croissance réalisés sur amidon de Bittner ou sur cellulose - matériaux biodégradables- la liaison substrat - engrais étant aisément hydrolisables.

L'élaboration du biocomposant, donc la bioactivité, a été réalisée entre 5 et 50% dans le cas du support cellulosique ou ligninique (8). Une bonne variante, techniquement réalisable, est représentée par la dispersion de l'agent bioactif dans une solution aqueuse de xanthogénat d'amidone, suivie d'une réticulation oxydative par des métaux de transition ou d'épiclorhydrine. Malheureusement le produit contient trop de sodium qu'il le rend inutilisable pour l'agriculture.

PARTIE EXPERIMENTALE

En tant que support retardant nous avons utilisé le xanthane, un bouillon

xanthanique et de la cellulogénine obtenue dans la fabrication dirigée du fourfouroule.

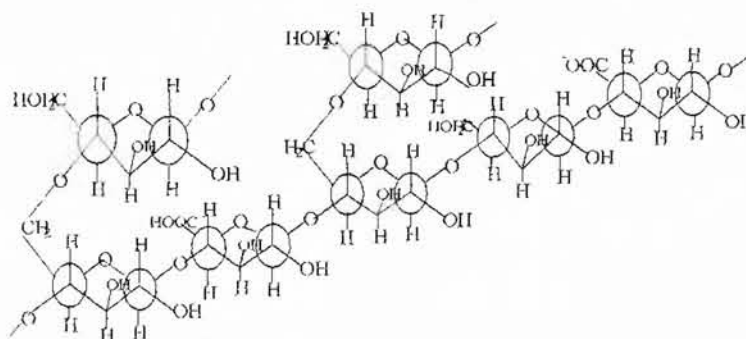


Figure 1. Formule de xanthan

La forte solubilité du xanthane dans l'eau a été énergiquement diminuée par l'élimination des cations, solution aqueuse de 1% de xanthane perclorée, par un cationite fort; l'éluat collecté et concentré jusqu'à 3% de xanthane (sous vide) a été traité par l'alcool isopropilique quand le xanthane précipité. Le polymère est séché et ensuite, toujours sous vide, est broyé. On a utilisé ensuite soit une solution 1% de xanthane précipité soit le bouillon xanthanique (avant la précipitation du xanthane) toujours en concentration de 1% exprimée en xanthane qui sont été traités par des solutions d'urée 50% et de phosphate mono-ammoniacal ou diammoniacal 30%, en volumes croissantes. Les sels obtenus ont été chauffés 30 minutes à l'ébullition.

Pour l'analyse on a minéralisé les échantillons par H_2SO_4 conc. et H_2O_2 30%. Le contenu en azote a été déterminé par distillation (Parnas-Wagner) et le phosphore par la méthode de molybdate (Lorentz).

RESULTATS ET DISCUSSIONS

Sur le tableau 1 sont présentés les résultats de l'analyse d'azote et dans le tableau 2 ceux du phosphore.

L'effet retardant du xanthane est appréciable même pour des quantités importantes de phosphore. Les engrais polymères préparés sur cette voie contiennent en moyenne 15-16% N total d'où 97-98% insoluble dans l'eau mais qui devient accessible aux plantes dès que la chaîne polyhydro-carbonatée de xanthane est coupée en petite morceaux par des microorganismes du sol (ou d'un milieu

nutritif quelconque). Dans le cas d'un bouillon xanthanique contenant 4,5% xanthane on a réussi à retarder 95% d'azote

ajouté sous forme d'urée. On obtient ainsi un produit organique et minéral ayant un contenu de 22% N, donc meilleur qu'un $(\text{NH}_4)_2\text{SO}_4$.

Tableau 1. Contenu en azote ajouté sous forme de $\text{CO}(\text{NH}_2)_2$ et le pourcentage de retardement.

Xanthan g	N total ajouté, %	N solub. en H_2O ajouté, %	N total trouvé après trait., %	N soluble en H_2O trouvé après trait., %	Perte %	Retardement %
1,0	6,43	6,43	6,24	0,44	3,05	93
1,0	18,64	18,64	17,96	0,49	3,82	97
1,0	23,77	23,77	23,44	0,39	3,07	98

Tableau 2. Contenu en azote et en phosphore ajoutés sous forme de $(\text{NH}_4)_2\text{HPO}_4 + (\text{NH}_4)\text{H}_2\text{PO}_4$

Xanthane g	N total ajouté %	N soluble ajouté, %	N total trouvé %	N soluble trouvé, %	Perte %	Retardement %
1,0	2,29	2,29	2,20	0,13	4,09	94
1,0	7,74	7,74	7,50	0,78	3,04	90
1,0	10,71	10,71	10,3	1,04	4,01	90

Tableau 2. Contenu en azote et en phosphore ajoutés sous forme de $(\text{NH}_4)_2\text{HPO}_4 + (\text{NH}_4)\text{H}_2\text{PO}_4$

P_2O_5 total ajouté, %	P_2O_5 soluble ajouté, %	P_2O_5 total trouvé, %	P_2O_5 soluble trouvé, %	Pertes, %	Retardement %
12,75	12,75	12,50	1,45	2,02	88,40
35,02	35,02	34,23	1,72	2,02	94,98
53,02	53,02	52,24	1,58	1,52	97,00

$$y = k \cdot x, \quad y = \text{retardement, \%}$$

$$x = 12,75 = 1, \quad x = 35,02 = 3$$

$$x = 53,02 = 4$$

$$k = \operatorname{tg} \alpha = 0,295$$

Retardement, %

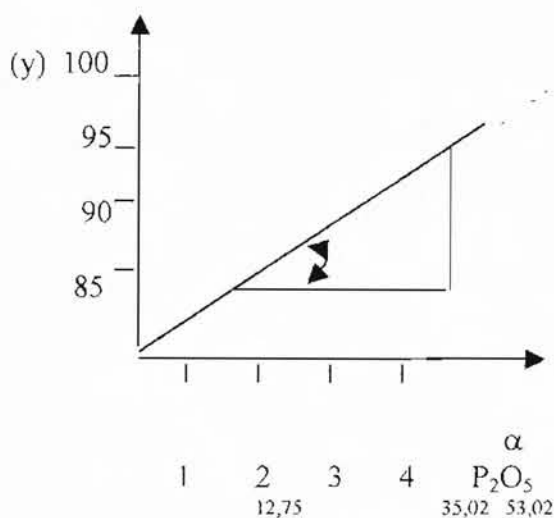


Fig. 2. La quantité de phosphore ajoutée à 1g xanthane

En ajoutant l'azote sous forme d'urée, le pourcentage de retardement est élevé, 97-98%, et sous forme de phosphates d'ammonium, de 90-94%. Quant aux phosphates, la retardation va de 88% à 97% au fur et à mesure que la quantité totale augmente, d'après l'équation d'une droite représentée sur la figure 2.

En utilisant le xanthane, le bouillon xanthanique comme support on a réussi à

retarder par voie chimique l'urée et des phosphates d'ammoniac.

En résulte des engrais complexes organiques et minéraux contenant l'azote et respectivement le phosphore insolubles dans l'eau, qui deviennement solubles après une dégradation microbologique du support organique. On a établi les limites du processus de retardation rapportées au support.

RÉFÉRENCES

1. D.Y.Chu, J.K. Thomas *J.Phys. Chem.* 17 (1984) 2142-2147.
2. P.J. Flory *J. Am. Chem. Soc.* 65 (1943) 372-382.

3. P. Alexander, R.J. Block, *Analytical Methods of Chemistry vol.3*, Pergamon Press, New York, 1961.

SYNERGISTIC EFFECTS OF SOME DYES WITH STERIC HINDERED PHENOLS IN I-PP THERMAL STABILIZATION

CRINELA DUMITRESCU, LAURA MONICA GORGHIU,

RADU LUCIAN OLTEANU, SILVIU JIPA

*Chemistry Department, Science Faculty, Valahia University of Targoviste
cdumi_13@yahoo.com*

ABSTRACT. *In this paper a new set of antioxidants is studied. They belong to H-acid class, having different chemical structures in comparison with "classical" stabilizers. The stabilization efficiency of these additives has been studied. The oxidation induction times and the oxidation rates were obtained for polymer systems containing 0.15 wt % of additive. One of the most sensitive procedures used for the determination of antioxidative ability is chemiluminescence.*

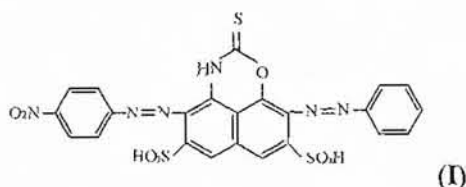
A kinetic treatment of the chemiluminescence data as well as synergetic effects are discussed.

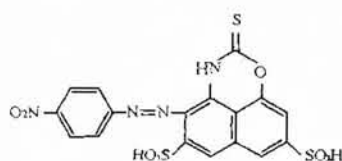
INTRODUCTION

The influence of color additives on thermal stability of isotactic polypropylene is assessed by chemiluminescence. The selected concentration for this study is 0.15 % (w/w). Kinetic parameters, namely, oxidation induction time (t_i), half life time of degradation ($t_{1/2}$) and maximum oxidation time (t_{max}), together with oxidation rate on propagation stage of thermal degradation were determined. Synergistic effect of color additives and Irganox 1076 is characterized [1-4].

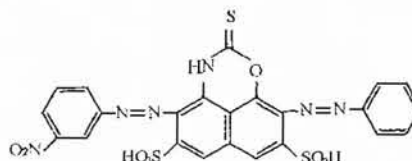
EXPERIMENTAL

The applications used iso-tactic polypropylene Moplen, Himont, Italy. The polymer was purified by dissolving in o-xylene at heat and repeated precipitation with methyl alcohol. The obtained powder was washed in acetone and dried under vacuum at room temperature. The additives used were azo dyes (I, II, III, IV).

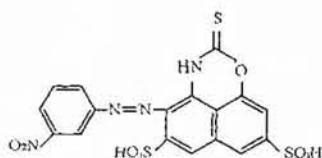




(II)



(III)



(IV)

In some samples, beside the organic dye was introduced the phenolic antioxidant Irganox-1076 [octa decyl - 3 - (3',5' - di tert - butyl - 4' - hydroxyphenyl) propionate] at 0,15% in weight. The samples used in thermal oxidation (170°C, air) were in the shape of

free powder (20 mg). The measurements of chemiluminescence (CL) were made with oxyluminograph OL-94 apparatus (ICPE - Bucharest) [5]. The CL-parameters used for the kinetic description of thermal oxidation process are presented in figure 1.

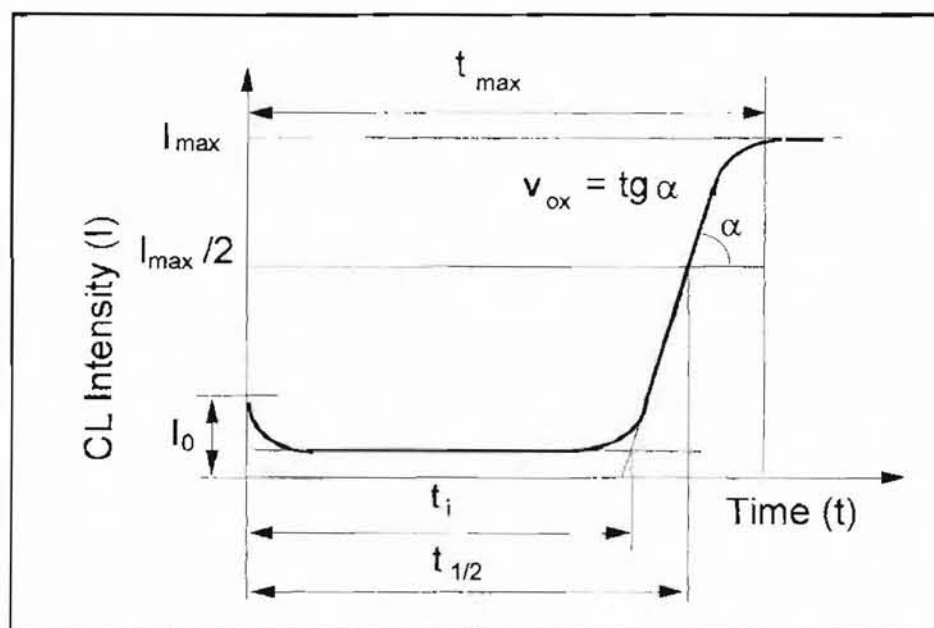


Fig. [1.] - Chemiluminescence diagram for oxidation of polymers

t_i - oxidation induction period, $t_{1/2}$ - required period for reaching half maximum CL intensity, v_{ox} - oxidation rate in propagation stage of oxidation, t_{max} - time elapsed from the beginning of CL determination until attainment of maximum CL intensity, I_{max} - maximum CL intensity, I_0 - initial CL intensity

RESULTS AND DISCUSSION

Figure 2, 3, 4, 5 shows the chemiluminescence curves obtained in isothermal regime (170°C, air) of the i-PP

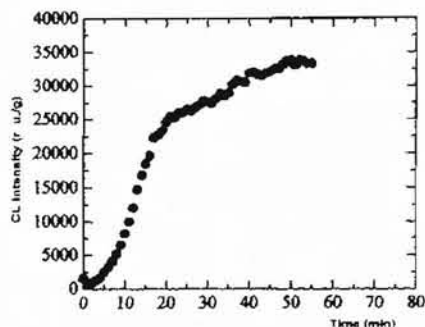


Fig.[2]-CL-curves (170°C, air) for i-PP with additives 0,15% **I**

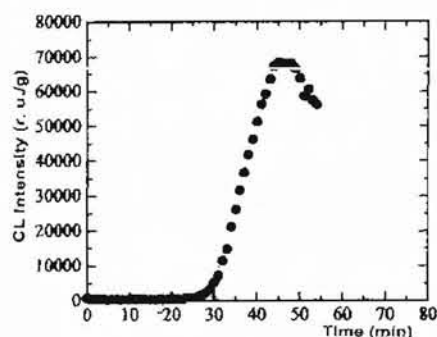


Fig.[4]-CL-curves (170°C, air) for i-PP with additives 0,15% **III**

Based on these data result that only the (**II**) and (**IV**) dyes have a significant protective effect concerning the length of the induction time (t_i or $t_{1/2}$) and also the low value of the maximum rate of oxidation (v_{ox}^{max}). These dyes have in common the monoazo structure with azo groups in position 2.

Can be observed that the induction time have a higher value relative to free

samples using such as additives the compounds (**I**), (**II**), (**III**) and (**IV**) relative to free additives sample.

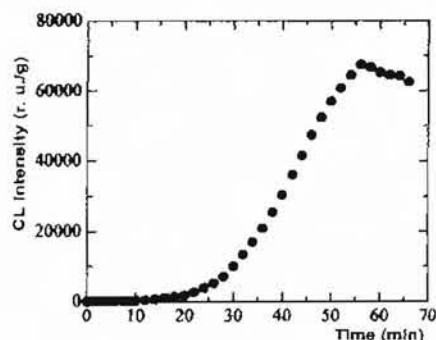


Fig.[3]-CL-curves (170°C, air) for i-PP with additives 0,15% **II**

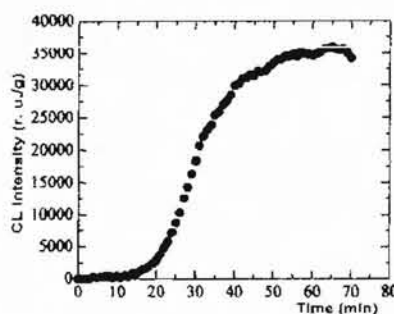


Fig.[5]-CL-curves (170°C, air) for i-PP with additives 0,15% **IV**

additives sample (table 1). The diazo dyes (**I**) and (**III**) have comparable induction times but lower than the firsts. The presence of azo group in position 7 do not improve the protective effect of the dye (see **I** and **III**).

On the basis of thermooxidation induction time parameter (t_i), we are able to range the antioxidant effect of these dyes as follows: **IV** > **II** > **III** > **I**.

The dyes with protective action presents an important cooperative effects with phenolic antioxidant Irganox-1076 (figure 6 and 7) (table 2). The cooperative factors (θ) presented in table II were calculated from the ratio between the

kinetic parameters of couple dye-antioxidant and the sum of kinetic parameters of individual additives [6]. When $\theta > 1$ a synergetic effect is present, additivation for $\theta = 1$, and an antagonistic effect when $\theta < 1$.

Table 1. The kinetic parameters of thermooxidation (170°C, air) of i-PP using as additives (0,15%) different azo dyes. Chemiluminescence data.

Pigment	t_i (min)	$t_{1/2}$ (min)	t_{max} (min)	V_{ox}^{max} (u.r./g/min)
None	4	13	33	2226
(I)	6	14	50	2060
(II)	28	41	56	2455
(III)	30	36	45	6683
(IV)	20	30	60	1869

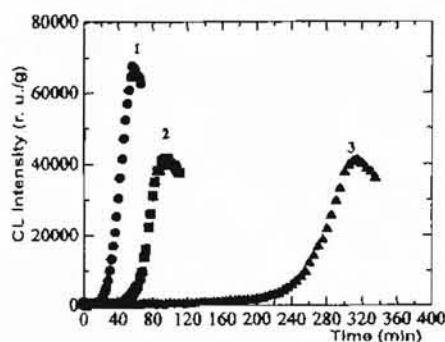


Fig. [6]-CL-curves (170°C, air) for i-PP with additives 0,15% **II** (1), 0,15% Irganox-1076 (2), and 0,15% **II** + 0,15% Irganox-1076 (3)

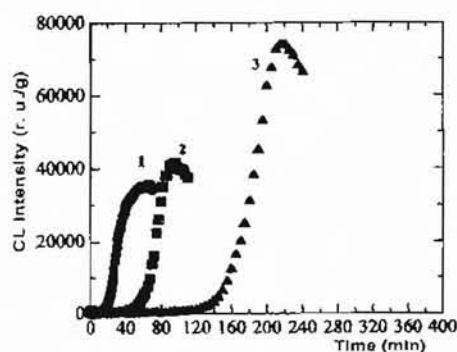


Fig. [7]-CL-curves (170°C, air) for i-PP with additives 0,15% **IV** (1), 0,15% Irganox-1076 (2), and 0,15% **IV** + 0,15% Irganox-1076 (3)

The synergistic effect of compounds (II) and (IV) with screened phenol Irganox-1076 can be explained by the

regeneration theory elaborated by Spetsig[7].

Table 2. The cooperative factors for binary systems azo dye / Irganox-1076.

Chemiluminescence data.

Additive	t_i (min)	$t_{1/2}$ (min)	t_{max} (min)	Cooperative factor		
				θ_{t_i}	$\theta_{t_{1/2}}$	$\theta_{t_{max}}$
0,15% Irganox 1076	58	72	97	-	-	-
0,15% (I)	6	14	50	-	-	-
0,15% (II)	28	41	56	-	-	-
0,15% (III)	30	36	45	-	-	-
0,15% (IV)	20	30	60	-	-	-
0,15% (II)+0,15% Irganox 1076	247	275	315	2,87	2,43	2,05
0,15% (IV)+0,15% Irganox 1076	160	184	220	2,05	1,80	1,40

CONCLUSIONS

The paper came with new arguments for using the chemiluminescence technique as rapidly and precise, for characterization of polymeric materials stability.

In this work the chemiluminescence method was used for study of thermooxidative degradation of i-PP with additives like different mono and diazo dyes substitution derivatives.

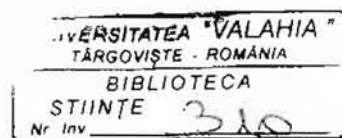
REFERENCES

[1]. *** *Handbook of Polyolefins. Synthesis and Properties*, Marcel Dekker

The synergetic effects were put in evidence between the dyes studied and a screened phenolic antioxidant (Irganox-1076) in protection at thermooxidation of the polymer. This result claim the necessity to analyse the organic dyes regarding the effect at thermooxidative stabilization of polymeric material and cooperative effects with the rest of additives from the receiver.

Inc., New York, Basel, Hong Kong, 1993, p. 705.

- [2]. ****Plastic Additives Handbook*, Hanser Publishers, Munich, Vienna, New York, 1987, p. 471.
- [3]. Kelleher, P. G., *J. Appl. Polym. Sci.* **10**, (1966), 843.
- [4]. Takahashi, T., Suzuki, K., *Kobunshi Kagaku*, **23**, (1966), 792.
- [5]. Jipa, S., Constantinescu, V., Setnescu, R., Setnescu, T., *Brevet RO nr. 110367* of 30th November 1995.
- [6]. Latocha, C., Uhniat, M., Balcerovich, A. W., *Polym. Degrad. Stab.* **7**, (1984), 189
- [7]. Rychla, L.M., Rychly, J., Vavrekova, V., *J. Eur Polym.*, **14**, (1978), 1033.



REVERSIBLE TRANSITIONS INDUCED BY LIGHT

IONICA IONITĂ, CRINELA DUMITRESCU

Chemistry Department, Science Faculty, Valahia University of Targoviste

ABSTRACT: Photoresponsive system are system which respond to light energy beyond merely absorbing and releasing it as heat. Storage of the light energy for varying lengths of time, to reappear as fluorescence, photophorescence and chemical or even mechanical energy are properties of photoresponsive system. The system that utilize photochromic azo dyes as the absorbing chromophores. In the attendant absorption process, light energy becomes stored up in what is probably best called chemical energy, since the chromophores became isomerised, the processes observed are reversible.

AZOIC DYES

One stereochemistry factor, which plays an important part on colour azo dyes, is their possibility to give cis-trans isomerization.

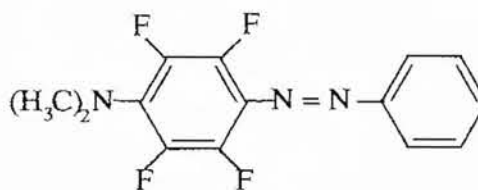
The trans - form are much stabile at room temperature, in while that cis isomer can be generated only through photochemical methods. Absorption spectra of that two isomer forms at one azo dye are always different and thus, exposing of a dye to light cause detectable quantities of cis - isomer is observed a change of colour which will be reversible at removed the source of light.

This phenomena is called photochromie or phototropism and is uncalled for dyes with industrial application.

The photochromic degree depended decisive of cuantic efficiency and thermal stability of cis - form.

Fortunately strong electronic donor groups in azobenzene system reduced sensitive the life - time at cis - isomer and thus, photochromia wasn't a major problem for dyes producers.

Yet, some azobenzene dyes with electronic donor groups present a pronounce photochromic phenomena [1]:

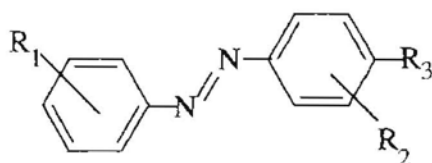


(I)

The dye with upper part structure (I) is rapid converted at cis- form through his solution exposure at light day and after

four hour in the dark, at room temperature still contain only 10% trans – form [2].

The compound (II) was synthesized from azobenzene and present photochromic properties and good reversibility [3]:

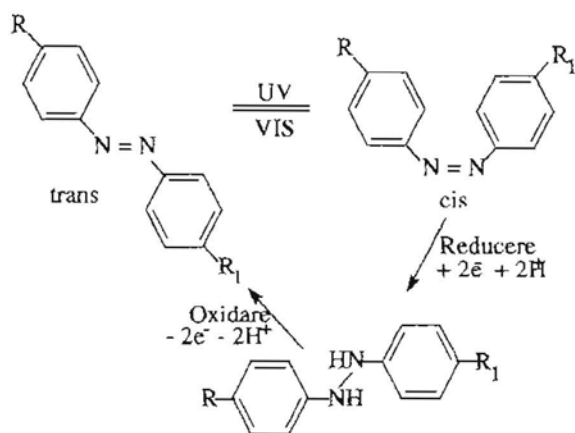


(II)

where: R_1, R_2 - halogen, halogen group in o- or m- position

R_3 - OH or polymer with OH groups

The azobenzene derivatives can be switched from trans to cis by UV irradiation. The relatively unstable cis – isomer may be electrochemically oxidized to trans – azobenzene, as can see in the scheme below [4]:



Using the photoelectrochemical properties of a Langmuir-Blodgett film (a

monoatomic layer of long molecules that are arranged parallel one to another at right angles to the plane of the film) of 4 - octyl - 4'-(5-carboxypentamethylene –oxy)-azobenzene ($R = n\text{-C}_8\text{H}_{17}$, $R_1 = \text{O} - \text{CH}_2\text{CH}_2\text{CH}_2\text{CH}_2\text{CH}_2\text{-COOH}$ on a transparent SnO_2 glass substrate, this work like an electrode [4].

PHOTOCHROMIC POLYMERS

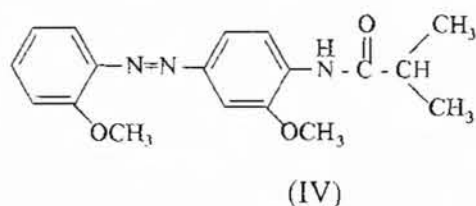
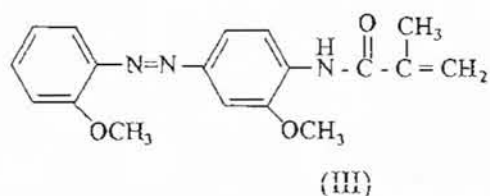
The cis – trans isomeric change principle in relative to $-\text{N}=\text{N}-$ bond was used for the syntheses of the azo photochromic polymers.

The macromolecule conformation influence the photochromic properties, the influence being pithy in the polyelectrolyts with contains the azo group in the lateral chain.

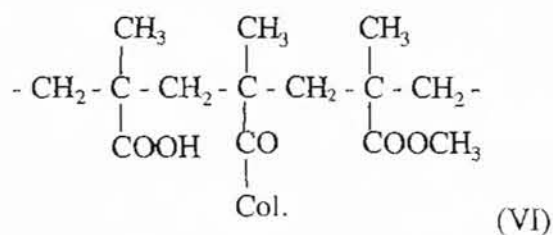
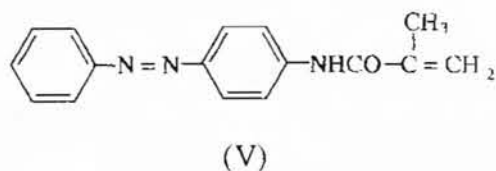
The conformational transitions of the polyelectrolyts depend by the ionisation grade, rave influence not only the unfolding of the photoinduce reaction, also the one in the dark. From this reason, the wavelength of the isosbestic point from the absorption spectrum of the acrylic acid copolymer and N - (2, 2' - dimethoxyazobenzene) - acrylamida (III, IV), depends by the pH of the solution and it reduces with the degree of viscosity (pH = 5-7) as a result of the polyelectrolyt conformation change.

This phenomena determines also the reduce of the reaction rate in the dark of the compound (IV), at $\text{pH} = 6 - 9$, though in this pH domain the isomerization rate for the photochromic monomer increases by the catalytic action of the HO^- ions.

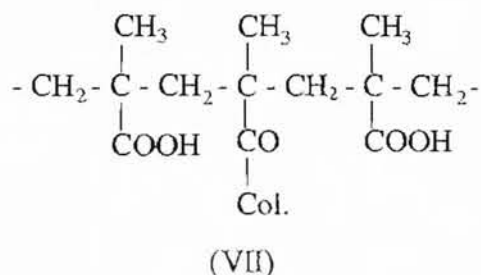
The conclusion it might be that the cis - trans isomerization reaction rate it isn't influenced only by the pH, but also by the polyelectrolyt type [5].



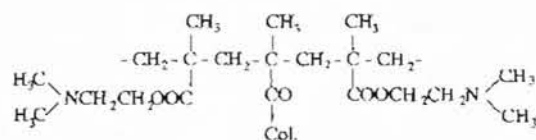
A monoazoic dyes (V) with a simple constitution insoluble in water, with contains a polymerisable lateral chain it was copolymerise with: methacrylic acid, his derivatives or with a monomer mixture, so it forms the hydrosoluble polyelectrolyts (VI-IX) [6]:



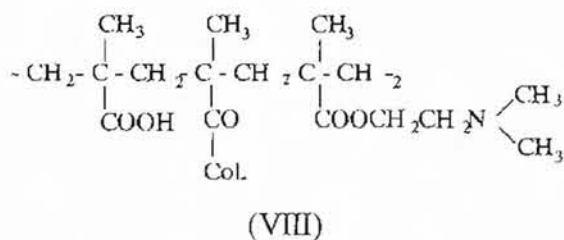
Methacrylic acid: methacrylic acid
methylester = 60:40 Mol. %



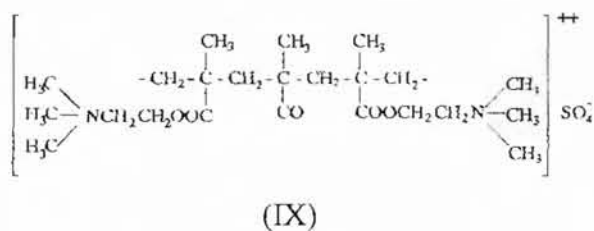
100% methacrylic acid



100% methacrylic acid (2-dimethylamino-
ethylester-1)



methacrylic acid - (2-dimethylamino-
ethylester-1) : methacrylic acid = 50:50
Mol. %



100% methacrylic acid -(2-dimethylamino-ethylester-1) processed with dimethylsulfat

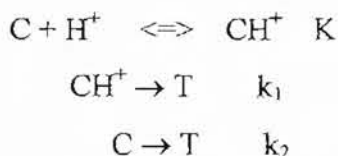
The polyelectrolyts thus obtained have a molecular weight between 75000 and 22500.

For dark reaction when cis-trans conversion takes place, kinetics are apparent first order in all dye systems, so that $K_d(C)$ is defined:

$$\frac{-d(C)}{dt} = k_d(C)$$

where (C) equals cis form concentration

Assuming that H^+ is in rapid equilibrium with the cis form characterized by equilibrium constant K then a mechanism consistent with the data is:



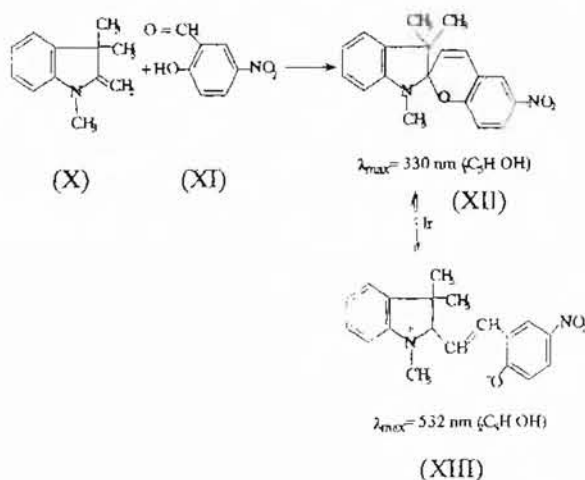
in which the k 's are rate constants. In the k_1 step, the reverse step (rate constant k_{-1}) is not included because addition of H^+ or other catalysts to a solution of dye in the trans form (T) does not cause a discernible absorption spectral shift by the free dyes toward that of the cis form. It must be pointed out that is true only in the dark, in water. For other conditions it isn't true [7].

The same situation holds for the k_2 step; the reverse reaction k_{-2} may will be important under different solvents and

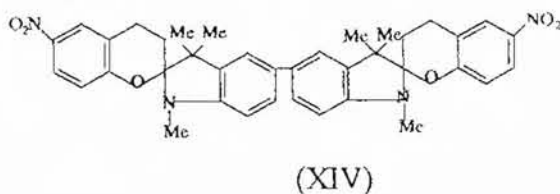
temperature conditions. This step is probably not a simple one step reaction as noted by several others for no aqueous system. For the present that activity of water is a constant at $25^\circ C$ and is a factor in k_2 [7].

Photochromic substances, especially those from spiranic type have been introduced in latest years in cosmetic produces with a view to 'worsen' make-up at accidently exposure to intense light with a big fund of ultraviolet.

One classic example is constituted by spiropyran (XII), which is prepared through condensation of Fisher base with nitrosalicyl aldehyde.



The same action has the (XVII) dye used especially for irritant skin oil, nail varnish, dyes for hair etc [8].



CONCLUSIONS

Photochromic substances present a vast practice utility in a lot of domains series like: the protective of lens in the presence of UV and visible radiation, because the closing of colour at light increase molecular extension of dyes, so the incident radiation in eyes is more reduced; protector windscreens for all the transport vehicles, sensors which can put in

evidence illuminated intensity in some precincts through changed own colour and in cosmetics.

The cis-trans photoisomerization of polymer azo compounds constitute a model for adjusted enzymatic activity through intermediated photochromic effectors, which is connected with constitutive proteins of active centre.

REFERENCES

- [1]. I. Popov, V. T. Skripkina, S. P. Protsyk, A. A. Skrynikova, B. M. Krasovitskii, L. M. Yagupol'skii, *Ukrain Khim. Zhun.*, 1991, 57/8, 843
- [2]. R. Brode, J. H. Gould, G. M. Wyman, *J. Amer. Chem. Soc.*, 1952, 74, 4641
- [3]. Y. Katsura, M. Uehara, M. Taniguch, K. Katimura (Seiko Epson Corp.), *Jpn. Kokai Tokkyo Koho Jap. Pat.* 05, 125, 030 (Cl. C07C245/08) 1993 cf. *Chem. Abstr.* 1993, p. 119, 191962y
- [4]. H. Zollinger, "Color Chemistry", Ed. II, VCH Meinheim - New York - Basel - Cambridge, 1991, p. 329 - 331
- [5]. H. Fink, *Plaste und Kautschuk*, 18, 1971, 645
- [6]. H. Fink, *Veröffentlichung in Vorbereitung*
- [7]. R. Lavrien, J. C. B. Waddington, *J. Amer. chem. Soc.* Bd. 86, 1964, p. 2315
- [8]. Fischer, Y. Hirshberg, *J. Chem. Soc.*, 1952, 4522

INORGANIC POLLUTANTS IN THE AIR, FORMED IN PHOTOCHEMICAL PROCESSES

ELENA GRIGORESCU

"I.H. Rădulescu" High School, 26 Unirii Blvd., 0200 Târgoviste, Romania

INTRODUCTION

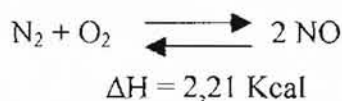
The photochemical reactions involved in the air pollution have mostly been studied during the last few years, to demonstrate their important role in the "photochemical smog" manifestation phenomena.

Any process which, adding certain chemical compounds to the ordinary air components, can alter its physical and chemical properties so that these should be detected by the inhabitants of the environment is called pollution.

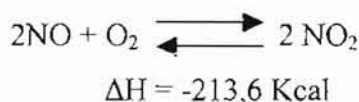
Two of the nitrogen oxides hold importance concerning the preservation of the environment.

NITROGEN OXIDES, POLLUTION SOURCES.

Nitrogen monoxide is produced at high temperatures, by burning fosile combustibles, gases, fuel oil, coal, in the air.



At a high temperature, the formed oxide dissociates rapidly. The equilibrium concentration of NO varies with temperature. It is reglectible under 550⁰ C, but becomes significant at 1700⁰ C. The formed NO can react with the oxygen, resulting NO₂ :



Nitrogenous anhydride is also produced in a small amount, mostly dissociated:



From the IR absorption spectres the conclusion is drawn that also nitrogenic anhydride formation occurs, which vanishes through an other reaction:



or else



From the experimental verifications resulted that high temperatures combustion, quick cooling and instant dilution occur, with the emission of high concentrations of nitrogen monoxide and low concentrations of nitrogen dioxide. *The stability of NO_2 decreases together with increasing temperature.*

The oxidation of NO to NO_2 with oxygen shows a specific particularity, namely that the forming rate decreases with the temperature increase. The rate also varies with the square of the NO concentration. Therefore, the oxydation rate of NO in the air decreases rapidly with the NO dilution. A lot of time is therefore necessary for the traces of NO from the atmosphere to be oxidated, but a photochemical mechanism taking place under the influence of solar light produces such an oxidation in much shorter time.

Biologically produced NO represents the higher amount of nitrogen oxides in the atmosphere.

The natural sources produce $50 \cdot 10^7$ t NO yearly, and those from human activities $5 \cdot 10^7$ t NO_x yearly.

The concentrations of nitrogen oxides in the cities atmosphere are 10-100 times higher than those from the outside cities atmosphere.

The average time of stability for NO_2 is about 3 days, and for NO is about 4 days.

The burning processes of coal, oil products, natural gas, and of the fuel used in the vehicles engines, contribute with about 90% at the nitrogen oxides concentrations. In industry, the nitrogen oxides are eliminated in the processing of HNO_3 , of the nitrogenous fertilizers, of H_2SO_4 (the bad chambers method), and in the dinitration and nitration process.

The process of electrocuting, engraving, welding, metal puriffication, explosive detonations, obtaining the liquid NO_2 based fuels used in the spacecrafts jet propulsion, are considered as *nitrogen oxides* sources.

The most serious nitrogen oxides pollution effects hold not on to the nitrogen oxides themselves, but on to the *role* they play in the *formation of the photochemical oxidants. (OX).*

A photochemical oxidant is any substance from the atmosphere produced by a photochemical process, capable to oxidate any materials insufficiently oxydated by the gaseous oxygen. These are very important components of the „smog“.

INTERACTIONS OF THE NITROGEN OXIDES IN THE ATMOSPHERE

The formation of the photochemical oxidants is due to a complex process of

interactions of some certain hydrocarbons and oxidation products of the hydrocarbons with the *photolytic cycle* of NO_2 .

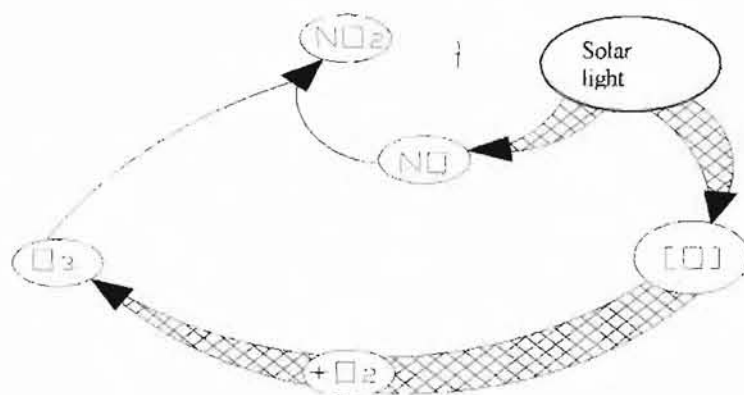


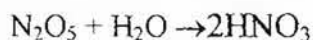
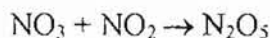
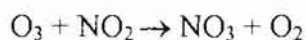
Fig. 1. The photolytic cycle of the nitrogen dioxide

The UV rays have enough energy to break the N-O bounds and to form new species of NO and [O]. The atomic oxygen reacts with the O_2 molecules from the air and form O_3 , the main oxidant from the environmental air.

During an ordinary day in a city, the ambient level of the nitrogen oxides follows a regular pattern, related to the solar light and to the traffic. Before the day break, the concentrations of NO and NO_2 keep level. Once the human activities enhance between 6-8 in the morning, the NO concentration rise, due mainly to the streets traffic. As the solar light intensify

providing UV radiations, the NO concentration increase, due to the conversion of primary NO into secondary NO_2 . As the NO concentration decrease, O_3 starts to accumulate up to a concentration value lower than 0,1 p.p.m. As the solar light intensity diminishes and the automotive traffic intensifies, toward evening, between the hours 17-20 the NO concentration starts growing again. The solar energy can no more transform NO into NO_2 .

The final product of the pollution with nitrogen oxides is HNO_3 , but in a big proportion this is passed into nitrates.



FORMING PROCESSES OF THE „PHOTOCHEMICAL SMOG“

As a consequence of a reaction between atomic oxygen and hydrocarbon an intermediary species is formed, very reactive, called *hydrocarbon free radical* RO^*_2 .

The hydrocarbons concentration for air originates in natural sources, biological processes, coal, oil, petrol evaporation, emissions of unburned fuel in the exhaust gases, evaporation of organic solvents, dyes, varnishes.

The free radicals react rapidly with NO to form NO_2 . This way, NO is replaced from the cycle, the O_3 transforming mechanism is eliminated and the O_3 concentration in the air is getting higher.

The free radicals can react with the oxygen and with the NO_2 to form peroxyacetyl nitrates with other hydrocarbons and oxygenated species, forming other, undesirable organic products.

The mixture of products resulting from the hydrocarbons interactions within the photolytic cycle of NO_2 is called „photochemical smog“. This is shaped out of O_3 and CO, peroxyacetyl nitrates and other organic compounds: aldehydes, cetones, alkyl nitrates, and so forth.

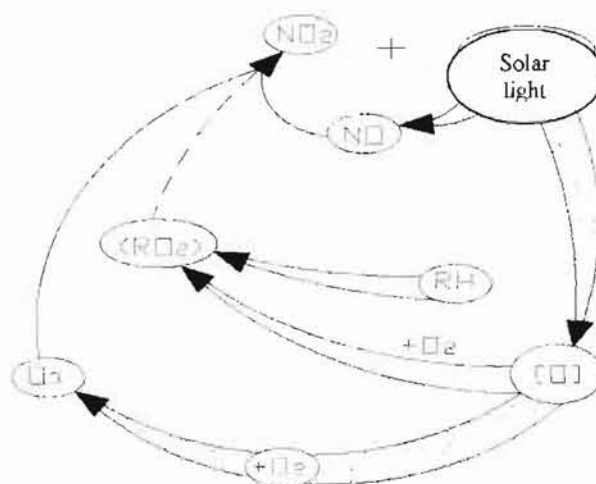
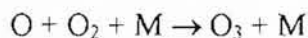
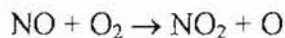


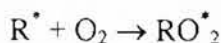
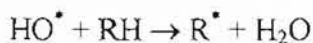
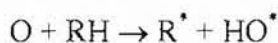
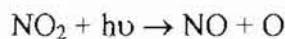
Fig. 2. The interaction of the photolytic cycle of NO_2 with the hydrocarbons

The action of the solar light triggers the oxidation processes:

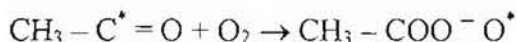
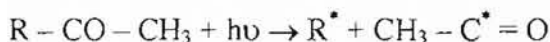
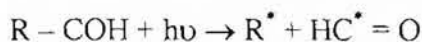


These compounds make up the „photochemical smog” or the oxidant mist, present in the atmosphere of the big, intensively circulated cities.

Significant amounts of O_3 , free radicals, intermediaries and other oxidation products, show up in the atmosphere, as a result of the photochemical processes:



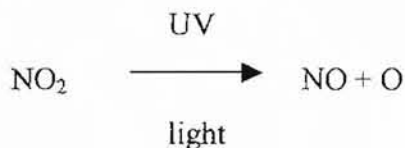
The peroxyacetyl nitrate from the polluted atmosphere appears according to the reactions:



The nitrogen dioxide is a much more efficient absorbent in the fraction of

the UV light which reaches the surface of the Earth.

The absorption by the NO_2 of the UV radiations with wave lengths ranging between 3000-4000 Å, is followed by the reactions:



M being considered a molecule from the system.

Together with the increase of the ultraviolet light intensity, one can observe a quick and almost quantitative oxidation of the NO to the NO_2 . This photochemical oxidation is unusual, because the absorption capacity of NO_2 increases with the irradiation.

In terms of an undisturbed photolytic cycle of the NO_2 , ozone and NO are formed and destroyed in equal amounts.

Pollution is a danger to people, animals, plants, and to the state of some materials.

Preserving the environment we live in, is and will be an essential problem of the mankind.

REFERENCES

1. N. Negoiu, A. Kriza – Poluanți anorganici în aer, Ed. Academiei 1977.
2. Control techniques for nitrogen oxide emissions from stationary Sources, AP – 67 (1970)
3. Air Quality Criteria for Photochemical oxidants, AP – 63 (1976)
4. E.R. Stephens, J. Air Wather Pollut, 4, 79 (1961).

VARIATIONAL FORMULATION OF THE IMPULSIVE TRACTION FOR A PLASTIC MATERIAL

CONSTANTIN GHIȚĂ

Department of Mathematics, "Valahia" University, Targoviste, Romania

ABSTRACT: *We analyze the cvasi-static equilibrium of a plastic body governed by a nonlinear differential constitutive law; the directional linear hardening is expressed in terms of a hidden variable: the dimensionless plastic work. We obtain a result which gives an inferior bound for the intensity impulsive factor on a side of the boundary.*

INTRODUCTION

An existence result to a dynamical contact problem with friction, based on the penalization and regularization methods was proved in [8] for a viscoelastic material with short memory. A quasi-static behaviour of a linear visco-elastic body with fading memory and dynamic boundary conditions was investigated in [1].

Analytical expressions in the duality of functional spaces of some constitutive laws and some friction laws have been described in several works of J. J. Moreau (for example [9]). Variational formulations in distributional spaces of a Coulomb friction law, especially for the case of elastic structures, appear in french papers (example [2]). Some contributions about variational formulation of a few elasto-

visco-plastic structures with short memory can be found in the author works [6], [7] and [10]. There we have imposed for the directional hardening case admissibility conditions at the quasi-statical loading and have selected some technological parameters.

The elasto-plastic structures case, having geometrical and physical nonlinearities was treated in the duality of spaces, based on a compensatory functional appear in the works of Y. Gao [3 - 5].

In this work we have given an elasto-plastic deformation process model with directional hardening in the context of unilateral contact and Coulomb friction on the same side of the boundary. Following a way of thinking initiated by Y. Gao, about estimation of an impulsive factor of

superficial loading (a measure for the traction), we formulate in the sequel a variational inequality on a time-independent statical admissible set of a variational space. Now we get a similar result about impulsive factor in the conditions of directional linear hardening and superficial friction in a finite period of time during a quasi-static loading. The dependence of this factor is essential on the superpotentials: complementary power developed by the stress tensors, superficial dissipated power by friction.

PRELIMINARY CONCEPTS AND FRICTIONAL CONTACT PROBLEM

A body occupies a regular domain Ω of \mathbb{R}^3 referred to a rectangular cartesian system (Euler system) $Ox_1x_2x_3$, Ω is an open, bounded, connected subset of \mathbb{R}^3 , with a boundary Γ (a Lipschitz boundary is sufficient). Γ is decomposed into three mutually disjoint parts $\Gamma_u, \Gamma_F, \Gamma_s$, the body is clamped on Γ_u ; we assume that on Γ_u the displacements are given. The body is submitted to given forces f on another part Γ_F and unilateral contact conditions with Coulomb friction against a rigid obstacle on Γ_s of the boundary.

Let U be the space of admissible displacements and \dot{U} the space of

admissible velocities; the space \dot{U} is paired with the admissible forces space F by a bilinear form, expressed by $(f, u)_e$ - the density of external power. Let E be a strain *Green* space, Σ the dual space of E , the *Kirchhoff* stress space. A strain tensor ε is paired with a stress tensor σ by the bilinear form $(\sigma, \varepsilon) = \sigma : \varepsilon$ - internal energy. For a large deformation, we take \dot{E} the admissible strain rate space, the dual pair of $\dot{\varepsilon} \in \dot{E}$ and $\sigma \in \Sigma$ is given by $(\sigma, \dot{\varepsilon})_{int} = \sigma : \dot{\varepsilon} = \text{Tr}(\dot{\varepsilon} \sigma^T) = \dot{\varepsilon}_{ij} \sigma_{ij}$ - the density of internal power [3-5].

At initial state the body has a null configuration, $u(0) = \dot{u}(0) = 0$; during a quasi-static deformation process, the body is subjected to a uniform loading: by forces b in Ω , surface impulsive traction $\bar{f} = v(u, \sigma, \theta) \bar{t}$, $\|\bar{t}\| = 1$, on the part Γ_F of the boundary, here θ is a hidden variable of the material. We seek the loading factor v_σ on Γ_F related to a solution (u, σ, θ^*) of the abstract governing equations modeling the local behavior of a plastic material with hardening, θ^* is a conjugate factor of θ :

$\dot{\varepsilon} = A_t(u) \dot{u}$ in Ω , $\dot{u} = 0$ on Γ_u , $\forall t \in [0, T]$ (geometric relation);

$A_t^*(u) \sigma + b = 0$ in Ω , $A_t^*(u) \sigma \bar{t} = v$ on Γ_F , $\forall t \in [0, T]$ (equilibrium equation);

$-R \in \partial\phi(\dot{u})$ on Γ_s , $-R = A_t^*(u)\sigma$ on Γ_s ;
 $\forall t \in [0, T]$ (unilateral contact with
 Coulomb's friction);
 $(\dot{\varepsilon}, -\dot{\theta}) \in \partial\psi^c(\sigma, \theta^*)$, $\theta^* = H\theta$ in Ω ,
 $\forall t \in [0, T]$ (constitutive law).

DEFINITIONS AND NOTATIONS

Let $\varepsilon: U \rightarrow E$ be the Green-Saint-Venant map,

$$\varepsilon(v) = \frac{1}{2}(\nabla v + \nabla v^T + \nabla v \nabla v^T), \text{ the}$$

directional derivative of ε at $u \in U$ in the direction $v \in U$ is defined by

$$\frac{d\varepsilon}{dv}(u) = \frac{1}{2}[\nabla v + \nabla v^T + \nabla u \nabla u^T + \nabla u^T \nabla u]$$

$$\frac{d\varepsilon}{dv}(u) = A_t(u)v, \text{ which emphasize the}$$

nonlinear map, namely *tangent geometric mapping*.

$$\text{But } \frac{d\varepsilon}{dt}(u) = A_t(u)\dot{u} = [(I + \nabla u^T)\nabla]_{\text{sym}} \dot{u},$$

and if we take $u = v + \delta u$, assuming that v is time independent, we investigate the relation-ship between the two geometric maps $A_t(u)$, $A_t(v)$. Indeed, a simple calculus of the *Gâteaux derivative* of a strain rate tensor gives the following relation:

$$A_t(u)\dot{u} = \frac{d}{dt}\varepsilon(u) = \frac{d}{dt}\varepsilon(v + \delta u) = A_t(v + \delta u)\delta\dot{u} =$$

$$= \frac{1}{2}[\nabla\delta\dot{u} + \nabla\delta\dot{u}^T + \nabla\delta\dot{u}\nabla v^T + \nabla\delta\dot{u}^T\nabla v] +$$

$$+ \frac{1}{2}[\nabla\delta\dot{u}\nabla\delta u^T + \nabla\delta\dot{u}^T\nabla\delta u] =$$

$$= A_t(v)\delta\dot{u} + A_n(\delta u)\delta\dot{u}, \text{ where}$$

$$A_n(w)v = \frac{1}{2}[\nabla v \nabla w^T + \nabla v^T \nabla w] = A_n^t(v)w$$

is *compensatory operator* associated with a displacement perturbation.

Now, we define its conjugate operator $A_t^*(u)$ by a Gauss-ian transformation

$$\langle A_t(u)\dot{u}, \sigma \rangle_\Omega = \langle \dot{u}, A_t^*(u)\sigma \rangle_\Omega,$$

$$\text{where: } \langle \cdot, \cdot \rangle_\Omega = \int_\Omega (\cdot, \cdot)_{\text{int}} dx,$$

$$(\cdot, \cdot)_\Omega = \int_\Omega (\cdot, \cdot)_{\text{ext}} dx + \int_\Gamma (\cdot, \cdot) dx_s, \quad \text{are}$$

global internal and external powers.

We refer to the compensatory map, taking

$$\frac{d}{dt}(\nabla\delta u \nabla\delta u^T) = 2A_n(\delta u)\delta\dot{u} \quad \text{and}$$

integrating on $[0, t_f]$, where t_f is a final time of loading; we obtain

$$\begin{aligned}
 G(\delta u, \tau)(t_f) &= 2 \int_0^{t_f} \langle A_n(\delta u)\delta\dot{u}, \tau \rangle_\Omega dt = \\
 &= \int_\Omega \nabla\delta u \nabla\delta u^T : \tau dx(t_f) = (G(u(t_f)) - v, \tau)
 \end{aligned}$$

that is so called *gap function* associated to the compensatory operator $A_n(\delta u)$ -- [3 - 5].

Denote by θ an internal variable,

$$\theta(t) = \frac{1}{\mu(\Omega)\sigma_c} \int_0^t \langle A_t(u) \dot{u}, \sigma \rangle_{\Omega} dt, \text{ having}$$

$\theta(0)=0$, a time function, as a dimensionless plastic power, where σ_c is a material constant, an yield threshold at a deformation by traction and $\mu(\Omega)$ is a measure of Ω (volume). Let Θ be the space of admissible hardening factor θ , Θ^* the space of θ^* , conjugate function of θ , $\theta^*=H\theta$, where H is a positive tensor.

UNILATERAL CONTACT WITH COULOMB FRICTION

Let K be a subset of U , K is the set of an admissible displacements of every boundary point on Γ_s ; $u(t) \in K \Leftrightarrow g(u) \geq 0$, for all time, where $g: U \rightarrow \mathbb{R}$ is a contact intensity factor. For a displacement $u(t) \in K$ of a boundary point on Γ_s , we associate $V_K(u)$ the set of admissible velocities of the frontier points,

$$V_K(u) = \left\{ v \in \dot{U} / \nabla g(u)v \in Rg(u) + R_+ \right\} [2].$$

We remark that

$$\dot{u} \in V_K(u) \Leftrightarrow$$

$$g(u)(t) = (\alpha g(u)(0) + \beta) e^{-\alpha t} - \frac{\beta}{\alpha} \text{ for some}$$

parameters $\alpha \in \mathbb{R}$, $\beta \in \mathbb{R}_+$.

Suppose that *Signorini - Fichera* boundary condition hold on Γ_s , expressing

the contact with a unilateral support, having a nonlinear intensity g

$$(3.1) \quad g(u) \geq 0, R_N(u) \geq 0, R_N(u)g(u)=0 \text{ where } R = (I + \nabla u^T) \nabla \sigma \text{ is a reaction of the rigid obstacle, } R_N = R \cdot \bar{n}.$$

Lemma 1: Let $u \in W^{1,1}([0, T], \mathbb{R}^3)$,

then the conditions (3.1) are equivalent to the subdifferential

$$\text{inclusion} - R_N(u) \in \partial \psi_{V_K(u)}(\dot{u}) [2].$$

If Coulomb's friction holds in Γ_s with given normal forces R_N , there exists $|R_T| \leq \mu |R_N|$, more precisely, if $|R_T| < \mu |R_N|$, then $\dot{u}_T = 0$ and if $|R_T| = \mu |R_N|$, then there exists $\lambda \geq 0$, such that $\dot{u}_T = -\lambda R_T$, where μ is the friction coefficient [2], [9].

Lemma 2: Let $u \in W^{1,1}([0, T], \mathbb{R}^3)$ a

displacement of a boundary point, then Coulomb's friction law is equivalent to a variational inequality.

$$R_T(u)(v_T - \dot{u}_T) + \mu |R_N| (|v_T| - |\dot{u}_T|) \geq 0,$$

$$\forall v \in V_K(u)$$

The last relation is an explicit writing of the subdifferential inclusion

$$-R_T(u(t)) \in \partial \Phi_T(\dot{u}(t)), \forall t \in [0, T],$$

$$\Phi_T(v) = \int_{\Gamma} \mu |R_N| |v_T| d\sigma$$

Summarizing the two results, we deduce the following

Proposition 1. The behavior of the body on Γ_s , if $u \in W^{1,1}([0, T], R^3)$, is characterized by the inequality $u(0) \in K$, $R(u(t))(v - \dot{u}(t)) + \mu |R_N(u(t))| (|v_\tau| - |\dot{u}(t)|_\tau) \geq 0$, $\forall v \in V_K(u(t))$, a.e. $t \in [0, T]$

VARIATIONAL FORMULATION AND EVALUATION OF INTENSITY LOAD.

Let $C \subset \Sigma \times \Theta^*$ be a convex nonempty subset

$$C = \{(\sigma, \theta^*) \in \Sigma \times \Theta^* / \varphi(\sigma, \theta^*) \leq 0 \text{ in } \Omega\},$$

where $\varphi(\sigma, \theta^*) = T(\sigma) - \eta(\theta^*) - \sigma_c$, ψ_C

is so called *complementary plastic*

superpotential, $\partial\psi_C(.,.) \subset \dot{E} \times \Theta$ is a

convex subset. The duality between

$\dot{E} \times \Theta$ and $\Sigma \times \Theta^*$ is given by (see also [5], [7]):

$$\langle (\tau, \theta^*), (\dot{\varepsilon}, -\dot{\theta}) \rangle = \langle \tau, A_t(u)\dot{u} \rangle + \langle \theta^*, -\dot{\theta} \rangle_\tau,$$

where $\langle \theta^*, -\dot{\theta} \rangle_\tau = \langle \dot{\theta}^*, \theta \rangle - \theta(T)\theta^*(T)$.

The constitutive equation of the hardening plastic material may be written in an

inequality form

$$(A_t(u)\dot{u}, \tau - \sigma) + \langle -\dot{\theta}, \phi^* - \theta^* \rangle \leq$$

$$\psi_C(\tau, \phi^*) - \psi_C(\tau, \theta^*), \forall (\tau, \phi^*) \in \Sigma \times \Theta^*$$

We take

$$S_{ad} = \{ (v, \tau, \phi^*) \in U \times \Sigma \times \Theta^* / A_t^*(v)\tau = b \text{ in } \Omega, \\ A_t^*(v)\tau - v(\tau, v)\bar{I} = 0 \text{ on } \Gamma_F$$

the time independent statically admissible

set and we have:

Theorem 1: Suppose that H^{-1} is a positive definite matrix, G a non-negative gap function, $(u, \bar{t}) > 0$ on Γ_t , then

$$v_\sigma \geq v(v, \tau, \phi) - t_f \left[\int_{\Omega} \{ \psi_C(\tau, \phi^*) + \phi(-R_\tau) \} dx \right],$$

$$\forall (v, \tau, \phi^*) \in S_{ad} \quad \forall t \in [0, t_f], \text{ where } \psi_C \text{ and}$$

ϕ are superpotentials, $v(v, \tau, \phi^*)$ is an admissible intensity factor on a part Γ_t , t_f is a final time of quasi-static loading on Γ .

The last result gives an inferior bound for the intensity impulsive factor on Γ_t .

REFERENCES

[1] C. A. Bosello & G. Gentili, *Some quasi-static problems with elastic and viscous boundary conditions in linear viscoelasticity*, Quart.of Appl Math,

volume LIV, no. 1, 1996 p. 687-696;

[2] A. Cimetiere, A. Leger & C. Naejus, *A functional framework for the Signorini problem with Coulomb's friction*,

EDF, Directions des Etudes et Recherches, 1994;

[3] Y. Gao & G. Strang, *Geometric nonlinearity potential energy, complementary energy, and the gap function*. Quart. Of Appl. Math. XLVII, 1989, p.487-504;

[4] Y. Gao & T. Wierzbicki, *Bounding theorem in finite plasticity with hardening effect*, Quart. Appl. Math. XLVII, 1989, p.395-403;

[5] Y. Gao, *Dynamically loaded rigid - plastic analysis under large deformation*, Quart. Appl. Math. XLVIII, 1990, p.731-739;

[6] C. Ghiță, *Metalurgie Matematică. Analiză nestandard a proceselor metalurgice*, Ed. Academiei Române, 1995;

[7] C. Ghiță, *The quasi-static equilibrium of a system with anisotropic hardening*, Rev. Roum. Math. Pures. Appl., XXIX, nr.1, 1984, p.43-54;

[8] J. Jarušek & C. Eck, *Dynamical contact problems with friction in linear viscoelasticity*, C. R. Acad. Sci. Paris, t. 322, s. 1, 1996, p. 497-502;

[9] J. J. Moreau, *On unilateral constraints, friction and plasticity*, New Variational Techniques in Mathematical Physics, G. Capriz & G. Stampacchia, Ed. Cremonese, Roma, 1973;

[10] Nguyen Quoc Son, *Problemes de plasticité et de rupture*, Publ Math d'Orsay, nr.82-08, 1981, Orsay.

[11] P. D. Panagiotopoulos, *Multivalued Boundary Integral Equation for Inequality Problems. The convex case*, Acta Mechanica 70, 1987, p.145-167.

A METHOD OF COMPACTNESS FOR HAMMERSTEIN EQUATIONS AND APPLICATIONS

CRISTINEL MORTICI

Department of Mathematics, "Valahia" University, Targoviste, Romania
e-mail: cmortici@valahia.ro

ABSTRACT: *This paper contains homotopy arguments and continuation methods for nonlinear operator equations of Hammerstein type. Using the Leray-Schauder, it obtains existence results for the problem of forced oscillations of a pendulum with finite amplitude.*

INTRODUCTION

Roughly speaking, the degree of F at y relative to D , written $d(F, D, y)$, is a measure of the number of the solutions of the equation $F(x) = y$ in D .

L.E.J. Brouwer introduced in 1912 the finite dimensional topological degree, uniquely defined by four axioms: the existence condition, the additivity with respect to the domain, the invariance under homotopies and the normalization.

In 1934, Leray-Schauder extended the degree to compact perturbations of the identity in infinite dimensional Banach spaces.

Some properties of the topological degree are of interest in the theory of abstract Hammerstein equations.

Proposition 1.1. *Let $F: \overline{D} \subset X \rightarrow X$ be such that $I - F$ is compact and let $y \in X \setminus F(\partial D)$. Then the Leray-Schauder degree $d(F, D, y)$ satisfies the following properties:*

- a) *The degree is continuous in F .*
- b) *If $H \in C([0, 1] \times D, X)$ is such that $I - H(t, \cdot)$ is compact, for every $t \in [0, 1]$ and $y \in X \setminus H([0, 1] \times \partial D)$, then the degree*

$$d(H(t, \cdot), D, y) = \text{constant}, \quad \forall t \in [0, 1].$$

- c) *If $d(F, D, y) \neq 0$, then $y \in F(D)$.*
- d) *The degree for the identity function $I: X \rightarrow X$ is*

$$d(I, D, y) = \begin{cases} 1 & , \quad y \in D \\ 0 & , \quad y \notin D \end{cases}.$$

For proof and details see [2], [6].

THE RESULTS

Let X be a real Banach space, with strictly convex dual space X^* . This means that the unit sphere of X^* contains no line-segments,

$$\begin{aligned} \|(1-t)x + ty\| &< 1, \\ \forall t \in [0, 1], \|x\| = \|y\| = 1, x \neq y. \end{aligned}$$

In other words, the space X^* is strictly convex if $x, y \in X^*$ with $\|x\| = \|y\| = 1$ and $\|(1-t)x + ty\| = 1$ holds if and only if $x = y$.

We mention a basic result due to Asplund (e.g. [2]): For every $a > 1$, there exists an equivalent norm $\|\cdot\|_a$ which is strictly convex together with its dual norm and such that

$$\frac{1}{a} \|\cdot\|_a \leq \|\cdot\| \leq a \|\cdot\|_a.$$

In virtue of this theorem, the assumption on strict convexity is not an essential restriction for reflexive Banach spaces.

The map $J: X \rightarrow 2^{X^*}$ given by

$$Jx = \{f \in X^* \mid \langle f, x \rangle = \|x\|^2 = \|f\|^2\}$$

is called the duality map, where $\langle f, x \rangle$ denotes the duality between X and X^* , i.e. the action of the functional $f \in X^*$ to the element $x \in X$.

According to Hahn-Banach theorem, to each $x \in X$ there corresponds an $f \in X^*$

satisfying $\|f\| = \|x\|$ and $\langle f, x \rangle = \|x\|^2$.

Therefore Jx is a non-empty set of X^* , for every $x \in X$, that is $D(J) = X$. It follows also from the definition that J is odd ($J(-x) = -Jx$), positively homogeneous ($J(\lambda x) = \lambda J(x)$, for all $\lambda \geq 0$), bounded, bijective and norm preserving.

It is easy to see that if the dual space X^* is strictly convex, then Jx is a single valued map. In what follows, the reflexive Banach space will be considered equivalently renormed as strictly convex spaces and we may assume that J is an operator.

Let us consider the semilinear abstract equation $Lx + N(x) = 0$, where $L: D(L) \subset X \rightarrow X^*$ is linear and $N: X \rightarrow X^*$ is nonlinear.

If L has a continuous inverse $A := L^{-1}$, then (2.1) can be written as $(I + AN)x = 0$, where $N: X \rightarrow X^*$ is nonlinear and $A: X^* \rightarrow X$ is linear such that $R(N) \subset D(A)$.

An equation of the form (2.2) is called Hammerstein equation.

Note that the operator $AN: X \rightarrow X$ is compact if A is compact and N is bounded and demicontinuous.

Indeed, N transforms bounded sets of X in bounded sets of X^* and further, A

carries bounded sets of X^* in relatively compact sets of X . Finally, the continuity of AN follows from the fact that A is completely continuous.

In conclusion, $I + AN$ is compact perturbation of the identity map, so the Leray-Schauder degree can be considered. We give the following existence result:

Theorem 2.1. *Let $A: X^* \rightarrow X$ be a compact linear map and let $N: X \rightarrow X^*$ be a bounded demicontinuous operator. Assume that there exists a bounded, open set $0 \in D \subset X$ such that* (2.3)
 $\langle N(x), x \rangle \geq 0, \quad \forall x \in \partial D.$

Then the equation $(I + AN)x = 0$ has at least one solution $x \in \bar{D}$.

Proof. We use the method of elliptic super-regularization due to Browder and Ton (see [1]). For every $\varepsilon > 0$, we consider the perturbation $N_\varepsilon: X \rightarrow X^*$, defined by

$$N_\varepsilon x := Nx + \varepsilon Jx, \quad x \in D(N).$$

It is easy to see that the operator $P_\varepsilon := AN_\varepsilon: X \rightarrow X$ is compact.

First, we prove that for every $\varepsilon > 0$, the equation

$$(2.4) \quad (I + P_\varepsilon)x = 0$$

has at least one solution denoted $x_\varepsilon \in D$. Let us consider the Leray-Schauder homotopy

$$H(t, x) = x + tP_\varepsilon x, \quad x \in \bar{D}, t \in [0, 1].$$

In order to use the property of invariance to homotopy of the Leray-Schauder degree, we must show that $0 \notin H([0, 1], \partial D)$.

If assume by contrary that $H(t, x) = 0$ for some $x \in \partial D, t \in [0, 1]$, then

$$0 = \langle N_\varepsilon x, x + tP_\varepsilon x \rangle = \langle N_\varepsilon x, x \rangle + t \langle N_\varepsilon x, AN_\varepsilon x \rangle.$$

Since A is linear, monotone, it follows

$$0 \geq \langle N_\varepsilon x, x \rangle = \langle Nx, x \rangle + \varepsilon \|x\|^2 \geq \varepsilon \|x\|^2,$$

thus $x = 0 \in \partial D$, contradiction.

Therefore $0 \notin H([0, 1], \partial D)$ and consequently

$$\begin{aligned} d(I + P_\varepsilon, D, 0) &= d(H(1, \cdot), D, 0) = \\ &= d(H(0, \cdot), D, 0) = d(I, D, 0) = 1. \end{aligned}$$

We obtained that $d(I + P_\varepsilon, D, 0) \neq 0$, so the equation (2.4) has at least one solution $x_\varepsilon \in D$. From the equality

$$(I + AN)x_\varepsilon = -\varepsilon AJx_\varepsilon$$

it follows that $x_\varepsilon \rightarrow x$ in X as $\varepsilon \rightarrow 0$, that is $0 \in \overline{(I + AN)(D)}$. Since AN is compact, we have $0 \in (I + AN)(\bar{D})$, which proves the assertion.

APPLICATION

We are now in position to indicate how the existence results from the previous

section can be applied to the problem of the forced oscillations of a pendulum.

Let $X = C([0, 1])$ be the real Banach space of all continuous functions $f: [0, 1] \rightarrow \mathbf{R}$ endowed with the uniform convergence norm

$$\|x\| = \sup_{t \in [0, 1]} |x(t)|, \quad x \in X.$$

The problem of the forced oscillations of a pendulum with finite amplitude is described by the following system

$$(3.1) \quad \begin{cases} -x''(t) = a \sin x(t) - z(t), & t \in [0, 1] \\ x(0) = x(1) \end{cases}$$

where $x(t)$ is the amplitude of the oscillation, $a > 0$ is a real constant depending on the pendulum length and the driving function $z(t)$ is continuous, odd, periodic.

The problem (3.1) can be written in the abstract form

$$(3.2) \quad Lx + N(x) = 0,$$

where $Lx = -x''$ is linear with

$$D(L) = \{x \in C([0, 1]) | x(0) = x(1) = 0\}$$

and the nonlinearity N is the superposition

operator relative to $f(t, \xi) = -a \sin \xi + z(t)$,

$$Nx(t) = -a \sin x(t) + z(t), \\ x \in C([0, 1]), t \in [0, 1].$$

It is well known that L is invertible with continuous inverse

$$(3.3) \quad Ax(t) = L^{-1}x(t) := \int_0^1 G(t, s)x(s)ds, \\ x \in X, t \in [0, 1],$$

where $G: [0, 1] \times [0, 1] \rightarrow \mathbf{R}$ given by

$$G(t, s) = \begin{cases} s(1-t) & , 0 \leq s \leq t \leq 1 \\ t(1-s) & , 0 \leq t < s \leq 1 \end{cases}$$

The operator $A: D(A) \subset X \rightarrow X^*$ is compact because G is continuous. The equation (3.2) can be written as an Hammerstein equation

$$(I + AN)x = 0,$$

where $AN: X \rightarrow X$ is given by

$$ANx(t) = \int_0^1 G(t, s)f(s, x(s))ds, \quad x \in X.$$

The function G is continuous and satisfies the usually Caratheodory conditions and growth conditions which assure the compactness of AN .

According to the theorem, the equation (3.2) and consequently the equation (3.1) has at least one solution.

REFERENCES

[1] - F.E. Browder, B.A. Ton, *Nonlinear Functional Equations in Banach*

Spaces and Elliptic Super-regularization, Math. Z., 105(1968), 1-16.

- [2] – K. Deimling, *Nonlinear Functional Analysis*, Springer Verlag, Berlin, 1995.
- [3] – C.L. Dolph, G.J. Minty, *On Nonlinear Integral Equations of the Hammerstein Type*, in *Nonlinear Integral Equations*, Univ. Wisconsin Press Madison, 1964, 99-154.
- [4] – J. Mawhin, *Topological Degree Methods in Nonlinear Boundary Value Problems*, Reg. Conf. Ser. Math., 40, AMS, Providence, 1979.
- [5] – J. Mawhin, *Topological Degree Methods in Nonlinear Boundary Value Problems*, Reg. Conf. Ser. Math., 40, AMS, Providence, 1979.
- [6] – C. Mortici, *Variational Methods for Perturbed Laplace Problem*, Analele Univ. Timisoara, 1998.
- [7] – S. Sburlan, *Lectii de Analiza Neliniara. Gradul Topologic*, Ed. Academiei, Bucuresti, 1985.
- [8] – I.V. Skrypnik, *The Solvability of Nonlinear Equations with Monotone Operators*, Dopovidi Akad. Nauk Ukran. RSR, Ser. A, 1970, 32-35.
- [9] – I.V. Skrypnik, *Methods for Analysis of Nonlinear Elliptic Boundary Value Problems*, Transl. Math. Monographs, 139(1994), AMS.

SOME PROPERTIES OF MAXIMAL RING OF QUOTIENTS

ANDREEA MIHAELA PANAIT

Department of Mathematics, "Valahia" University, Targoviste, Romania

e-mail: augustandre@yahoo.com

ABSTRACT: In the present paper are given the construction of the maximal ring of quotients and are demonstrated two properties of maximal ring of quotients.

This article tries to present some properties of maximal ring of quotients studied closely.

First I want to present scantily the construction of maximal ring of quotients. The context for this notion is: let R be a ring, F an additive topology on R , $(\mathcal{T}, \mathcal{F})$ a torsion theory with respect to F and t the radical associated to $(\mathcal{T}, \mathcal{F})$. We introduce on F the next relation: if $I, J \in F$, then we define $I \prec J$ if I contain J .

Evidently " \prec " is an order relation.

Also we observe that F with this relation becomes an arranged filtered relation.

If we denote the category of left R -modules with ${}_R\mathcal{C}$ and if M is a R -module, $I, J \in F$, $I \prec J$ then we define a canonical homomorphism like this:

$Hom_R(I, M) \rightarrow Hom_R(J, M)$ which associates to the homomorphism $\alpha: I \rightarrow M$ the homomorphism

$\alpha|_J: J \rightarrow M$. It demonstrated that the family $\{Hom_R(I, M)\}_{I \in F}$ became an inductive sistem.

Then we define:

$$M_F = \varinjlim_{I \in F} (I, M/I(M))$$

and we denote **the module of quotients of M with respect to F** .

In the particular case where $M = {}_R R$ it obtains a ring structure which is called **the ring of quotients of R with respect to F** .

Now let R be a ring, $F = D$ the additive topology of the left dense ideals of R accordingly to the torsion theory of Lambek.

The ring R_D is the **maximal ring of quotients of R** , and is denoted by Q_m .

Then:

$$Q_m = \varinjlim_{I \in D} Hom_R(I, R/I(R))$$

We consider:

$\mathcal{A}_D = \{M \in {}_R\mathcal{C} \mid \forall x \in M, I_R(x) \in D\}$ the

torsion class of additive topology D . It results:

$\mathcal{A}_D = \{M \in {}_R\mathcal{C} \mid \forall x \in M, I_R(x) \text{ dense in } R\}$

Let be

$\mathcal{L} = \{M \in {}_R\mathcal{C} \mid \text{Hom}_R(M, E({}_R R)) = 0\}$. Then

$\mathcal{A}_D = \mathcal{L}$. So that $R \in \mathcal{A}_D$ equivalent with $R \in \mathcal{L}$.

But ${}_R R \leq E({}_R R)$, then

$\text{Hom}_R(M, E({}_R R)) \neq 0$.

So ${}_R R \notin \mathcal{L}$, ${}_R R \notin \mathcal{A}_D$. It follows that the

${}_R R$ is D -without torsion, then $\iota({}_R R) = 0$.

So we have:

$$Q_m = \lim_{I \in D} \text{Hom}_R(I, R)$$

In the next part of this article I will try to present one condition which make the Q_m a Q_m -injective module.

Therefore, we introduce the following set:

$$\mathcal{M} = \left\{ I \leq {}_R R \mid \begin{array}{l} \exists \alpha : I \rightarrow R \text{ homomorphism which can't be} \\ \text{extended to } \beta : J \rightarrow R \text{ homomorphism, for every } J \leq {}_R R \text{ with } I \subseteq J \end{array} \right\}$$

We demonstrate that every ideal of \mathcal{M} is essential in ${}_R R$. Let be $I \in \mathcal{M}$. We suppose that exist $K \leq {}_R R$ with $K \cap I = \{0\}$.

In this case every homomorphism $\alpha : I \rightarrow R$ can be extended to $\beta : J \rightarrow R$, that is a contradiction to $I \in \mathcal{M}$. So the

supposition is false and it results that every ideal of \mathcal{M} is essential in ${}_R R$.

Proposition 1. Q_m is Q_m -injective module if and only:

$$\{\lambda \in R \mid I\lambda = 0\} = 0, \text{ for every } I \in \mathcal{M}.$$

Proof: " \Rightarrow " We suppose that Q_m is Q_m -injective module.

Let be $I \in \mathcal{M}$. It results $I \leq {}_R R$ and from the [3] we know that for every homomorphism $\alpha : I \rightarrow R$, exists a dense left ideal J of R and a homomorphism $\beta : J \rightarrow R$, with $I \subseteq J$ and $\beta|_I = \alpha$.

But J is dense in R and $I \subseteq J$, then I is dense in R , so with the definition it obtains for every $a \in R$, $\{\lambda \in R \mid (I : a)\lambda = 0\} = 0$.

For $a = I$ we obtain: $\{\lambda \in R \mid (I : 1)\lambda = 0\} = 0 \Leftrightarrow \{\lambda \in R \mid I\lambda = 0\} = 0$. So we did this implication.

We suppose that $\{\lambda \in R \mid I\lambda = 0\} = 0$, for every $I \in \mathcal{M}$.

Let be $J \leq {}_R R$, and $\alpha : J \rightarrow R$. By Zorn lemma we may say that it exists a homomorphism $\beta : K \rightarrow R$ which extends α and can't be extended to a left ideal L which contains K .

So, $K \in \mathcal{M}$ and $\{\lambda \in R \mid I\lambda = 0\} = 0$.

Also from [3] we can say that is enough to show that K is a dense ideal of R , which is equivalent with $\{\lambda \in R \mid (K : a)\lambda = 0\} = 0$, for every a .

Let be $a \in R$. We define

$$\varphi : (K : a) \rightarrow R, \varphi(c) = \beta(ca), c \in K.$$

We will try to show that φ can't be extended to a left ideal which contains $(K : a)$. We suppose that exists

$$P \supsetneq_{*} (K : a) \quad \text{and} \quad \psi : P \rightarrow R \quad \text{with}$$

$$\psi|_{(K : a)} = \varphi.$$

We define

$$\gamma : K + Pa \rightarrow R, \gamma(k + pa) = \beta(k) + \psi(p).$$

If $k + pa = 0$, then $p \in (K : a)$ and $\psi(p) = \varphi(p) = \beta(pa)$.

Thus

$$\gamma(k + pa) = \beta(k) + \beta(pa) = \beta(k + pa).$$

In conclusion γ extends β . But $P \supsetneq_{*} (K : a)$ and $\exists p \in P$ with $pa \notin K$, and $K \subsetneq K + Pa$.

With this affirmation we deny the

maximality of P .

So, φ can't be extended to a left ideal which contains $(K : a)$. By the definition $(K : a) \in \mathcal{M}$, and $\{\lambda \in R \mid (K : a)\lambda = 0\} = 0$.

Q.e.d

The following proposition will show that if R is a boolean ring(i.e. a commutative regular ring with all elements idempotent), then Q_m is boolean.

Proposition 2. The maximal ring of quotients of a boolean ring is boolean.

Proof: Let R be a boolean ring and Q_m its maximal ring of quotients.

$$Q_m = \varinjlim_{I \in D} \text{Hom}_R(I, R)$$

We will show that all the elements of Q_m are idempotent. Let be $a \in Q_m$, $a = \hat{\xi}$, $\xi : I \rightarrow R, (I \in D)$. With R boolean ring we say that $\xi^2 = \xi$. So, it results: $\hat{\xi}^2 = \hat{\xi}$, and therefore $a^2 = a$. Since $a \in Q_m$, we obtain that Q_m is a boolean ring.

Q.e.d.

REFERENCES:

[1] C.Nastasescu – “ Inele, module, categorii “, Editura Academiei, Bucuresti, 1976

[2] Bo Stenstrom – “ Rings and Modules of Quotients “, Springer Verlag, Heidelberg-New York, 1971

[3] Bo Stenstrom – “Rings of quotients “, Springer Verlag, Berlin-Heidelberg-New York, 1975

CURVILINEAR INTEGRAL $I(C)$ FOR PROBLEMS OF VARIATIONS CALCULUS ON SUPERMANIFOLDS

VALENTIN GABRIEL CRISTEA

Department of Mathematics, "Valahia" University valentin_cristea@yahoo.com

ABSTRACT: A proposition for the curvilinear integral $I(C)$ for piecewise superdifferentiable supercurve is given.
Mathematics Subject Classification (1991): 58A50

Let V be a supervector space as in [1], V^* be the dual supervector space as in [2], M be a supermanifold in sense Rogers as in [4] and $T(M)$ be the tangent superspace or superbundle over M as in [2].

We consider B_L the Grassmann algebra over the reals with generators $1^{(L)}, \beta_1^{(L)}, \dots, \beta_L^{(L)}$ with L positive integer and $B_L^{m,n} = (B_L)_0^m \oplus (B_L)_1^n$ [4] where $B_L = (B_L)_0 \oplus (B_L)_1$ [5].

Definition 1. A function $f: B_L^{m,n} \rightarrow B_L$ is called a superdifferentiable function [4]

if there exist $f_\mu \in C^\infty(B_L^{m,n}, \mathbf{R})$ [4] such that:

$$f(x, \theta) = \sum_{\mu \in M_n} f_\mu(x, \theta) \theta^\mu \quad [4]$$

where $M_n = \{ (\mu_1, \dots, \mu_n) / 1 \leq \mu_1 < \dots < \mu_n \leq n \}$ [3].

Definition 2. Let L be a superdifferentiable function on $T(M) \times B_L$. Then L defines a superdifferentiable map of $T(M) \times B_L \rightarrow T^*(M) \times B_L$ called the Legendre supertransformation, given in local coordinates by

$$x' \circ L_1 = x' \quad (\forall) 1 \leq i \leq m, \quad \theta^\alpha \circ L_1 = \theta^\alpha \quad (\forall) 1 \leq \alpha \leq n, \quad t \circ L_1 = t,$$

$$y' \circ L_1 = (\partial L / \partial x') \quad (\forall) 1 \leq i \leq m, \quad \text{and} \quad \delta^\alpha \circ L_1 = (\partial L / \partial \theta^\alpha) \quad (\forall) 1 \leq \alpha \leq n.$$

If this map is an immersion [2] of $T(M) \times B_L$ into $T^*(M) \times B_L$, then the function L will be called a regular super-Lagrangian. In this

$$H(y, \delta) = \langle L_1^{-1}(y, \delta), (y, \delta) \rangle - L \circ L_1^{-1}(y, \delta)$$

with the scalar product defined in [1] and we put $\omega = \bar{\theta} - Hdt$ where $\bar{\theta} = \rho^*(\theta)$ with θ fundamental 1-superform on $T^*(M)$ and $\rho^*: T^*(M) \times B_L \rightarrow T^*(M)$ is the projection of $T^*(M) \times B_L$ on $T^*(M)$ and $R_a^*\theta = Ada^{-1}\theta$ where R_a is the action on the right on M through the Lie supergroup $GL(m, n)$ [2], $a \in GL(m, n)$ and the interior automorphism of $GL(m, n)$ Ada^{-1} defines an interior automorphism of the Lie superalgebra $gl(m, n)$ [2].

Definition 3. The function $C: [b, k] \rightarrow M$ is called a superdifferentiable supercurve [1] if the functions $x^i \circ C$ (\forall) $1 \leq i \leq m$ and $\theta^\alpha \circ C$ (\forall) $1 \leq \alpha \leq n$ are superdifferentiable (**Definition 1.**), the

case, the map L_1^{-1} comes locally in a similar way from a function H on $T^*(M) \times B_L$ called the super-Hamiltonian:

functions $\varepsilon_L \circ x^i \circ C$ (\forall) $1 \leq i \leq m$ and $\varepsilon_L \circ \theta^\alpha \circ C$ (\forall) $1 \leq \alpha \leq n$ are differentiable in \mathbf{R} , the application $\varepsilon_L: B_L \rightarrow \mathbf{R}$ that is given by $\varepsilon_L(\sum_{\mu \in M_L} d^\mu \beta_\mu) = d^\Phi$ with $\beta_\Phi = 1^{(L)}$ and (x^i, θ^α) are the coordinates of a point $p \in M$.

Then we have the following theorem:

Theorem 1. Let $C: [b, k] \rightarrow M$ be a superdifferentiable supercurve and we put $\bar{C} = L_1 \circ \tilde{C}$ with $\tilde{C}(t) = (\dot{C}(t), t)$. Then we have:

$$\int_b^k L(\tilde{C}(s))ds = \int_{[b, k]} \bar{C}^* \omega$$

where $\omega = \bar{\theta} - Hdt$.

REFERENCES

[1]. CRISTEA, V.G., Existences and uniqueness theorem for Frenet frame supercurves, Max-Planck-Institut fuer Mathematik, Preprint Series 1999 (94)

[2]. DEWITT, B., Supermanifolds, Cambridge, Univ. Press, Cambridge, London, 1984

[3] KOSTANT, B., Graded manifolds, graded Lie theory and prquantization, Lect.

Notes in Math. no. 570, Springer-Verlag
1977

[4] ROGERS, A., Graded manifolds,
supermanifolds and infinite-dimensional
Grassmann algebras, Commun. Math. Phys.
105, 375-384 (1986)

[5] SCHEUNERT, M., The theory of
Lie superalgebras, Lect. Notes in Math. no.
716, Springer-Verlag 1979

[6] STERNBERG, S., Lectures on
differential geometry, Prentice-Hall, Inc.
Englewood Cliffs, New Jersey 1964

UN THÉORÈME DE SURJECTIVITÉ POUR OPÉRATEURS MONOTONES DANS ESPACES DE HILBERT

DINU TEODORESCU,

Département de Mathématiques, Faculté des Sciences, Université „Valahia” Târgoviste,

RÉSUMÉ: En utilisant un théorème de surjectivité de F. Browder, on montre qu'une classe d'opérateurs monotones dans espaces de Hilbert réels ont la propriété d'être inversables. Le résultat établi peut être appliqué pour étudier l'existence et l'unicité de la solution des équations opératoriennes nonlinéaires dans espaces de Hilbert réels.

Soit E un espace linéaire normé sur le corp K ($K = \mathbb{R}, \mathbb{C}$) et $A : E \rightarrow E$ un opérateur. S'il existe $\omega > 0$ tel que $\|A(x) - A(y)\| \leq \omega \|x - y\|$ pour tous $x, y \in E$, on dit que A est un opérateur Lipschitz de constante ω . Pour $\lambda > 0$ on définit les opérateurs:

$$A_\lambda : E \rightarrow E, A_\lambda = A + \lambda I$$

$$\text{et } B_\lambda : E \rightarrow E, B_\lambda = A - \lambda I,$$

où I est l'identité de E .

Il est évident que:

Proposition 1. Si A est un opérateur Lipschitz de constante ω , alors les opérateurs A_λ et B_λ sont opérateurs Lipschitz de constante $\omega + \lambda$.

Proposition 2. Soient $\varepsilon > 0$ et A un opérateur Lipschitz de constante ω . Alors les opérateurs $A_{\omega+\varepsilon}$ et $B_{\omega+\varepsilon}$ sont opérateurs Lipschitz injectifs de constante $2\omega + \varepsilon$.

Démonstration: On va montrer l'injectivité des opérateurs $A_{\omega+\varepsilon}$ et $B_{\omega+\varepsilon}$.

Soient $x, y \in E$. $A_{\omega+\varepsilon}(t) = A(t) + (\omega + \varepsilon)t$, $B_{\omega+\varepsilon}(t) = A(t) - (\omega + \varepsilon)t$ pour tout $t \in E$, et on obtient:

$$\begin{aligned} (\omega + \varepsilon)\|x - y\| &= \|A_{\omega+\varepsilon}(x) - A(x) - A_{\omega+\varepsilon}(y) + A(y)\| \leq \\ &\leq \|A_{\omega+\varepsilon}(x) - A_{\omega+\varepsilon}(y)\| + \|A(x) - A(y)\| \leq \|A_{\omega+\varepsilon}(x) - A_{\omega+\varepsilon}(y)\| + \omega\|x - y\| \end{aligned}$$

$$\begin{aligned} \text{et } (\omega + \varepsilon)\|x - y\| &= \|A(x) - B_{\omega+\varepsilon}(x) - A(y) + B_{\omega+\varepsilon}(y)\| \leq \\ &\leq \|A(x) - A(y)\| + \|B_{\omega+\varepsilon}(x) - B_{\omega+\varepsilon}(y)\| \leq \omega\|x - y\| + \|B_{\omega+\varepsilon}(x) - B_{\omega+\varepsilon}(y)\|. \end{aligned}$$

Donc:

$$\varepsilon\|x - y\| \leq \|A_{\omega+\varepsilon}(x) - A_{\omega+\varepsilon}(y)\| \quad \forall x, y \in E \quad (1)$$

$$\text{et} \quad \varepsilon \|x - y\| \leq \|B_{\omega+\varepsilon}(x) - B_{\omega+\varepsilon}(y)\| \quad \forall x, y \in E \quad (2)$$

En vertu de (1) et (2), il résulte que les opérateurs $A_{\omega+\varepsilon}$ et $B_{\omega+\varepsilon}$ sont injectifs.

Dans ce qui suit H sera un espace de Hilbert réel et $\langle \bullet, \bullet \rangle$ sera le produit scalaire sur H . Soit $A : H \rightarrow H$ un

opérateur. On dit que A est un opérateur monotone et

$$\langle A(x_1) - A(x_2), x_1 - x_2 \rangle \geq 0,$$

$$\forall x_1, x_2 \in H.$$

On dit que A est un opérateur fort monotone s'il existe $a > 0$ tel que :

$$\langle A(x_1) - A(x_2), x_1 - x_2 \rangle \geq a \|x_1 - x_2\|^2 \quad \forall x_1, x_2 \in H$$

Il est évident qu'un opérateur fort monotone est monotone.

On dit que A est un opérateur hémicontinu et

$$\lim_{t \rightarrow 0} \langle A(x + ty), u \rangle = \langle A(x), u \rangle \quad \forall x, y, u \in H$$

(autrement dit $\lim_{t \rightarrow 0} A(x + ty) = A(x)$ dans la topologie faible de H).

On dit que l'opérateur A satisfait une condition de coercivité de type (b) et

$$\lim_{\|x\| \rightarrow \infty} \frac{\langle A(x), x \rangle}{\|x\|} = +\infty.$$

Dans cette situation on dit simplement que A est un opérateur de type (b).

Proposition 3. Tout opérateur Lipschitz $A : H \rightarrow H$ est hémicontinu. (En particulier, si $A : H \rightarrow H$ est un opérateur Lipschitz de constante ω , alors

les opérateurs $A_{\omega+\varepsilon}$ et $B_{\omega+\varepsilon}$ sont hémicontinus).

Démonstration: Soient $x, y, u \in H$ et $(t_n)_n \subset \mathbb{R}$ avec $t_n \xrightarrow[n]{} 0$.

$$\begin{aligned} |\langle A(x + t_n y), u \rangle - \langle A(x), u \rangle| &= |\langle A(x + t_n y) - A(x), u \rangle| \leq \\ &\leq \|u\| \cdot \|A(x + t_n y) - A(x)\| \leq \|u\| \cdot \omega \|x + t_n y - x\| = \omega \|u\| \cdot \|y\| \cdot |t_n| \xrightarrow[n]{} 0 \end{aligned}$$

$$\text{donc} \quad \lim_{t \rightarrow 0} \langle A(x + ty), u \rangle = \langle A(x), u \rangle.$$

Proposition 4. Tout opérateur fort monotone $A : H \rightarrow H$ est un opérateur de type (b).

Démonstration: A soyaient un opérateur fort monotone, il résulte l'existence de $a > 0$ tel que

$$\langle A(x) - A(y), x - y \rangle \geq a\|x - y\|^2 \quad \forall x, y \in H.$$

Pour $y=0$ on obtient:

$$\langle A(x) - A(0), x \rangle \geq a\|x\|^2 \Rightarrow \langle A(x), x \rangle \geq a\|x\|^2 + \langle A(0), x \rangle \quad \forall x \in H.$$

De l'inégalité Cauchy-Schwartz on obtient

$$|\langle A(0), x \rangle| \leq \|A(0)\| \cdot \|x\|$$

et comme H est un espace réel il résulte que:

$$-\langle A(0), x \rangle \leq \|A(0)\| \cdot \|x\| \Rightarrow \langle A(0), x \rangle \geq -\|A(0)\| \cdot \|x\| \quad \forall x \in H.$$

$$\text{Donc } \langle A(x), x \rangle \geq a\|x\|^2 - \|A(0)\| \cdot \|x\| \quad \forall x \in H \Rightarrow$$

$$\Rightarrow \frac{\langle A(x), x \rangle}{\|x\|} \geq a\|x\| - \|A(0)\| \quad \forall x \in H \text{ cu } x \neq 0 \Rightarrow \lim_{\|x\| \rightarrow +\infty} \frac{\langle A(x), x \rangle}{\|x\|} = +\infty.$$

Proposition 5. Soient $A : H \rightarrow H$

un opérateur Lipschitz de constante ω et $\varepsilon > 0$. Alors $A_{\omega+\varepsilon} = (\omega + \varepsilon)I + A$ est un opérateur fort monotone.

Démonstration:

Soient

$x_1, x_2 \in H$. De l'inégalité Cauchy-Schwartz, comme H est un espace de Hilbert réel, il , résulte que:

$$\begin{aligned} -\langle A(x_1) - A(x_2), x_1 - x_2 \rangle &\leq |\langle A(x_1) - A(x_2), x_1 - x_2 \rangle| \\ &\leq \|A(x_1) - A(x_2)\| \cdot \|x_1 - x_2\| \leq \omega\|x_1 - x_2\|^2 \end{aligned}$$

$$\text{donc: } \langle A_{\omega+\varepsilon}(x_1) - A_{\omega+\varepsilon}(x_2), x_1 - x_2 \rangle =$$

$$\begin{aligned} &= \langle A(x_1) + (\omega + \varepsilon)x_1 - A(x_2) - (\omega + \varepsilon)x_2, x_1 - x_2 \rangle = \\ &= \langle A(x_1) - A(x_2), x_1 - x_2 \rangle + \omega\|x_1 - x_2\|^2 + \varepsilon\|x_1 - x_2\|^2 \geq \varepsilon\|x_1 - x_2\|^2. \end{aligned}$$

Soit $U_{\omega+\varepsilon} = -B_{\omega+\varepsilon} = (\omega + \varepsilon)I - A$,

où A est un opérateur Lipschitz de constante ω et $\varepsilon > 0$. En vertu de la proposition 2 ,

$U_{\omega+\varepsilon}$ est un opérateur Lipschitz injectif de constante $2\omega + \varepsilon$, qui satisfait:

$$\varepsilon\|x - y\| \leq \|U_{\omega+\varepsilon}(x) - U_{\omega+\varepsilon}(y)\| \quad \forall x, y \in H \quad (3).$$

Proposition 6. Soient $A : H \rightarrow H$ un opérateur Lipschitz de constante ω et $\varepsilon > 0$. Alors $U_{\omega+\varepsilon}$ est un opérateur fort monotone.

$$\langle A(x_1) - A(x_2), x_1 - x_2 \rangle \leq \omega \|x_1 - x_2\|^2. \text{ Donc:}$$

$$\begin{aligned} & \langle U_{\omega+\varepsilon}(x_1) - U_{\omega+\varepsilon}(x_2), x_1 - x_2 \rangle = \\ & = \langle (\omega + \varepsilon)x_1 - A(x_1) - (\omega + \varepsilon)x_2 + A(x_2), x_1 - x_2 \rangle = \\ & = \omega \|x_1 - x_2\|^2 + \varepsilon \|x_1 - x_2\|^2 - \langle A(x_1) - A(x_2), x_1 - x_2 \rangle \geq \varepsilon \|x_1 - x_2\|^2. \end{aligned}$$

Théorème (F. Browder, voir [1]).

Soit H un espace de Hilbert réel. Tout opérateur $V: H \rightarrow H$ de type (b), monotone et hémicontinu est surjectif.

Théorème: Soient $A : H \rightarrow H$ un opérateur Lipschitz de constante ω et $\varepsilon > 0$. Alors les opérateurs $A_{\omega+\varepsilon}$ et $U_{\omega+\varepsilon}$ sont inversibles.

Démonstration: Soit V un des opérateurs $A_{\omega+\varepsilon}$ et $U_{\omega+\varepsilon}$. On a montré

$$\|A_{\omega+\varepsilon}^{-1}(x) - A_{\omega+\varepsilon}^{-1}(y)\| \leq \frac{1}{\varepsilon} \|x - y\| \quad \forall x, y \in H$$

$$\text{et} \quad \|U_{\omega+\varepsilon}^{-1}(x) - U_{\omega+\varepsilon}^{-1}(y)\| \leq \frac{1}{\varepsilon} \|x - y\| \quad \forall x, y \in H.$$

Donc pour $\varepsilon > 1$, les opérateurs $A_{\omega+\varepsilon}^{-1}$ et $U_{\omega+\varepsilon}^{-1}$ sont des contractions et en

BIBLIOGRAPHIE:

- [1] R. Cristescu - Analiză funcțională - Editura Didactică și Pedagogică, București, 1983;
[2] Gh. Moroșanu - Ecuații neliniare de evoluție și aplicații - Editura Academiei R.S.R., București, 1986;

Démonstration: Soient $x_1, x_2 \in H$. En vertu des mêmes arguments que lesquels utilisés dans la démonstration de proposition 5, on obtient:

que V est un opérateur injectif.

En vertu des propositions 5 et 6 V est un opérateur fort monotone, donc V est monotone et en vertu de la proposition 4 il est un opérateur de type (b). V est aussi opérateur hémicontinu, soyaant opérateur Lipschitz. En vertu du Théorème de Browder, V est donc surjectif. Par conséquent V est inversable.

Remarque: En vertu de (1) et (3) on obtient:

vertu du théorème Picard-Banach ils admettent point fixe unique.

- [3] S. Sburlan- Gradul topologic - Lecții asupra ecuațiilor neliniare - Editura Academiei R.S.R., București, 1983.